The Role Of Mixed Emulsifier Systems In The Preparation Of Emulsions And Latexes.

THE ROLE OF MIXED EMULSIFIER SYSTEMS IN THE PREPARATION OF EMULSIONS AND LATEXES

by

YUNGNIEN JOHN CHOU

A Dissertation

Presented to the Graduate Committee

of Lehigh University

in Candidacy for the Degree of

Doctor of Philosophy

in

Polymer Science and Engineering

Lehigh University

1978

CERTIFICATE OF APPROVAL

Approved and recommended for acceptance as a dissertation in partial fulfillment of the requirements for the degree of Doctor of Philosophy.

June 2, 1978
(date)

J.W. Vanderhoff
M.S. El-Aasser
(Professors in Charge)

Accepted June 2, 1978
(date)

Special committee directing the doctoral work of Mr. Yungnien John Chou

J.W. Vanderhoff,
Co-Chairman

M.S. El-Aasser,
Co-Chairman

F.M. Fowkes

F.J. Micale

G.W. Poehlein

ACKNOWLEDGEMENTS

The author is indebted to many individuals for their assistance and encouragement during this research. Their constant help and advice contributed immeasurably to its successful completion.

Among these many individuals, the author is especially indebted to Dr. John W. Vanderhoff who gave guidance, encouragement and suggestions during the course of this research. His generous assistance, patience and understanding has made this work possible.

Also appreciation is given to Dr. Mohamed S. El-Aasser, Co-advisor, for his interest, assistance and suggestions which made possible the author's overcoming of many problems.

Appreciation is also expressed to the Dissertation Committee members Dr. Gary W. Poehlein, Dr. Fredrick M. Fowkes and Dr. Fortunato J. Micale for their interest, support and providing constructive proposals and help whenever called upon.

The author sincerely appreciates the financial support from a University Scholarship and the Emulsion Polymers Institute at Lehigh University.

The author wishes to thank Mrs. Olga Shaffer for proofreading the drafts. Special thanks are due Mr. Paul Krumrine, Mr. David Sudol, Mr. George Pauli and Ms.

Tina Vital for their constant help.

The author also wishes to thank Mrs. Doris Lewis for her careful typing of the final drafts.

Last, but not least, the author is most grateful to those whose encouragement, understanding, love and personal sacrifices made the completion of this study a reality; his children, Leslie, Johnny and Luann and his wife, Chaochin.

TABLE OF CONTENTS

Table of Contents (continued)

Table of Contents (continued)

Table of Contents (continued)

LIST OF FIGURES

Figures (continued)

Figures (continued)

Figures (continued)

Figures (continued)

Figures (continued)

LIST OF TABLES

List of Tables (continued)

Page

CHAPTER 5

List of Tables (continued)

List of Tables (continued)

Page

ABSTRACT

Mixed emulsifiers, ionic surfactants and fatty alcohols, have been widely used in the preparation of stable emulsions and latexes in comparison to similar amounts of ionic emulsifier alone. The mechanism for emulsification is of a great interest to study.

The direct investigation is difficult if not impossible. Therefore, information concerning the mechanism of emulsification using an ionic emulsifier-cetyl alcohol and other long-chain alcohols mixtures was obtained through various indirect investigations.

The conductometric titration information obtained by titrating the oil phase into the aqueous single and the mixed emulsifier systems show different conductometric titration curves. This implies a completely different emulsification process for the two systems. In comparison, the titration in aqueous hexadecyltrimethylammonium bromide solution gave a decrease (solubilization) to an inflection point, followed by a slower decrease (emulsification). For the mixed emulsifier system, with increasing oil concentration, the conductance decreased to a minimum, then increased to a maximum, and decreased slowly thereafter. The titration rate and the pre-emulsification time affect the conductance change.

The adsorption isotherm indicates that cetyl alcohol can replace a certain amount of ionic surfactant from the surface of the emulsion droplets.

Complex rod formation was observed by transmission electron microscopy in the mixed emulsifier system and this complex formation was verified as crystalline by a electron diffraction pattern. This indicates that cetyl alcohol and the ionic surfactant were oriented alternatingly and regularly in the complex rod formation.

In the mixed emulsifier system the presence of the rod formation has an important influence in the emulsification process. The styrene emulsion droplet size was approximately 500 nm at the first inflection point and then the size decreased significantly while the conductance increased only slightly. These results suggest that the formation of crystalline hexadecyltrimethylammonium bromide-cetyl alcohol aggregates, which break down during the emulsification process, releasing hexadecyltrimethylammonium and bromide ions to the aqueous phase, to maintain the optimum ratio on the droplet surface.

The experimental results are correlated with a mathematical model of the conductometric titration process.

The ultracentrifugation data verified that the stability of the emulsion prepared by using a mixed

emulsifier system is directly related to the conductometric titration curve. A mechanism for stability of the emulsion has been proposed. A set of advanced interpretation of ultraviolet spectra in terms of relative peak heights has also been proposed.

CHAPTER 1 GENERAL INTRODUCTION

1-1 Background

The trend toward using water-based coatings in replacing organic solvent-based coatings systems, is becoming increasingly important. The advantages are both economical and environmental (1-5).

Water-based polymers can be divided into three classes (6-9): a) solution polymers (water reducibles); b) solubilized polymers (colloidal dispersions); c) latexes (aqueous dispersions or emulsions). These three types vary significantly in their physical and mechanical properties and thus provide a considerable formulation range for coatings chemists. The main differences among the three classes are summarized in Table 1-1 (6).

Table 1-1 Summary of Three Classes of Water-Based Polymers

Property	Solution Polymers	Solubilized Polymers	Latexes
Appearance	clear	translucent	Apaque
Particle size	--	20-100 nm	$\geq$ 100 nm
Self-crowding capacity constant	0	1.0→0	~ 1.9
Molecular weight	20,000-50,000	20,000-200,000	1 million
Viscosity	Viscosity very dependent on polymer molecular weight	more viscosity sensitive, somewhat dependent on polymer molecular weight	low, independent of polymer molecular weight

The lower viscosity, higher solid content, and higher molecular weight properties of latexes make them highly desirable in surface coating, textile sizing and paper coatings, etc.

The word "latex", originally coined to denote the milky sap from certain plants, such as the India-rubber tree (Hevea brasiliensis), has been extended to aqueous dispersions of synthetic latexes produced by emulsion polymerization, as well as to artificial latexes produced by emulsification of polymer solutions. In the other words, "latex" is a term for a polymeric substance in a colloid dispersion; the dispersion medium usually is water. Latexes can be classified into one of three main categories, depending on their origins: (a) natural latexes, (b) synthetic latexes, and (c) artificial latexes (10).

Natural latexes are limited in their production, variety and the geographic location. This results largely because of the quantity and special formulation demanded. However the use of synthetic and artifical latexes can compensate for these limitations. Emulsion polymerization is a good method for preparing certain specific synthetic latexes, not being applicable to all polymers, such as polymers already made, or those whose monomer or initiator/ catalyst will react with water. Furthermore, emulsion

polymerization is accomplished by a free radical polymerization mechanism and therefore cannot produce latexes by condensation polymerization. Examples of such polymers are reclaimed rubber, polyurethane, epoxy, ethyl cellulose, stereoregular rubber, polyester, polypropylene or polyamide. For these cases, emulsification of the polymer solution into water using conventional emulsifiers and emulsification technique is the only way to produce an artificial latex. Unfortunately, it has not been possible to prepare a latex using the emulsification technique with an average particle size smaller than 1000 nm using a practical concentration of emulsifier. Therefore, the stable latexes prepared by emulsification are difficult to obtain. This implies that the stability of commercial polymer emulsions as prepared by emulsification is often not competitive with that of latexes prepared by emulsion polymerization, which usually have particle sizes in the range 100-300 nm. A new emulsification technique has been developed by the Emulsion Polymers Institute at Lehigh University using mixed emulsifiers, a combination of surfactant and fatty alcohol, to give emulsion droplets of about the same size as latex particles produced by emulsion polymerization (40).

The author was involved in the "Exploratory Development of Improved Water Base Coatings" project. The purpose of this work has to develop water-based analogs of the

solvent-based epoxy, curing agent primers and a polyurethane top coat which is presently used by the Air Force. Epon 828, Epon 1001, Versamid 100, Versamid 125, as well as Desmodur N-100 prepolymer adducts were successfully prepared by using the new emulsification technique.

Mixed emulsifiers are effective in preparing latexes from ethylcellulose, polyethylene carbonate, polystyrene, polyvinylacetate, etc.

The mixed emulsifier concept was originally derived from microemulsions. These are prepared with mixed emulsifiers constituting 15-25% of the total weight and produce significantly smaller particles, in the size range 8-80 nm (11). Microemulsions apparently are homogeneous transparent systems of low viscosity and contain a high percentage of oil and water. Microemulsions have attracted considerable interest ever since their introduction in 1935 by Schulman et al (12). In the new emulsification technique, the amount of mixed emulsifiers can be cut down to 1-2%. The excellent stability of the emulsion prepared by the mixed emulsifier system is assumed to be due to the presence of fatty alcohol which may confer stability because of 1) a steric effect resulting from surface coverage of the droplet, 2) liquid crystal formed on the surface of the droplet, 3) complex monolayers formed with ionic surfactant on the surface of the droplet, 4) reduction of electrostatic

repulsion between ionic molecules on the surface of the droplet, 5) reduction of interfacial tension between droplet and water.

A great deal of research has been done concerning the interfacial phenomena of microemulsions (11, 13-17).

The treatment of microemulsions as colloidal systems (18-21) and recent theoretical contributions (22, 23) have given rise to a pronounced progress in the field.

The influences of the chain length, the cation portion of surfactant and the nature of the solvent on the formulation of microemulsions were studied by Gerbacia and Rosano (24). From NMR studies and free energy of absorption of the alcohol, it was concluded that the alcohol-sulfactant interaction is weak.

Cetyl alcohol, cetostearyl and stearyl alcohols were found to lower the interfacial tension between liquid paraffin and the ionic surfactant. These fatty alcohols also affected the critical micelle concentration (CMC) of the ionic surfactant, which lowering was greater decreased with increasing length of the fatty alcohol (13).

An increase in the chain length of alcohols has been found to increase the surface activity (14, 15) as well as the solubilizing power of the ionic surfactant (16, 17). Schulman et al (24, 25) have postulated the phenomenon of "penetration" as a process in the formation of the film

"complex" at the interface. The degree of interaction is thought to depend on the chain length, shape of the hydrocarbon chain, polarity of the hydrophilic group (26) and degree of hydrophobic saturation (27). The incorporation of dodecanol into sodium lauryl surfate has been found to cause a decrease in static surface tension and its rate of decrease (28). Furthermore, cetyl alcohol has been found to improve the quality of emulsions consisting of liquid paraffin, water and sodium lauryl sulfate (29). Brown and co-workers (30) have observed that a much higher ratio of alcohol to surfactant is required to maintain an appreciable interfacial viscosity above the CMC. Cockbain (31) has found that alcohols with chain length greater than C_5 do not lower the concentration of soap required for aggregation of oil particles although these alcohols do have a greater effect on the CMC. Using soap concentrations considerably higher than the CMC, he noted maximum and minimum states of particle aggregation. Prince (32) has suggested that an oil-soluble compound with a low chemical potential will effect a greater lowering of the tension between the oil and aqueous phase even though it is less strongly interfacially absorped.

Wan & Poon proposed (13) that in the mixed emulsifier system that the interfacial layer is occupied by an alcohol film

penetrated by liquid paraffin molecules, suggesting that the alcohol hydroxy groups within the aqueous phase have not completely reduced the unsymmetrical force of the water molecules.

The ionic surfactant and alcohol molecules in this interface are oriented with their functional group in the water and hydrocarbon part in the oil phase. As the number of these molecules per unit area is increased, they begin to crowd one another, thereby developing a lateral two dimensional pressure, π . Early in the study of these monomolecular films it was observed that the surface tension, γ_i, of the interface decreased in proportion to this development of pressure among its tenants. This idea is expressed in the thermodynamic equation

$$\gamma_i = \gamma_{o/w} - \pi$$

where $\gamma_{o/w}$ is the interfacial tension of oil phase and water phase.

Prince (32, 33) pointed out that the role of alcohol was two fold: in addition to the increase of interfacial pressure by the specific penetration of alcohol molecules into the interfacial layer by means of alcohol-surfactant association, it also causes an initial reduction of the o/w interfacial tension in the system.

Prince (34) also proposed a concept of how a mixed emulsifier system can determine the properties of an

emulsion system. This leads to an explanation of the role that Griffins hydrophilic-lipophilic balance (HLB) scheme (35) plays with π .

Shah suggested (36, 37) that elongated aggregates in the microemulsion are concerned with multi-phase birefingent areas observed at higher water contents.

The importance of mixed emulsifiers in the preparation of latexes enhanced interest in the detailed study of the mechanism of emulsion formation using mixed emulsifier systems.

1-2 Emulsification and Stability

In discussing emulsions it is necessary to be able to distinguish each of the two phases present. The phase which is present in the form of finely divided droplets is called the disperse or internal phase. The disperse phase may also be referred to as the nondisperse or discontinuous phase. The phase which forms the matrix in which these droplets are suspended is called the continuous or external phase.

The emulsification of any oil phase into an aqueous phase is the result of two competing processes: 1) the breaking of the bulk oil phase into droplets and, 2) the recombination of the formed droplets back into the bulk phase. Thermodynamics is found useful in discussing the emulsification process. The Gibbs equation for free

energy is given as:

$$dG = -SdT + \sum u_i\ n_i + VdP + \gamma dA$$

where S and V are entropy and volume, respectively.

Assuming temperature (T), surface potential (u_i), the number of moles (n_i) and pressure (P) are constants, then

$$dG = \gamma dA$$

where γ is the surface tension and A is the surface area. Therefore, from the free energy point of view, the recombination of the formed droplets process is favorable at constant surface tension.

Surface-active agents which are added to an emulsion to increase its stability by interfacial action are known as emulsifiers or emulsifying agents. Efficiency of emulsification is increased by the action of mechanical devices such as simple stirrers, homogenizers, ultrasonifiers, or colloid mills. These methods use physical means to break the oil phase into small droplets. The efficiency of emulsification is determined by the ability to quickly form fine droplets and the stabilization of the formed droplets.

The conventional emulsification of an oil in water by mechanical shear gives an average emulsion droplet with 1000 nm diameter. The emulsions also have broad particle-size distributions. Most commercial latexes for coating applications prepared by emulsion polymerization

have average particle diameters in the range of 100 nm to 300 nm. These particles are 5-10 fold smaller than particles made by conventional emulsification techniques.

Stoke's law shows that the rate of sedimentation of spherical particles is $(D^2/18\eta)\ (d_p-d_m)\ g$, where D is the particle diameter, η the viscosity of the medium, d_p and d_m the densities of the particles and the medium, respectively, and g the gravitational constant.

The tendency for colloidal particles to settle upon standing is offset by their Brownian motion and convection currents arising from small temperature gradients in the sample. Brownian motion is explained as movement that is caused by the actual collisions of particles in the suspending medium. Convection currents depend upon the sample size and storage conditions. One criterion proposed for settling is that a particle sedimentation rate of only 1 mm in 24 hours will be offset by the thermal convection and Brownian motion within the sample (38). Substituting this sedimentation rate into the Stoke's law equation, the critical particle size for settling can be calculated.

Since particle size of the emulsion plays an important role in terms of stability, it becomes significant that it has not been possible to prepare oil in water emulsions with average particle sizes smaller than about 1000 nm

using a practical concentration of emulsifier. However, it was shown (39) that anionic emulsions of styrene in water with droplet sizes as small as 200 nm can be prepared using 1-2% or less of the sodium lauryl sulfate-cetyl alcohol mixed emulsifier system. The analogous cationic polyamide, epoxy emulsions with similar ranges of droplet sizes were prepared using the hexadecyltrimethylammonium bromide-cetyl alcohol mixed emulsifier system (40).

In the preparation of emulsions and latexes, two systems can be used: 1) the conventional emulsification technique which involves a simple surfactant and, 2) the mixed emulsifier system, from here on referred to as the new emulsification technique.

The new emulsification technique is described as follows:

a) The polymer is dissolved in a suitable aqueous-immiscible solvent, in order to reduce its viscosity to a acceptable level for emulsification.

b) The polymer solution is then emulsified by pouring it into the mixed emulsifier system and agitating. It is then subjected to the Manton-Gaulin homogenizer to break down the particle size.

c) Remove the solvent from the emulsion by vacuum distillation.

The emulsions and latexes prepared by using the mixed

emulsifier system are stable and the particle size distribution is in the range of 100 nm to 500 nm, therefore studying the role of mixed emulsifier systems in the preparation of emulsions and latexes is of a great interest.

1-3 Purpose and Scope of the Present Investigation

The purposes of this study are 1) to find the mechanism of emulsion formation using mixed emulsifier systems, and to determine 2) whether the stability of the emulsions or latexes can be predicted by a simple instrumental measurement.

Since the direct study of this system is impossible to achieve, an indirect approach is used. This approach has made use of the following experimental methods.

A. Conductometric titration

titrating the oil phase into single and mixed emulsifier systems and following the conductance change

B. Absorption isotherm

titrating the surfactant solution into cleaned monodisperse latexes with and without the treatment of cetyl alcohol

C. Electron Microscopy

particle size measurement at positions along the characteristic conductometric curve

diffraction pattern observation of a mixed emulsifier structure

D. Ultraviolet Absorption

to study the concentration of benzene in water phase after centrifugation

E. Ultracentrifugation

to study the stability of the emulsion using IEC-B-35 model ultracentrifuge

F. Mathematical Modeling

single surfactant system

mixed emulsifier system

1-4 References

1. Bonov, Amer. Paint & Coatings J., 59, 9 (1975).

2. Anon, Product Fin, 39, 86 (1975).

3. F.X. Dwyer, Amer. Paint & Coatings J., 34, October 25 (1977).

4. R.G. Young, J. Coatings Technology, 49 (632), 76 (1977).

5. D. Campbell and R.W. Flynn, Amer. Paint & Coatings J., 55, March 6 (1978).

6. W.H. Brendley, Jr., and T.H. Haag, ACS ORPL Div. Meeting Preprints, 32 (2), 350 (1972).

7. J.L. Gardon and J.W. Prane (eds), Non-Polluting Coatings and Coating Processes, Plenum Press, New York, 5 (1973).

8. S. Paul, Prog.in Organic Coatings, 5, 80 (1977).

9. H. Goldschiedt, Ind. Fin. Surf. Coatings, 27 (323), 8 (1975).

10. D.C. Blackley, High Polymer Latices, 1, 4, Palmerton Publishing Co., N.Y. (1966).

11. K. Shinoda and S. Friberg, Advances in Colloid and Interface Science, 4, 281 (1975).

12. J.H. Schulman and E.K. Rideal, Proc. Roy. Soc. (London), B 122, 29 (1937).

13. L.S.C. Wan and P.K.C. Poon, Can. J. Pharm. Sci., 6 (4), 89 (1971).

14. A.F.W. Ward, Proc. Roy Soc. (London), A 176 412 (1940).

15. A.W. Ralston and R.N. Eggenberger, J. Amer. Chem. Soc., 68, 851 (1946).

16. H.B. Klevens, J. Am. Oil Chemist Soc., 26, 454 (1948).

17. H.B. Klevens, J. Amer. Chem. Soc., 72, 3581 and 3780 (1950).

18. A.W. Adamson, J. Colloid Interface Sci., 29 261 (1969).

19. G. Gillberg,H. Lehtinen and S. Friberg, J. Colloid Interface Sci, 33, 40 (1970).

20. K. Shinoda and H. Kunieda, J. Colloid Interface Sci., 42, 381 (1973).

21. S.I. Ahmed, K. Shinoda, and S. Friberg, J. Colloid Interface Sci., 47, 32 (1974).

22. E. Ruckenstein, and J.C. Chi, J. Chem. Soc. Faraday Trans., II, 71, 1690 (1975).

23. H. Reiss, J. Colloid Interface Sci. 53, 61 (1975).

24. W. Gerbacia and H.L. Rosano, J. Colloid and Interface Sci. 44 (2), 242 (1973).

25. J.H. Schulman and E. Stenhagen, Nature, 141, 785 (1938).

26. J. Marsden and J.H. Schulman, Trans. Faraday Soc., 34, 748 (1938).

27. D.G. Dervichian, "Surface Phenomenon in Chemistry and Biology," Pergamon Press, 70 (1958).

28. E.J. Burck and R.C. Newman, J. Colloid Sci., 9, 498 (1954).

29. A. Axon, J. Pharm. Pharmacol, 8, 762 (1956).

30. A.G. Brown, W.G. Thuman and J.W. McBain, J. Colloid Sci., 8, 491 (1953).

31. E.G. Cockbain, Trans. Faraday Soc., 48, 185 (1952).

32. L.M. Prince, J. Colloid. Interface Sci., 23, 165 (1967).

33. L.M. Prince, J. Colloid Interface Sci., 29, 216 (1969).

34. L.M. Prince, J. Soc. Cosmetic Chemists, 21, 193 (1970).

35. W.C. Griffin, Emulsions, Encyclopedia of Chemical Technology, 8, 2nd ed., John Wiley & Sons, Inc., New York 131, 1965.

36. D.O. Shah and R.M. Hamlin, Science, 171, 485 (1971).

37. J.W. Falco, R.D. Walker, Jr., and D.O. Shah A.I. Ch. E., 20, 510 (1974).

38. J. Th.G. Overbeek, in "Colloid Science," 1 80, ed. by H.R. Kruyt, Elsevier, N.Y. (1952).

39. J. Ugelstad, M.S. El-Aasser and J.W. Vanderhoff, Polymer Letters, 11 503 (1973).

40. Y.N. Chou, L.M. Confer, K. Earhart, M.S. El-Aasser, J.D. Hoffman and J. Vanderhoff etc., Gov. Rep. Announce Index (U.S.) 77 (16), 150 (1977).

CHAPTER 2 CONDUCTOMETRIC TITRATION

2-1 Introduction

Conductometric titration is a rapid, simple and accurate experimental method for determining the conductance change of a conducting species that has changed physically or chemically. This technique has been widely used. It is most commonly used for acid-base titrations (1-3). Vanderhoff et al (4-6) applied this method for surface characterization of colloid systems. This method can also be used for studying the dissociation constant of acidic or basic substances (7) and the formation of metal complexes (8,9).

Conductometric titration has been extensively used as a method of following the solubilization process of various ionic surfactants as additives are added (10,11). Although there are many papers describing the effect of organic additives on the electrical conductance of surfactant solutions, little attempt has been made to relate the measurements in terms of the emulsification mechanism.

Lawrence and Pearson (12) reported large observed increases in electrical conductance as related to increasing counter ion activity of the surfactant.

Hyde et al (13) classified the additives into four general groups which have been studied from a conductance viewpoint (10-15). It is known that close to and slightly

above the critical micelle concentration (CMC), the micelles of an ionic surfactant of average chain length contain about 50 to 100 long-chain ions and about 80 to 90% of the counterions are tightly bound to the micelle (16,17). Based on available information, the most popular method of explaining the conductance change is to focus on the micelle formation. It is believed that conductance will decrease as the additive goes into the interior of the micelle and the only processes which increases the conductance is adsorption of additive into the surface layer of the micelle, in other words, this could enhance (dissociation) of the counterion.

In principle, conductometric titration can be employed in all kinds of investigations as long as the conductivity of the conducting species changes. The purpose of this study is to use the conductometric titration technique as a tool to understand the emulsification mechanism by titration of the oil phase into the single and mixed emulsifier system.

2-2 Theoretical Relationships

The resistance to the flow of non- Faradaic current is the quantity measured during a conductometric titration. The reciprocal of this quantity is the measured conductance, K, which has the units of mhos ($ohms^{-1}$). The numerical value of κ for a given solution is directly

proportional to the cross-sectional area A of the column of solution between two electrodes and inversely proportional to its length, l

$$K = \kappa A/l$$

where κ is the specific conductance (mho/cm) which, for an ideal solution, is proportional to its concentration. The ratio A/l, characteristic of the cell geometry, is termed the cell constant and, for a given cell, is best determined by conductance measured on a solution of known specific conductance. Using the platinum electrodes, potassium chloride solutions of concentration 71.1352, 7.41913 and 0.74526 g(KCl)/ g (solution) have κ= 0.11134, 0.012856 and 0.0014088 mho/cm, respectively (19).

The measured conductance is governed by the nature and concentration of the dissolved ionic species through the dependency of specific conductance on these quantities (2,3). This relation is as follows:

$$\Lambda = 1000\ \kappa/C$$

where Λ is the equivalent conductance (mho/cm^2) of the substance and C is its concentration in gram-equivalents/ liter. Λ is thus the specific conductance of a hypothetical solution containing one gram equivalent of the substance per cubic centimeter.

The relationship of conductance to concentration can be employed analytically (18). The value of measured

conductance can be used for the direct determination of the solution concentration of an ionic species. Therefore, the equation can be written as

$$K = b \sum(\lambda_i)(Z_i)(C_i)$$

where b is a collection of the various constants involved, λ represents the ionic equivalent conductance at infinite dilution of ions, C is the molar concentration, and Z is the ionic charge.

2-3 Experimental Processes

2-3-1 Materials

A. Oils used as dispersed phase

1. Benzene: manufactured by Fisher Scientific Company

2. Styrene monomer: manufactured by Dow Chemical Company purified as described in Appendix 1 (20)

B. Water used as the continuous phase

1. Deionized water was used

C. Mixed emulsifiers

1. Hexadecyltrimethylammonium bromide (HTAB), $C_{16}H_{33}N^{+}(CH_3)_3Br^{-}$ manufactured by Eastman Kodak

2. Sodium dodecyl sulfate (SDS), $C_{12}H_{25}SO_4Na$, manufactured by Fisher Scientific Co.

3. n-amyl alcohol $n\text{-}C_5H_{11}OH$, manufactured by Fisher Scientific Co.

4. Octanol $n\text{-}C_8H_{17}OH$, manufactured by Fisher Scientific Co.

5. dedocanol n-$C_{12}H_{25}OH$, manufactured by Eastman Kodak

6. cetyl alcohol $C_{16}H_{33}OH$, manufactured by Ashland Chemicals

7. cholesterol $C_{27}H_{46}O$ manufactured by Fisher Scientific Company

8. behenyl alcohol $C_{22}H_{45}OH$ manufactured by Ashland Chemicals

2-3-2 Preparation of a Mixed Emulsifier System

Mixed emulsifier systems were prepared by combining 0.15 gms of HTAB with various fatty alcohols at the desired molar ratios in 25 cc volumes of deionized water. Pre-emulsification was carried out under magnetic stirring at 63°C, which is greater then the melting point of most fatty alcohols, for 1.5 hours in 100 cc beaker which was permanently attached to glass jacket (Figure 2-1). The beaker was covered with a watch glass. Two valves of the glass jacket were connected to a water bath pump, constant temperature water being pumped through the jacket as illustrated. This process kept the beaker's contents at constant temperature.

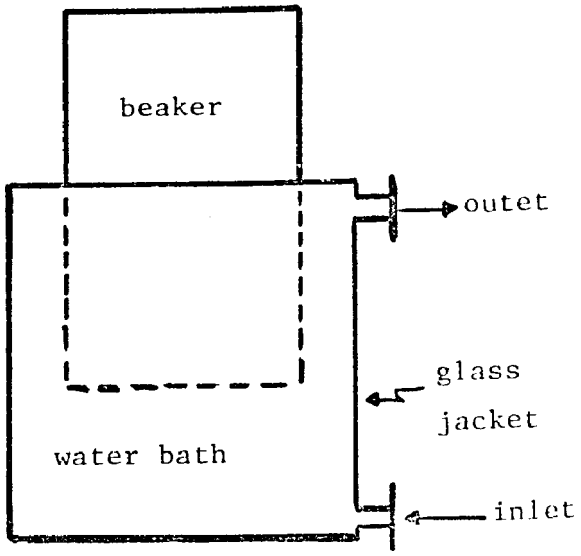

Figure 2-1 Jacketed glass container used for emulsification at constant temperature

2-3-3 Emulsification and Monitoring of Conductance Change

Electrodes were inserted into the mixed emulsifier system, and connected to the conductometric analyzer. The conductometric analyzer is capable of continuously producing an amplified voltage which is directly proportional to the conductivity of the emulsion being tested. The conductivity signal can be plotted by a recorder. A schematic of the apparatus is shown in Figure 2-2 (21).

The oil phase (benzene or styrene) was titrated into the mixed emulsifier system at a constant rate of 1 c.c./minute using an automatic constant flow rate burette and the conductance change was monitored.

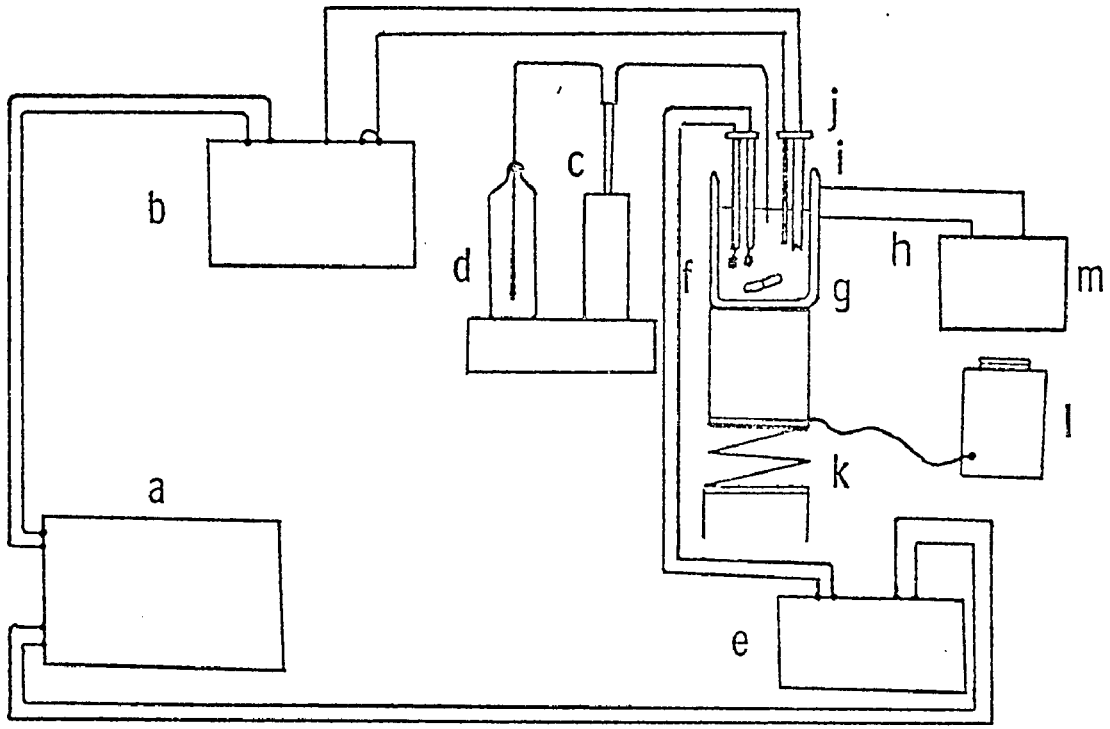

Figure 2.2. Apparatus for continuous conductometric titration. a. Two-channel recorder, b. pH meter, c. automatic constant-flow rate burette, d. titrant solution, e. conductometric analyzer, f. a pair of Pt electrodes, leaf type, g. magnetic bar, h. titration container, i. combination pH electrode, j. temperature compensator, k. jack, l. powerstat, m. constant-temperature circulator.

2-3-4 Parameters for Conductometric Titration

The experiments were varied as follows:

1. The presence and absence of fatty alcohol groups
2. The effect of varying the molar ratio of mixed emulsifier at a fixed concentration of ionic surfactant
3. The effect of varying the chain length of a fatty alcohol group at a fixed concentration and molar ratio
4. The effect of varying the rate of oil addition

2-4 Results and Discussions

Figure 2-3 shows the conductometric titration of benzene into 0.600% HTAB in the presence and absence of a fatty alcohol. Two distinctly different curves were observed. This suggests that the presence of a fatty alcohol in the surfactant system will produce oil in water emulsion by an emulsification mechanism which is different from a surfactant system devoid of fatty alcohol (22).

Titrating benzene into the single surfactant system showed an initial sharp decrease in conductivity. After a critical point (VO), the decreasing slope slowed down. Titrating benzene into the mixed emulsifier system showed an initial descending leg, followed by an ascending leg. After the critical point V2 a slowly decreasing leg was observed.

Figure 2-1 shows the effect of varying the molar

ratios of a mixed emulsifier used at a fixed concentration of ionic surfactant. The following phenomena were observed.

a. the initial conductance decreased to a certain extent with an increasing amount of cetyl alcohol

b. the extent of the descending leg decreased while the amount of cetyl alcohol in the mixed emulsifier system increased, and finally vanished

c. the slope of the descending leg decreased while the amount of cetyl alcohol in the mixed emulsifier system decreased

d. the curve with the least amount of cetyl alcohol approached the single surfactant system curve

e. the distance along the y-axis between the two critical points (V1 and V2) varied

Figure 2-5 shows the effect of varying the chain length of the fatty alcohol at a fixed concentration and fixed molar ratio. The following phenomena were observed.

a. the longer chain fatty alcohol produced a lower initial conductance

b. the ascending leg increased while the chain length of fatty alcohol increased

Figure 2-6 shows the effect of varying the rate of oil addition by comparing the titration of oil into the mixed emulsifier system at 1 cc per minute and titration of oil into the mixed emulsifier system dropwise for 5 to 10 minutes until equilibrium was reached. The titration curve was found to be time-dependent. This suggests that a diffusion-controlled process is involved in the initial descending leg.

Furthermore, the pre-emulsification is also important

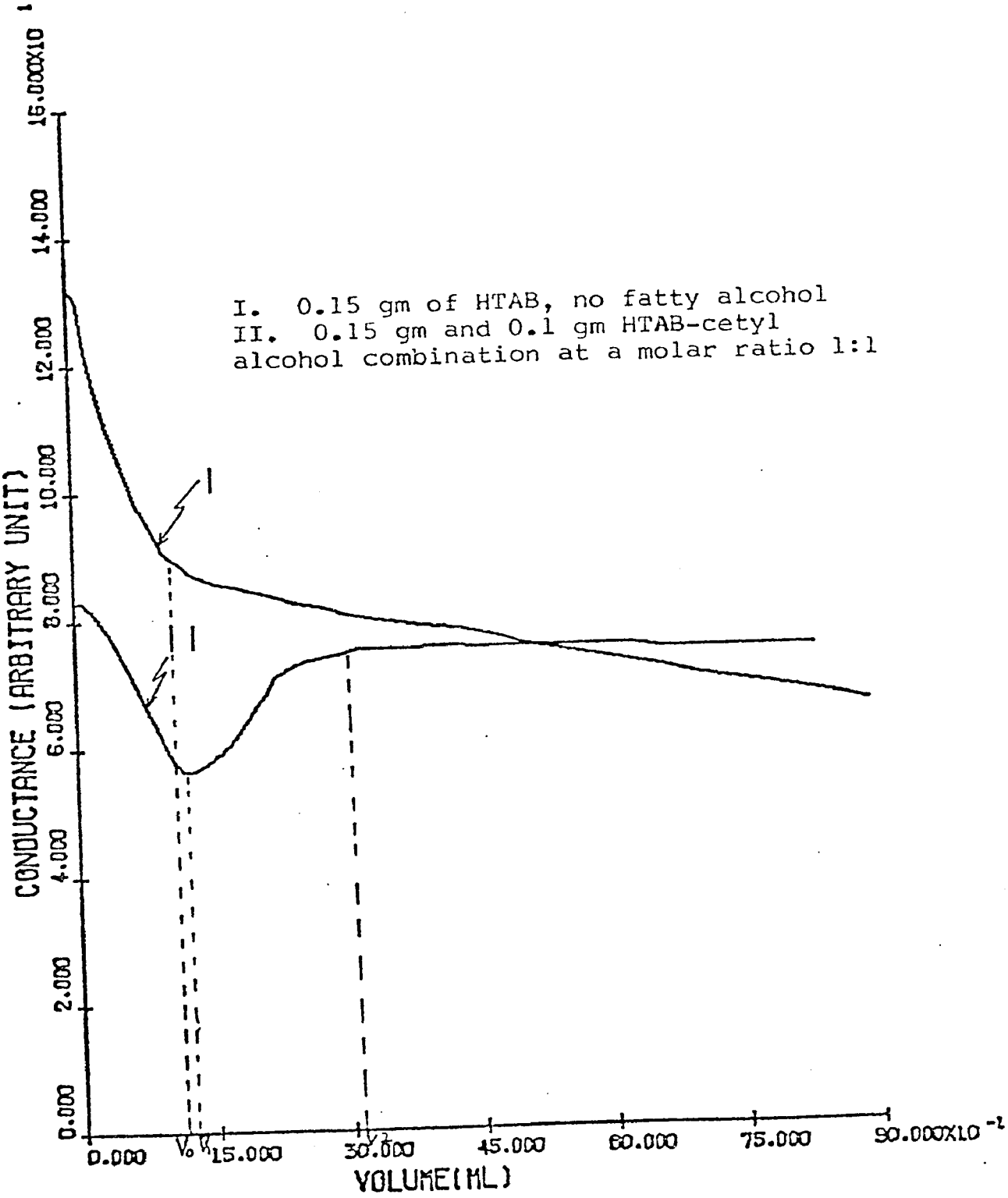

Figure 2-3 A comparison between the conductivity curves of benzene added to 25 c c of emulsifier solution in the presence and absence of fatty alcohol.

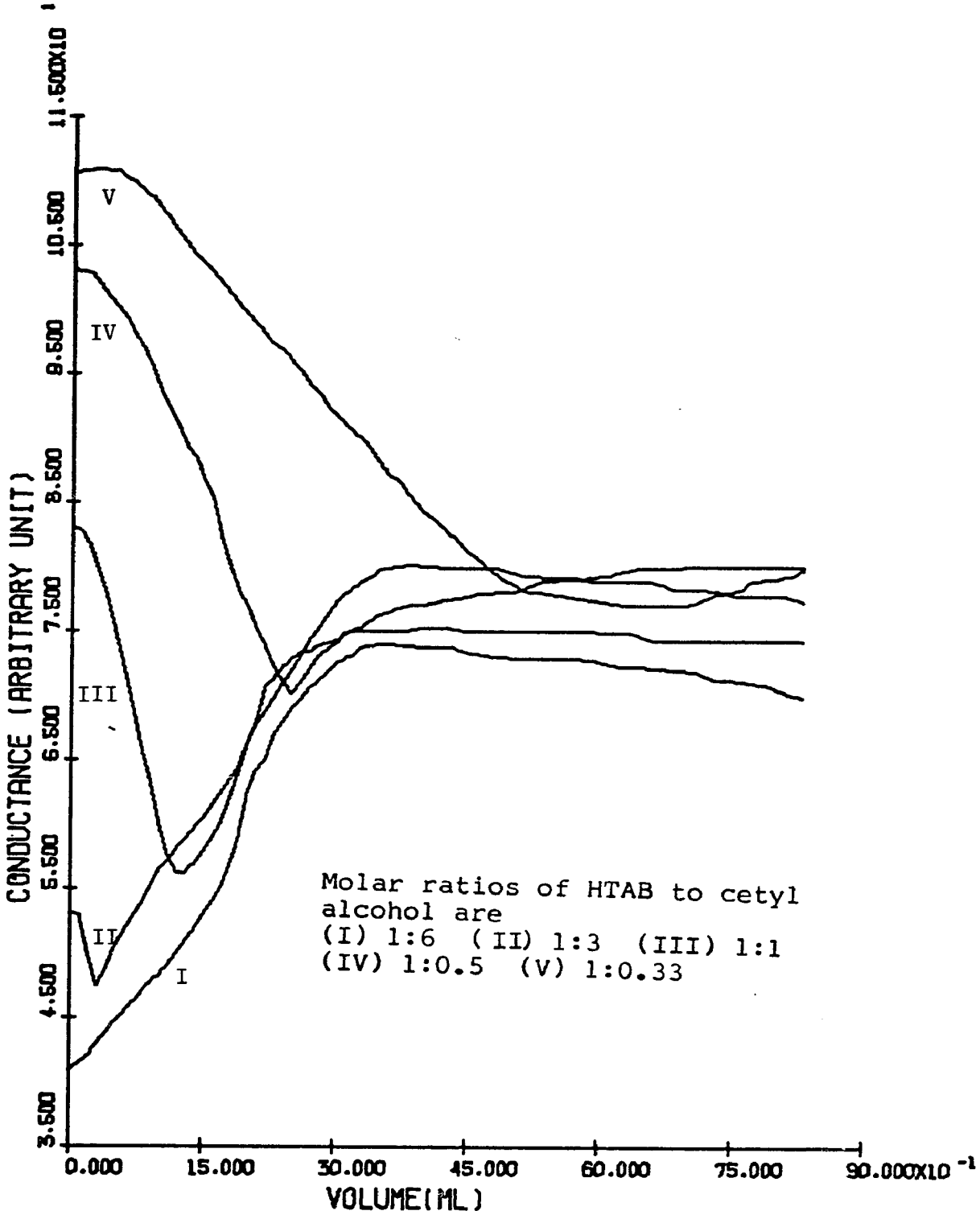

Figure 2-4 Conductometric titration curve for titrating benzene at constant rate of 1 c c /minute into 25 c c solution of 0.6% HTAB plus cetyl alcohol at various molar ratios.

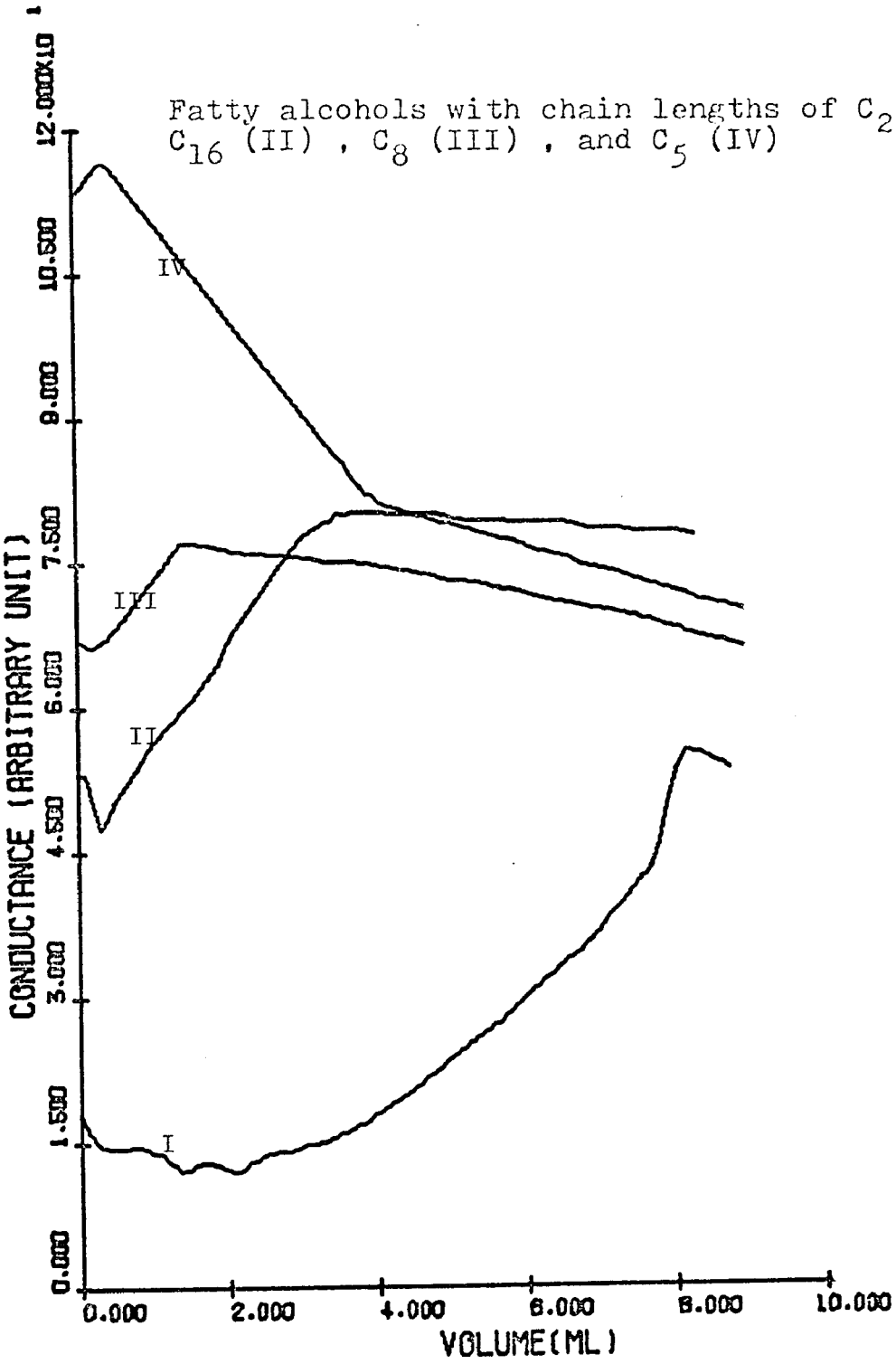

Figure 2-5 The effect of varying the chain length of the fatty alcohol on the conductivity curves of benzene added to aqueous solution of HTAB-fatty alcohol combination.

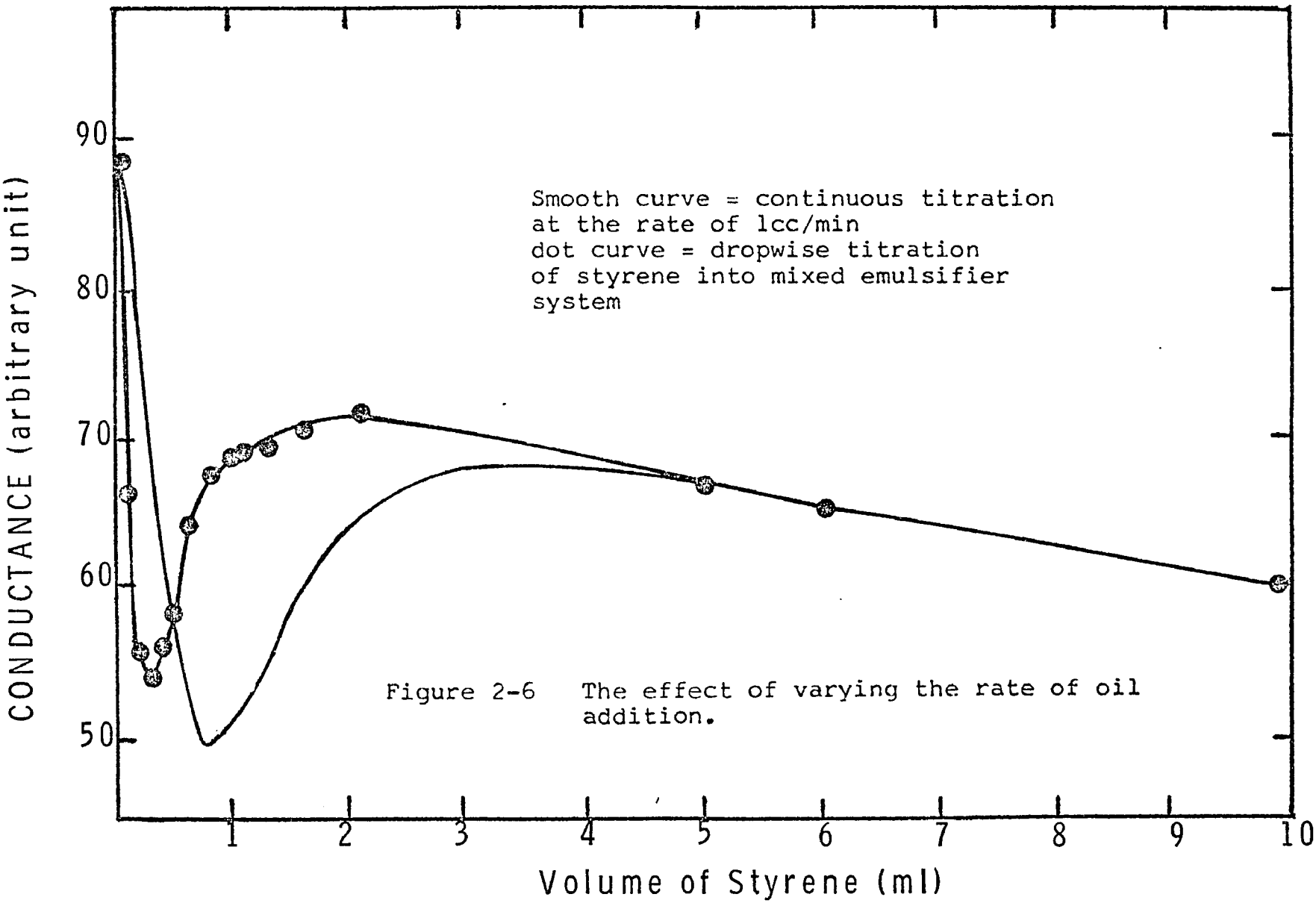

Figure 2-6 The effect of varying the rate of oil addition.

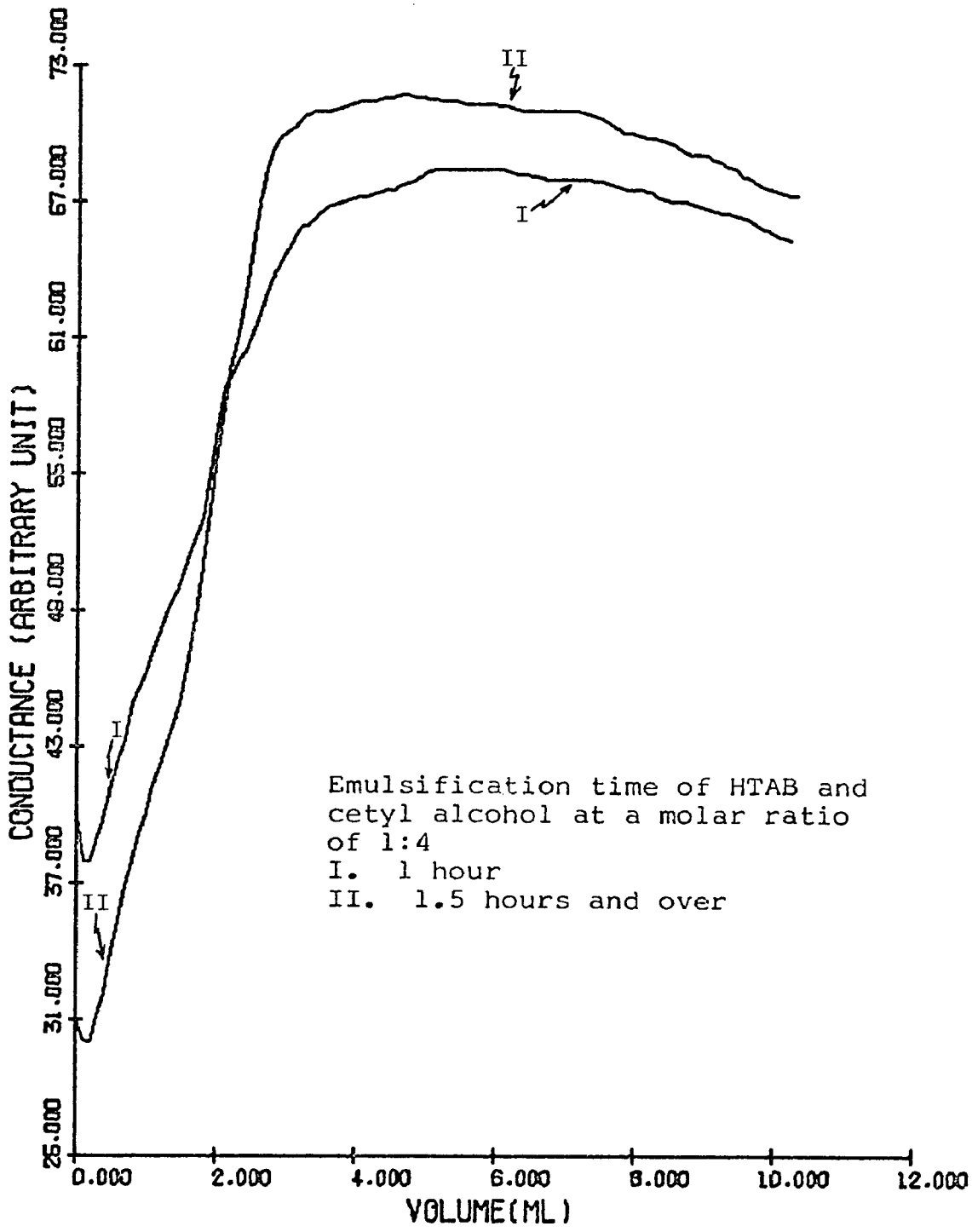

Figure 2-7 The effect of pre-emulsification time on the mixed emulsifier system.

in the preparation of a mixed emulsifier system. Figure 2-7 shows the difference in the conductometric titration of benzene into the HTAB and cetyl alcohol mixed emulsifier system at a molar ratio of 1:4. This difference is due to two different pre-emulsification times, 1 hour versus 1.5 hours. Reproducible conductometric titration curves were obtained when the pre-emulsification time exceeded 1.5 hours. When the pre-emulsification time was less than 1.5 hours higher initial conductance and lower equilibrium conductance was observed. It is believed that the pre-emulsification time is directly correlated to the formation of the mixed emulsifier system.

The conductivity data are complex functions of several parameters, and it is therefore impossible to make a complete interpretation of the above data. The various approaches used to interprete the conductivity data include droplet size distribution along the conductometric titration curve, the adsorption isotherm of the emulsifier, and the stability of the emulsions. Nevertheless, the role of mixed emulsifier in the preparation of emulsions and latexes will be the key point involved in interpreting the above data.

2-5 References

1. J.W. Loveland, "Conductometry and Oscillometry" in "Treatise on Analytical Chemistry" ed by I.M. Kolthoff and P.J. Elving, Interscience Publishers,

1 (4), 2569 (1967).

2. D.J. Gross and R.W. Murray, "Electroanalytical Method," in "Encylopedia of Chemical Technology," 2nd ed., Wiley, New York, 7, 776 (1965).

3. G.A. Schwartz, B.J. Barker, Talanta, 29 (9); 773 (1975).

4. H.J. van den Hul and J.W. Vanderhoff, J. Electroanal. Chem., 37, 161 (1972).

5. J.W. Goodwin, J. Hearn, C.C. Ho and R.H. Ottewill R.H., Brit. Polymer J., 5, 347 (1973).

6. J.W. Vanderhoff and H.J. van den Hul, J. Macromol. Sci. A7, 677 (1973).

7. A.K. Mandal and S.C. Lahiri, J. Prak. Chem. 319 (3), 377 (1977).

8. H. Yoshida, I. Hayshida and S. Hikime, Bunseki Kag, 26 (7), 461 (1977).

9. J. Schmidt, Z. Anorg. A.C., 431 (4), 284 (1977).

10. A.F.H. Ward and A.G. Chitale, Proc. 2nd Intern. Cong. on Surface Activity, vol. 1, 319 (1957).

11. K. Passinen and P. E.K. Wall, Acta. Chemica. Scand. 9, 1450 (1955).

12. A.S.C. Lawrence and J.T. Pearson, Trans. Faraday. Soc., 63, 495 (1967).

13. A.J. Hyde and D.M. Stevenson, C.R. Congr. Int. Deterg., 5th 1107 (1968).

14. A.J. Hyde, D.M. Langbridge and A.S.C. Lawrence, Faraday Soc. Discussion, 18, 239 (1954).

15. A.J. Hyde and D.M. Stevenson, Kolloid-Z, 232, 797 (1969).

16. K.J. Mysels and L.H. Princen, J. Phys. Chem., 63, 1696 (1959).

17. W. Prins and J.J. Hermans, Koninkl. Ned. Akad. Wetenschap Proc., B59, 298 (1956).

18. D.G. Davis, "Conductometric Titrations," in C.L. Wilson and D.W. Wilson, eds., "Comprehensive Analytical Chemistry," Vol II A, Elsevier Publishing Co., Amsterdam (1964).

19. D.J. Gross and R.W. Murray, Kirk-Othmer Encyclopedia of Chemical Technology, 7, 775, John Wiley & Sons. Inc., (1965).

20. E.A. Collins, J. Bares and F.W. Billmeyer, Jr., "Experiments in Polymer Science," a Wiley-Interscience Publication, 339 (1973).

21. W.C. Wu, Ph.D. dissertation, Lehigh University, 19 (1977).

22. M.S. El-Aasser, Y.N. Chou and J.W. Vanderhoff 51st Colloid and Surface Science Symposium, Grand Island, N.Y., 1 (1977).

CHAPTER 3 ADSORPTION ISOTHERM

3-1 Introduction

The soap titration method for the determination of surface area and particle size of synthetic latexes has been used extensively (1-5). The quantity of soap present in most latexes is sufficient to cover only a fraction of the available surface and, hence, the latex particles are capable of adsorbing more soap. Finally, all the available evidence points to the fact that the soap is adsorbed in a monomolecular layer by the polymer and that it exists in this form on the surface even at aqueous phase concentrations exceeding those required for micelle formation. These facts suggest the possibility of employing soap adsorption for determination of surface coverage of known-particle-size latexes.

The titration of latexes with emulsifier solution was proposed by Maron et al in 1944 (2) as a method of determining the surface area of latex particles, provided the molecular area of the emulsifier is known. The molecular area of sodium dodecyl sulfate has been reported by several workers. Cockbain (6) and Sawyer and Rehfeld (7) suggested a surface area of 50 $\mathring{A}^2$ for the SOS molecule on a polystyrene latex, while Vanderhoff and van den Hul obtained 46 $\mathring{A}^2$ (3) for the water-octane interface.

The relatively high surface tension of most latexes

such as polystyrene and styrene-butadiene copolymer indicates that practically all soap initially present is adsorbed (2). The concentration of unadsorbed soap is very low and is of insufficient quantity to yield micelles.

Adsorption isotherms are not all of the Langmuir type (9). Brunauer (8) considered that there are five principal adsorption forms. Brunauer, Emmett and Teller (10) showed how to extend the Langmuir approach to multilayer adsorption, and their equation has come to be known as the BET equation.

Using adsorption for surface area determination, as in the BET method, the usual practice is to determine the adsorption isotherm, and to find the quantity of adsorbate necessary to saturate the surface of the adsorbent with a monolayer. By determining the amount of emulsifier adsorbed by the known size monodisperse latex particles at the point of micellization, the effective surface area occupied by a molecule of emulsifier on the latex particle at the end point can be calculated.

The end point can be determined either by surface tension or conductance measurements. Both methods give identical results (2). When a given amount of a cleaned latex of known concentration and particle size is titrated conductometrically with standard soap solution, the point of intersection of the lines gives the quantity of added soap at which micellization sets in the aqueous phase.

This is the titration end point.

It was found (17) that only conductance is a reliable means of following the titration, since surface tension measurements produced a curve from which it is difficult to ascertain the end point.

Maron et al (11) reported the concentration of unsorbed soap in solution (S_f) in the titration of latex with Daxad 11 was 0.77 g/l, and the CMC of Daxad 11 is 0.80 g/l. This verifies the results for the CMC found in aqueous solution. It has been reported (12) that the adsorption method can be extended to latexes prepared by cationic emulsifiers.

The purpose of this investigation is to discover the differences in adsorption isotherms between cleaned latexes with and without cetyl alcohol on the surface.

3-2 Calculation

The total amount of soap (S_T), must be equal to the concentration adsorbed on the latex surface (Sa) and the concentration of unadsorbed soap in solution (S_f) at the end point, i.e., $S_T = S_a + S_f$

S_f, the CMC of the added soap in the given latex, should be constant. S_T, the total concentration of added soap, is constant. Consequently, S_a can be obtained.

If Vo is the initial volume of cleaned monodisperse latex taken for titration, and the solid content "a" is

known. V is the volume of added soap necessary to reach the end point. Then at the CMC the amount of added soap is VxC, where C is the concentration of soap in weight percent.

The amount of the polymer in gram (m) is (Vo)(a)(de) de is the density of latex, the number of particles is $m/(4/3\pi r^3 d)$, where r is the radius of the monodisperse latex and d is the density of the polymer.

To obtain the amount of surfactant adsorbed by the latex, a correction must be applied for unadsorbed soap (S_f). This correction may amount to an appreciable fraction of the soap added. It is generally valid to assume that the concentration of unadsorbed soap at the end point is the same as CMC in pure water (11).

From the above information the surface area covered by one surfactant molecule (A) on the latex particle should be calculated using equation 3.1

$$A=\frac{\{(Vo)(a)(de)/(4/3\pi r^3 d)\} \times 4\pi r^2}{(V-Vi)\times(c/M)\times No} = \frac{3(Vo)(a)(de)(M)}{(V-Vi)(C)(No)(r)(d)} \quad (3-1)$$

Where Vo = the volume of monodisperse latex

a = the solids content of latex (weight percent)

de = density of latex

r = the radius of monodisperse latex

d = density of polymer

V = the volume of added surfactant solution at the end point

Vi = the volume of added surfactant solution reach CMC in aqueous solution

C = concentration of surfactant solution in weight percent

No = Avogadro's number

M = the molecular weight of the surfactant

The term $[Cx(V-Vi)xNo]/M$ represents the number of surfactant molecules used to cover the surface of monodisperse latexes.

3-3 Experimental Process

3-3-1 Materials

I. Monodisperse polystyrene latex with diameter 0.45 μm, (lot number LS-1108B) manufactured by Dow Chemical Company

II. Sodium dodecyl sulfate (SDS), manufactured by Eastman Kodak Company

III. Ion exchange resins, Dowex 1-X4 and Dowex 50W-X4, manufactured by Dow Chemical Company

3-3-2 Preparation of Samples

A) The resins used in this study are the 20-50 mesh Dowex 50W-X4 solfonic acid and Dowex 1-X4 quaternary ammonium resin. They were intensively conditioned following Vanderhoff's method (12,13); the resins were converted to the H^+ and OH^- form, respectively.

B) Prepare standard SDS solution of 1.0%, 4.694% and 5.089%.

C) Remove the surfactant and ionic species from the 0.45 μm diameter polystyrene monodisperse latexes

by adding excess amount of mixed, cleaned Dowex 1-X4 and Dowex 50W-X4 resins in the flask which contains the monodisperse latex. Agitate overnight, filter the latex with glasswool and put an excess amount of mixed resins in the filtered latex. Repeat the process twice more.

The cleaned latex, now referred to as C-1108B, has a measured solids content of 11.97%.

D) Add 0.1 gram cetyl alcohol in the beaker (as Figure 2-1) containing 50 cc of C-1108B cleaned latex. Stir at 63°C for 1.5 hours. This sample is referred to as C-1108B-CA.

3-3-3 Procedure

Titrate a known concentration of SDS dropwise into a) 25 cc deionized water b) 5 cc C-1108B+ 20 cc deionized water and c) 5 cc C-1108B-CA + 20 cc deionized water at 63°C respectively. Monitor the conductance change while adding the SDS solution.

The conductance and added volume of SDS solution are obtained at every addition. There are two written programs (Appendix 2 and Appendix 3) which will analyze the every pair of added volume of sulfactant solution and the conductance and gives the following plots.

a) the added volume of SDS solution against conductance

b) the concentration of SDS solution in molarity (M) against conductance

c) the (conductance/M) against $\sqrt{M}$

3-4 Results and Discussion

Maron et al developed the soap adsorption method for the determination of synthetic latex particle size and specific surface area. This method can employ only if the latex initially contains less soap than is required to cover all the surface of the latex particles to reach this titration end point. Nevertheless, for this investigation, all the latexes employed were cleaned latexes; therefore this condition can be met. However, the data obtained in this system shows that the plot of conductance against volume of added surfactant solution gives curved lines, creating a difficulty in determining the end point. In order to obtain a sharp end point, conductance and surfactant concentration in molarity (M) as well as (conductance/M) and $\sqrt{M}$ were plotted.

Assuming sodium dodecyl sulfate is a strong electrolyte, then the equivalent conductance should equal (14).

$$\Lambda = \Lambda_o - A\sqrt{M}$$

$$\frac{1000}{M}\kappa = \Lambda = \Lambda_o - A\sqrt{M}$$

$$\frac{\kappa}{M} = \frac{\Lambda_o}{1000} - \frac{A}{1000}\sqrt{M} = \text{Constant} - A'\sqrt{M}$$

where

κ = specific conductivity (ohm^{-1} cm^{-1})

Λ = equivalent conductivity (cm^2 $equiv^{-1}$ ohm^{-1})

M= the concentration of electrolyte

Λ_o=equivalent conductivity at infinite dilution

A' (the slope of K/M vs $\sqrt{M}$ plot) is a constant for one conducting species under constant conditions. It changes at the end point, so the intersection of two straight lines will be the end point. As we know K/M is very sensitive to error, when M is small, therefore K/M values can be disregarded.

Tables 3-1 to 3-3 show the data of titrating 1% SDS solution against 25 cc deionized water (Sample A), 5 cc C-1108B+20 cc deionized water (Sample B) and 5 cc C-1108B-CA+20 cc deionized water (Sample C) respectively. The corresponding plots were shown in Figures 3-1, Figure 3-7, Figures 3-2 and 3-8 as well as Figures 3-3 and 3-9.

Table 3-4 to 3-5 show the data of titrating 4.694% SDS solution against Sample A and Sample B, respectively. The corresponding plots are shown in Figures 3-4 and 3-10, Figures 3-5 and 3-11.

Table 3-6 shows the data of titrating 5.089% SDS solution against Sample C. The corresponding plots are shown in Figures 3-6 and 3-12.

Comparing Figure 3-1 to Figure 3-3, the end point was found to be 8.57×10^{-3}M for Sample A, 9.14×10^{-3}M for Sample B, and 7.43×10^{-3}M for Sample C. In order to calculate the

Table 3-1 Data obtained by titration of 1% SDS solution into 25 c.c. deionized water

COND	VOL	M	COND/M	$\sqrt{M}$
3.1000	.1000	.000133	22439.63	.011754
9.9000	.3000	.000411	24077.68	.020277
19.0000	.6000	.000813	23378.82	.028508
30.0000	1.0000	.001334	22494.42	.036519
42.5000	1.5000	.001963	21653.28	.044303
53.5000	2.0000	.002569	20829.97	.050681
73.0000	3.0000	.003715	19648.97	.060952
89.8000	4.0000	.004783	18775.63	.069158
100.6000	5.0000	.005779	17407.22	.076021
125.0000	7.0000	.007585	16479.43	.087093
150.0000	10.0000	.009907	15140.47	.099535
168.0000	13.0000	.011863	14162.17	.108916
200.0000	18.0000	.014515	13778.63	.120479
238.4000	27.0000	.018004	13241.16	.134181
243.9000	30.0000	.018914	12890.07	.137527
245.0000	35.0000	.020227	12112.38	.142222
256.0000	44.0000	.022112	11577.55	.148700
269.2000	50.0000	.023117	11645.19	.152042

Table 3-2 Data obtained by titration of 1% SDS solution into sample B

COND	VOL	M	COND/M	$\sqrt{M}$
6.2000	.1100	.000152	40815.57	.012325
11.7000	.3000	.000411	28455.44	.020277
17.0000	.5000	.000680	25003.41	.026075
29.2000	1.0000	.001334	21894.57	.036519
36.3000	1.3000	.001714	21178.70	.041400
43.0000	1.6000	.002086	20616.28	.045670
52.0000	2.0000	.002569	20244.98	.050681
63.2000	2.5000	.003152	20048.87	.056145
72.5000	3.0000	.003715	19514.39	.060952
90.2000	4.0000	.004783	18859.26	.069158
98.8000	4.5000	.005289	18678.70	.072729
104.8000	5.0000	.005779	18133.96	.076021
117.2000	6.0000	.006711	17462.98	.081923
128.8000	8.0000	.008406	15322.16	.091685
156.2000	10.0000	.009907	15766.28	.099535
180.6000	14.1000	.012504	14442.94	.111823
198.8000	18.0000	.014515	13695.96	.120479
224.0000	26.0000	.017678	12671.41	.132957
237.3000	34.0000	.019982	11900.50	.141359
248.8000	42.0000	.021737	11446.06	.147434
254.8000	46.0000	.022466	11341.75	.149886
258.8000	50.0000	.023117	11195.30	.152042

Table 3-3 Data obtained by titration of 1% SDS solution into sample C

COND	VOL	M	COND/M	$\sqrt{M}$
6.5000	.1000	.000138	47050.83	.011754
12.8000	.3100	.000425	30138.43	.020608
20.6000	.6000	.000813	25347.56	.028508
31.1000	1.0000	.001334	23319.22	.036519
45.7000	1.6000	.002086	21910.79	.045670
54.8000	2.0000	.002569	21335.09	.050691
75.5000	3.0000	.003715	20321.88	.060952
94.5000	4.0000	.004783	19758.32	.069158
108.5000	5.0000	.005779	18774.19	.076021
120.5000	6.0000	.006711	17954.68	.081923
132.1000	7.0000	.007585	17415.46	.087093
144.5000	8.0000	.008406	17189.85	.091685
153.9000	9.0000	.009179	16766.99	.095806
160.5000	10.0000	.009907	16200.31	.099535
183.3000	14.0000	.012448	15127.50	.111569
208.5000	19.0000	.014973	13924.68	.122366
220.5000	23.0000	.016615	13270.96	.128900
242.5000	33.0000	.019729	12291.53	.140460
256.1000	43.0000	.021927	11679.66	.148078
259.7000	50.0000	.023117	11234.23	.152042

Table 3-4 Data obtained by titration of 4.694% SDS solution into 25 c.c. deionized water

COND	VOL	M	COND/M	$\sqrt{M}$
13.0000	.0800	.000519	25039.06	.022786
19.5000	.1500	.000971	20087.16	.031157
32.3000	.3000	.001930	16735.51	.043932
40.2000	.4000	.002563	15683.28	.050628
71.0000	.8000	.005047	14067.77	.071042
86.5000	1.0000	.006260	13817.41	.079122
102.5000	1.2000	.007455	13749.31	.086342
124.9000	1.6000	.009790	12757.37	.098947
140.9000	2.0000	.012057	11686.43	.109803
153.9000	2.5000	.014797	10400.84	.121642
166.5000	3.0000	.017439	9547.47	.132057
177.9000	3.5000	.019989	8900.00	.141382
187.9000	4.0000	.022450	8369.55	.149835
211.9000	5.0000	.027128	7811.23	.164705
237.9000	6.0000	.031503	7551.65	.177491
245.9000	6.5000	.033587	7321.38	.183266
252.9000	7.0000	.035605	7102.94	.188693
257.9000	7.5000	.037561	6866.11	.193807
262.5000	8.0000	.039458	6652.58	.198641
266.1000	8.5000	.041299	6443.29	.203221
269.9000	9.0000	.043085	6241.15	.207569
272.3000	10.0000	.046504	5855.35	.215649

Table 3-5 Data obtained by titration of 4.694% SDS solution into sample B

COND	VOL	M	COND/M	$\sqrt{M}$
33.0000	.3000	.001930	17098.20	.043932
48.6000	.5000	.003191	15228.02	.056493
70.8000	.8000	.005047	14028.14	.071042
83.9000	1.0000	.006260	13402.09	.079122
115.5000	1.5000	.009213	12536.43	.095985
136.1000	2.0000	.012057	11288.31	.109803
151.9000	2.5000	.014797	10265.68	.121642
163.5000	3.0000	.017439	9375.44	.132057
175.3000	3.5000	.019989	8769.92	.141382
185.7000	4.0000	.022450	8316.09	.149835
197.9000	4.5000	.024829	7970.63	.157571
209.5000	5.0000	.027128	7722.76	.164705
225.5000	6.0300	.031630	7160.94	.177848
234.5000	6.5300	.033709	6956.50	.183601
241.5000	7.0300	.035724	6760.14	.189008
247.1000	7.5300	.037677	6558.42	.194105
251.9000	8.0300	.039570	6365.88	.198923
259.9000	9.0300	.043191	6017.52	.207823
266.9000	10.0300	.046604	5726.97	.215880
270.3000	11.0300	.049828	5424.65	.223222
273.9000	12.0300	.052878	5179.85	.229952

Table 3-6 Data obtained by titration of 5.0888% SDS solution into sample C

COND	VOL	M	COND/M	$\sqrt{M}$,
7.8000	.1000	.000648	12028.33	.025465
16.3000	.2100	.001356	12022.04	.036822
31.0000	.4000	.002563	12094.07	.050628
45.0000	.6000	.003815	11796.10	.061764
70.6000	.9900	.006200	11387.09	.078740
95.8000	1.3800	.008515	11157.23	.092275
110.0000	1.7000	.010353	10614.32	.101801
119.8000	2.1000	.012613	9498.26	.112307
134.5000	2.6000	.015333	8778.45	.123826
144.2000	3.0000	.017439	8268.74	.132057
157.0000	3.6000	.020488	7663.03	.143136
169.0000	4.1000	.022933	7369.41	.151435
179.0000	4.6000	.025295	7076.59	.159043
189.0000	5.1000	.027578	6853.23	.166067
197.0000	5.6000	.029787	6613.58	.172590
205.0000	6.1000	.031925	6421.28	.178676
214.0000	6.6000	.033995	6294.98	.184378
221.0000	7.1000	.036001	6138.70	.189740
226.0000	7.6000	.037945	5955.93	.194796
233.4000	8.6000	.041660	5602.46	.204108
240.6000	9.6000	.045160	5327.67	.212510

surface average of SDS on the latex surface based on equation 3-1, the volume at end point is required. By using the calculation shown in appendix 4, the volumes at the end point were 8.2 cc, 8.948 cc and 6.815 cc, these are shown in Figures 3-1, 3-2 and 3-3 respectively.

The surface coverage for cleaned latex without cetyl alcohol on surface was calculated using appendix 5 as 48.65 $\mathring{A}^2$ for every SDS molecule, this value is very close to the reported values 50 $\mathring{A}^2$ and 46 $\mathring{A}^2$.

Schick and Fowkes (19) reported that the presence of a C_{15} highly branched alcohol in an SDS solution will lower the CMC by 20%. The CMC of SDS in the presence of alcohol at 50°C is in the range of 5.7×10^{-3} to 8.7×10^{-3}M, (15,16,18) therefore it should be reasonable by taking CMC of sodium dodecyl sulfate in the presence of cetyl alcohol at 63°C is 7.2×10^{-3}M. This concentration amounts to 6.55 cc 1% of sodium dodecyl sulfate solution titrating into 25 cc deionized water. In this case, the surface area covered by a surfactant molecule on the cleaned latex with cetyl alcohol on the surface is 137.3 $\mathring{A}^2$; this value is much larger than the surface coverage for cleaned latex without cetyl alcohol on the surface.

This information indicates cetyl alcohol can substitute for certain amount of ionic surfactanton contributing the stability to the colloid system.

It has been reported (20,21) that n-octanol solubilized

in 1% hexdecyltrimethylammonium bromide solution to the extent of 20 molecules per micelle reduces the association number from 72 to 65 soap ions per micelle. The micellar weight, however remained approximately the same, suggesting simple replacement of soap molecules by alcohol.

Figures 3-4 to 3-6 show curved plots in both conductance against added volume and concentration of surfactant at high added volume while higher concentration of SDS solution were used. Nevertheless, the end point can still be found at 0.0098M, 0.0107M and 0.00808M for Figure 3-4, 3-5 3-6, respectively. The corresponding volumes at the end points are 1.60cc, 1.76cc and 1.20cc respectively. The surface coverage for cleaned latex without cetyl alcohol on surface is 48.45$\mathring{A}^2$. This value agrees well with the previous one.

The CMC of SDS in the presence of cetyl alcohol at 63^{o}C is 7.2×10^{-3}M. This concentration amounts to 1.064cc of 5.0888% SDS solution titrated into 25 cc deionized water. Based on this information, the surface area covered by a surfactant molecule on the cleaned latex with cetyl alcohol on the surface is 134$\mathring{A}^2$; it agrees well with the value obtained previously.

Assuming the cetyl alcohol in sample C was all adsorbed on the surface of the monodisperse polystyrene latex, then the surface area occupied by each cetyl alcohol molecule is 31.6$\mathring{A}^2$. The surface density of HTAB to

cetyl alcohol is 1:4.3, which corresponds to 20$\mathring{A}^2$ for cetyl alcohol and 48$\mathring{A}^2$ for HTAB on the surface of polystyrene latex.

Figures 3-7 to 3-9 show the plots of (conductance/M) against $\sqrt{M}$ for Samples A, B and C. This data is obtained by titrating samples A, B and C with 1% SDS solution.

A clear end point is shown at 0.0099M, 0.0104M and 0.002569M in Figure 3-7, Figure 3-8 and Figure 3-9, respectively. Except for the Sample C, the concentration at end point is too low compared to previous data; Samples A and B did agree reasonably well.

Figure 3-10 to Figure 3-12 repeat the work of Figure 3-7 to Figure 3-9, but varying the higher concentration of SDS solution; the concentrations at end point are 0.0098M, 0.016M and 0.008M, respectively. These results are acceptable.

All the data indicates that the SDS molecule has a larger surface area covered by a single surfactant molecule on the cleaned latex with cetyl alcohol on it than the cleaned latex without cetyl alcohol on it.

The titration of SDS solution into the Sample C system and the adsorption isotherm seem to behave strangely (Figure 3-3, Figure 3-6, Figure 3-9 and Figure 3-12). Consider the plot of conductance against the concentration of surfactant solution. The slope changed after a certain added volume, and on the plot of (conductance/M) against $\sqrt{M}$, two intercept points were found. Presumably, the excess

alcohol adsorped by polystyrene returned to aqueous phase and formed a complex with the sodium dodecyl sulfate molecules.

Ugelstad et al (22) studied the adsorption isotherm of emulsifier adsorbed on the styrene emulsion droplets as a function of stirring time. It was found that, in all cases, the amount of octadecyl pyridinium bromide (OPB) adsorbed on the styrene droplets rapidly reached a maximum value. As the stirring continued, the OPB was gradually transported back to the aqueous phase; a gradual coalescence of the emulsion was verified by electron microscopy. Therefore, the desorption of OPB is caused by the decrease in the total surface area of the droplets.

The amount of OPB adsorbed on the monomer droplets was also found to increase while in the presence of the mixed emulsifier containing cetyl alcohol (22). However, in the emulsification process, a mixed emulsifier system will produce smaller droplets than a single surfactant system. In other words, the larger surface area will be produced by the mixed emulsifier system in the preparation of emulsions; therefore, more ionic surfactant is needed to cover the surface.

The adsorption isotherm study of titrating SDS solution into a cleaned monodisperse latex at 63^{o}C is at constant total surface area because the assumption made is that there is no coagulation. The adsorption isotherm of the emulsifier adsorbed on the styrene emulsion droplets is studied under the condition that the total surface area varied due to different method of preparation as well as different stirring time. Therefore there is no contradiction between the two systems.

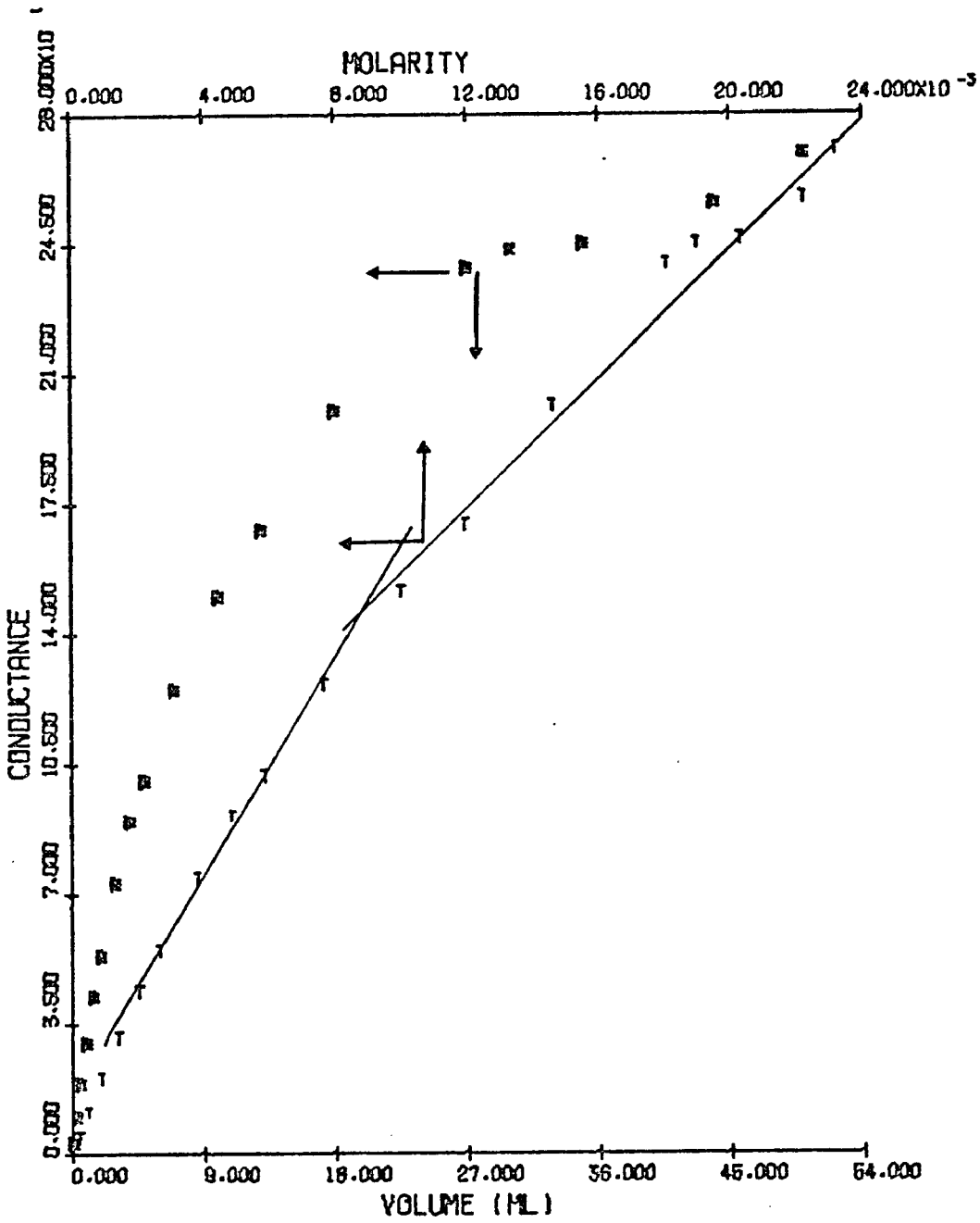

Figure 3-1 The conductance vs. the added volume in ml and the concentration in molarity of 1% sodium dodecyl sulfate solution against 25 cc deionized water

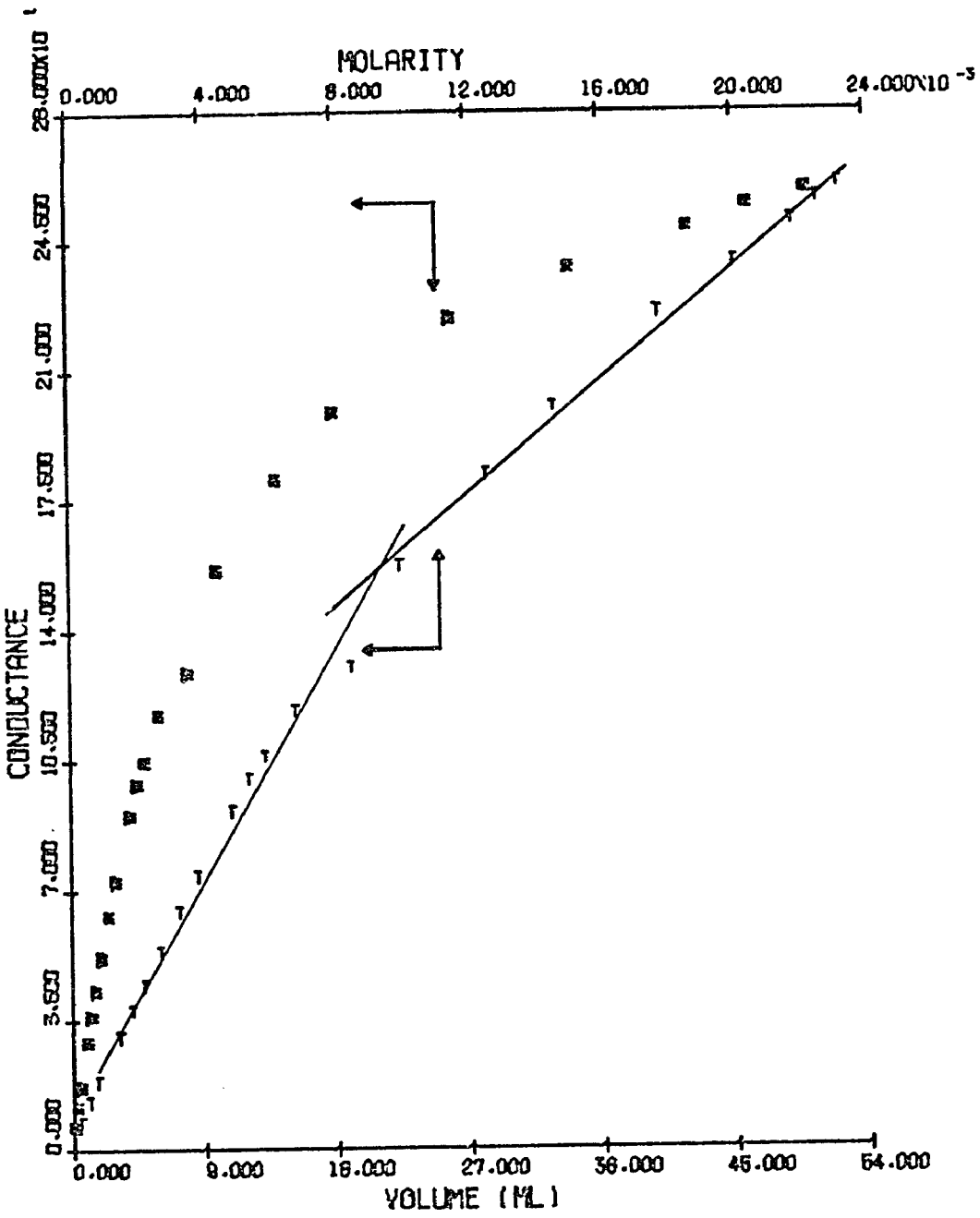

Figure 3-2 The conductance vs. the added volume in ml and the concentration in molarity of 1% sodium dodecyl sulfate solution against sample B.

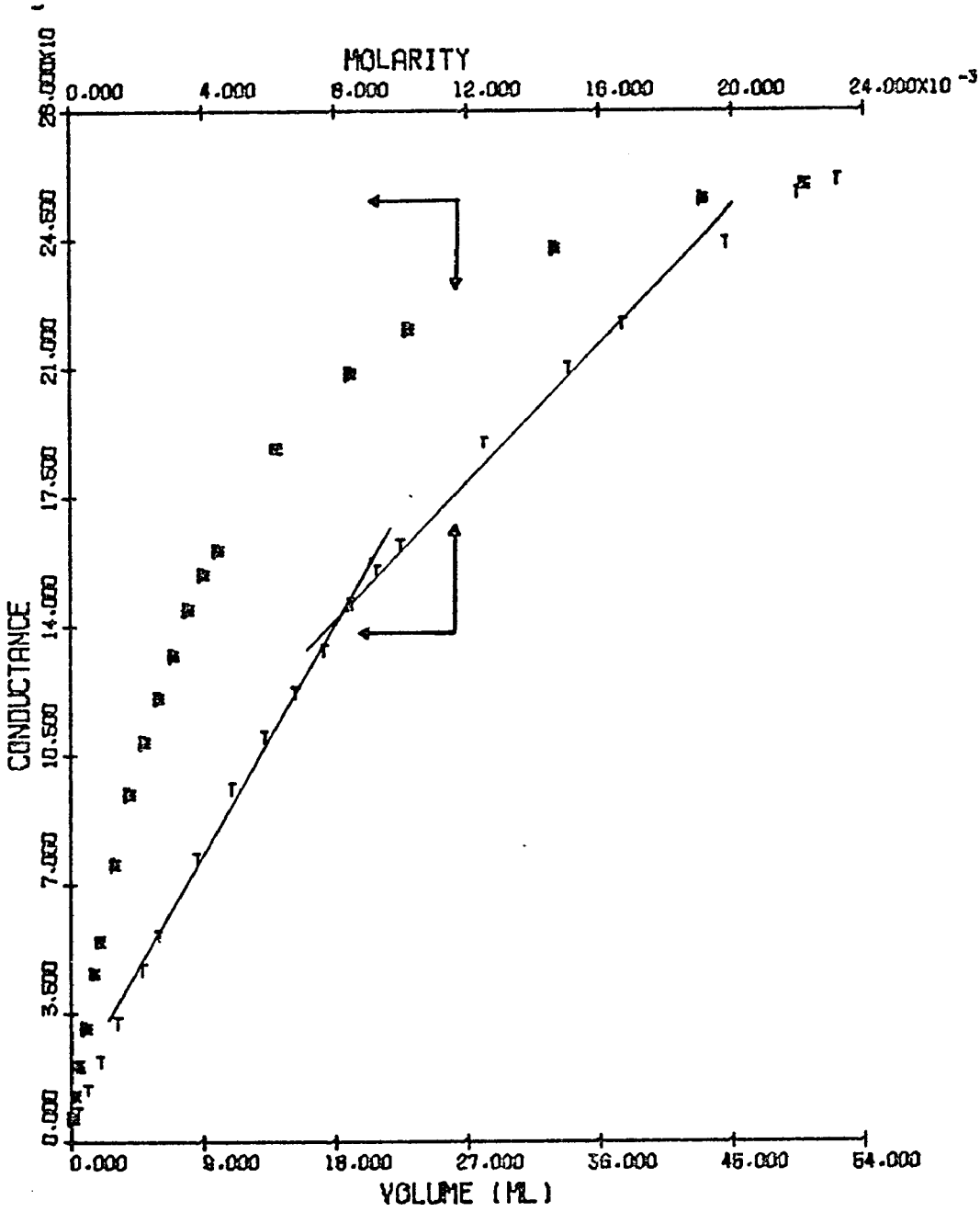

Figure 3-3 The conductance vs. the added volume in ml and the concentration in molarity of 1% sodium dodecyl sulfate solution against sample C.

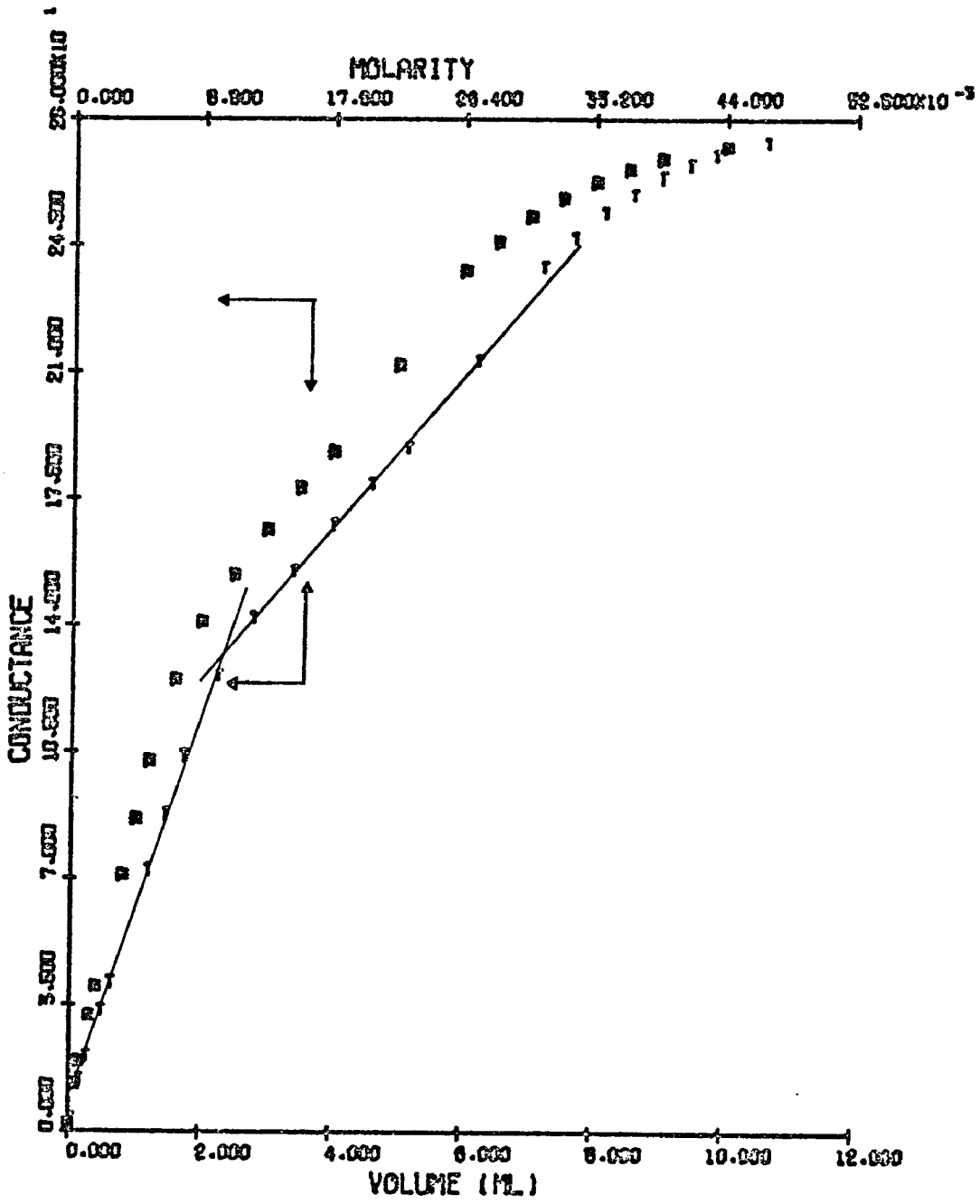

Figure 3-4 The conductance vs. the added volume in ml and the concentration in molarity of 4.69% sodium dodecyl sulfate soultion against 25 cc deionized water.

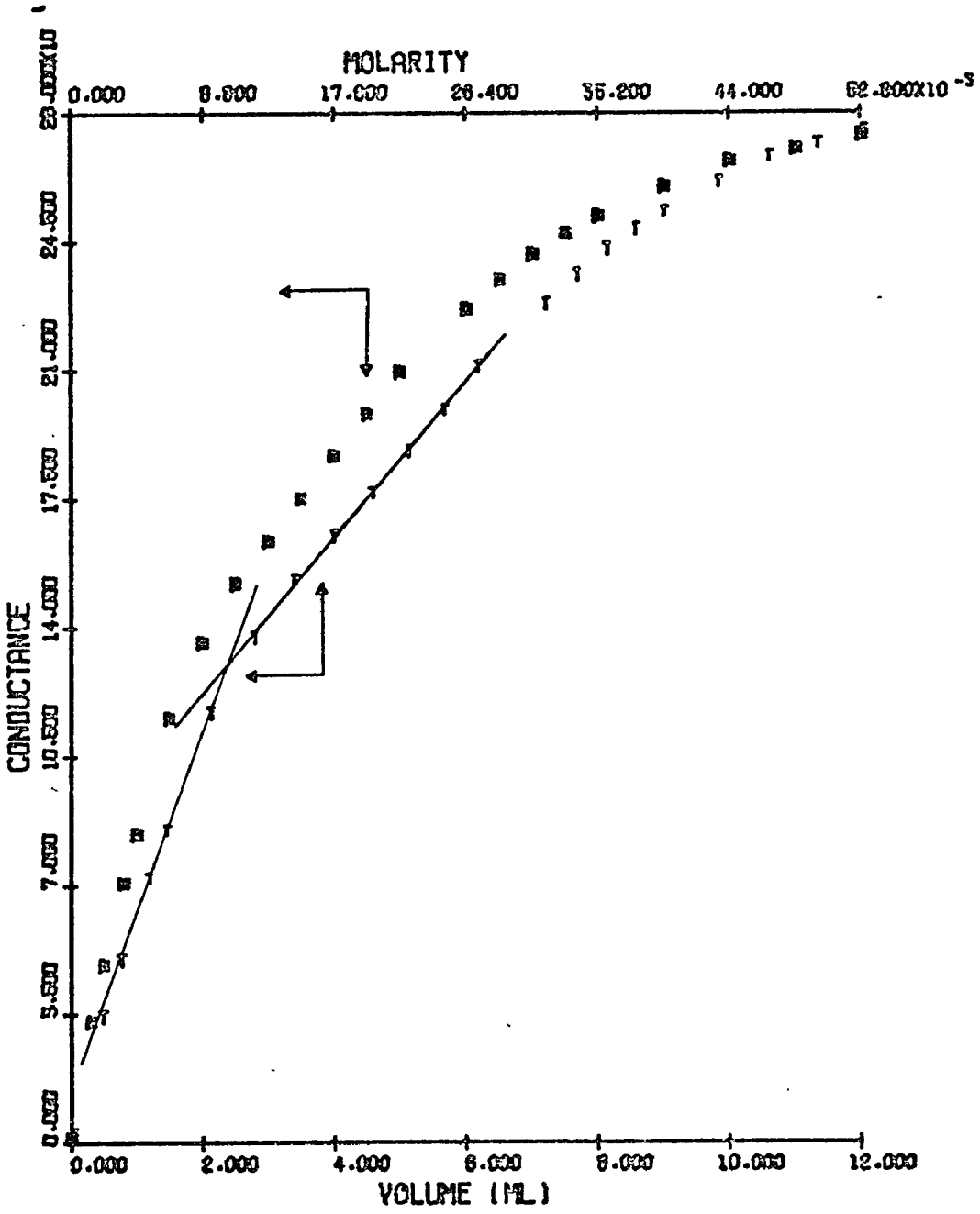

Figure 3-5 The conductance vs. the added volume in ml and the concentration in molarity of 4.694% sodium dodecyl sulfate solution against sample B.

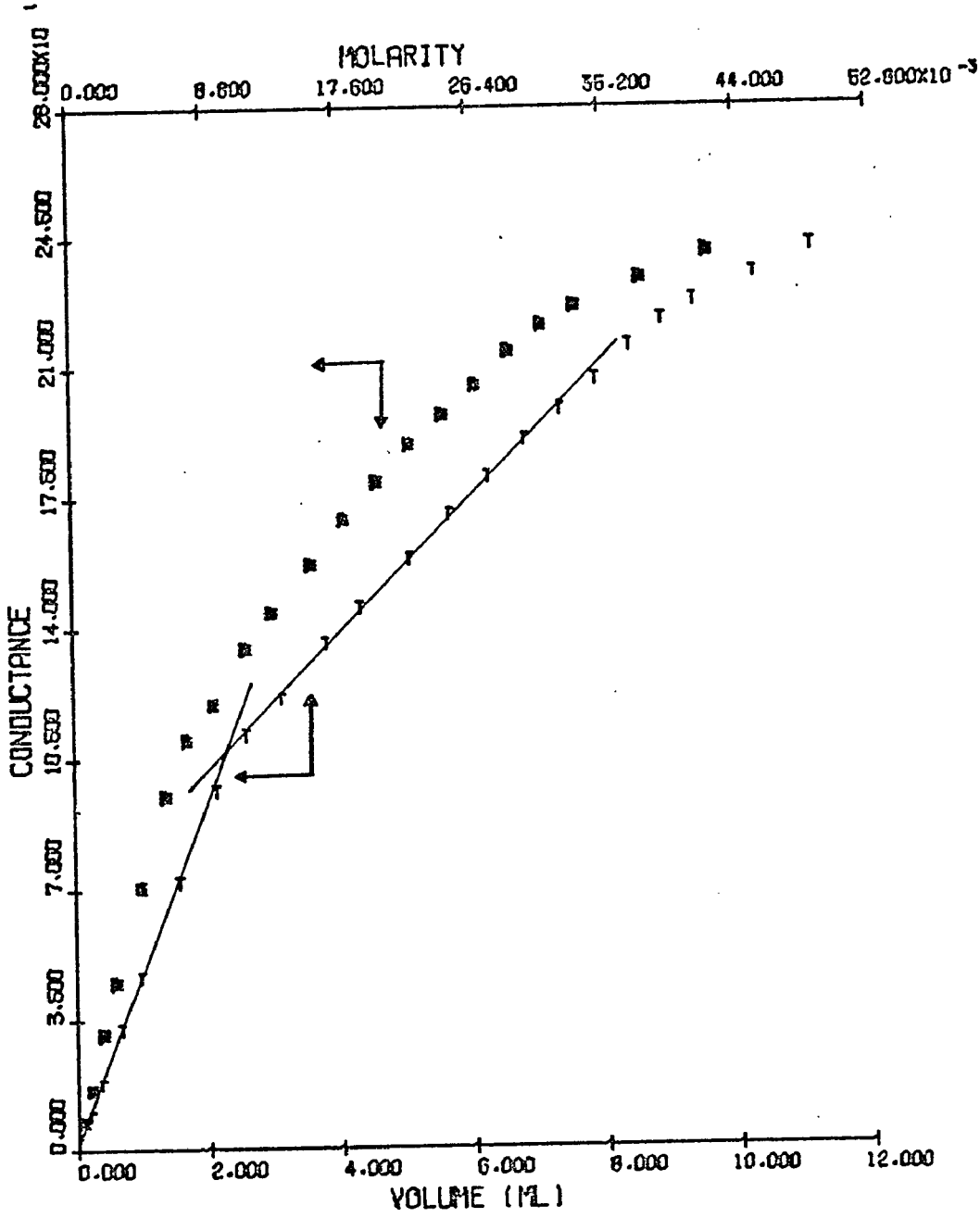

Figure 3-6 The conductance vs. the added volume in ml and the concentration in molarity of 5.0588% sodium dodecyl sulfate solution against sample C.

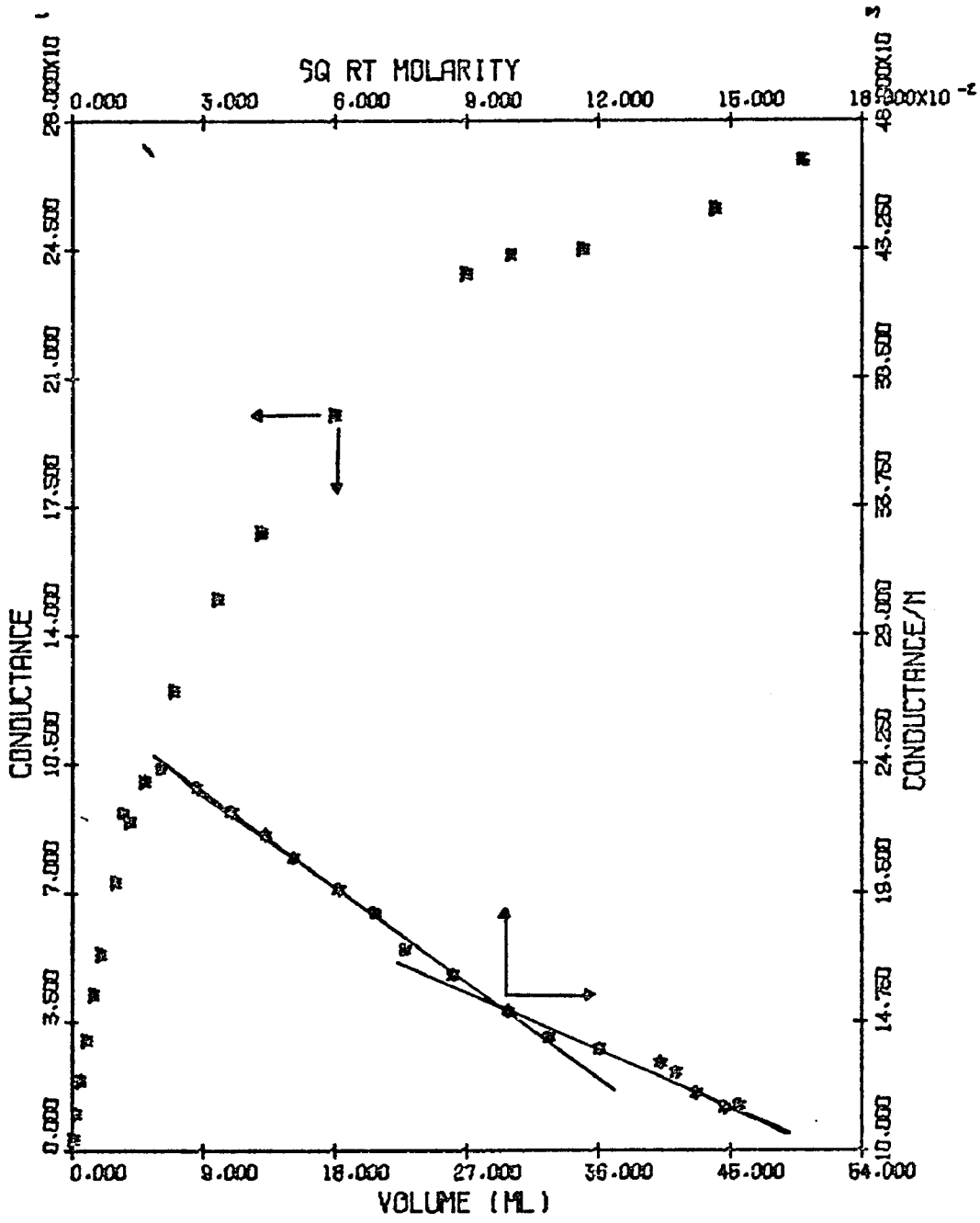

Figure 3-7 The comparison of two methods in finding the end point in terms of the concentration of the sodium dodecyl sulfate by titrating 1% sodium dodecyl fulfate solution against 25 cc deionized water.

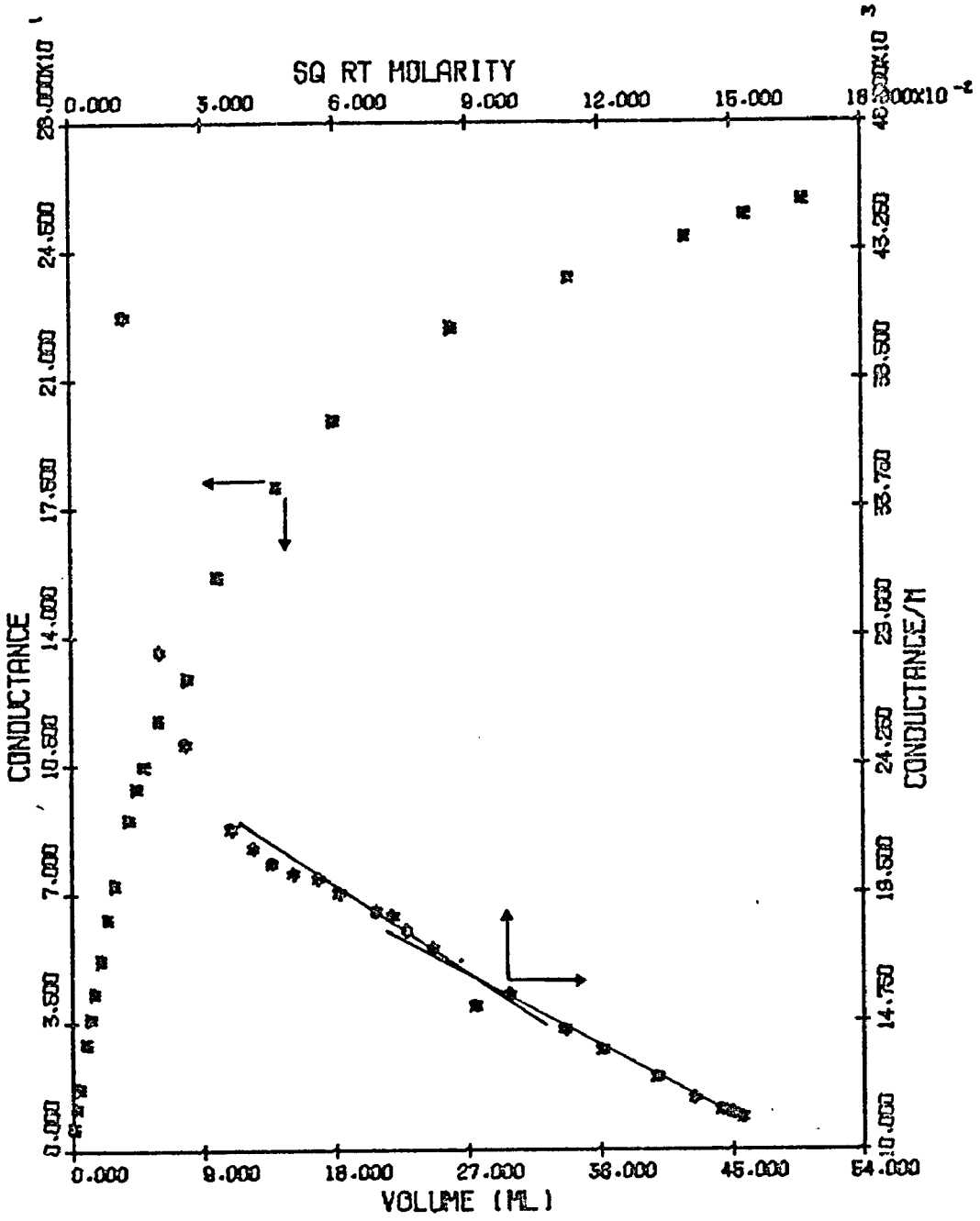

Figure 3-8 The comparison of two methods in finding the end point in terms of the concentration of the sodium dodecyl sulfate by titrating 1% sodium dodecyl sulfate solution against sample B.

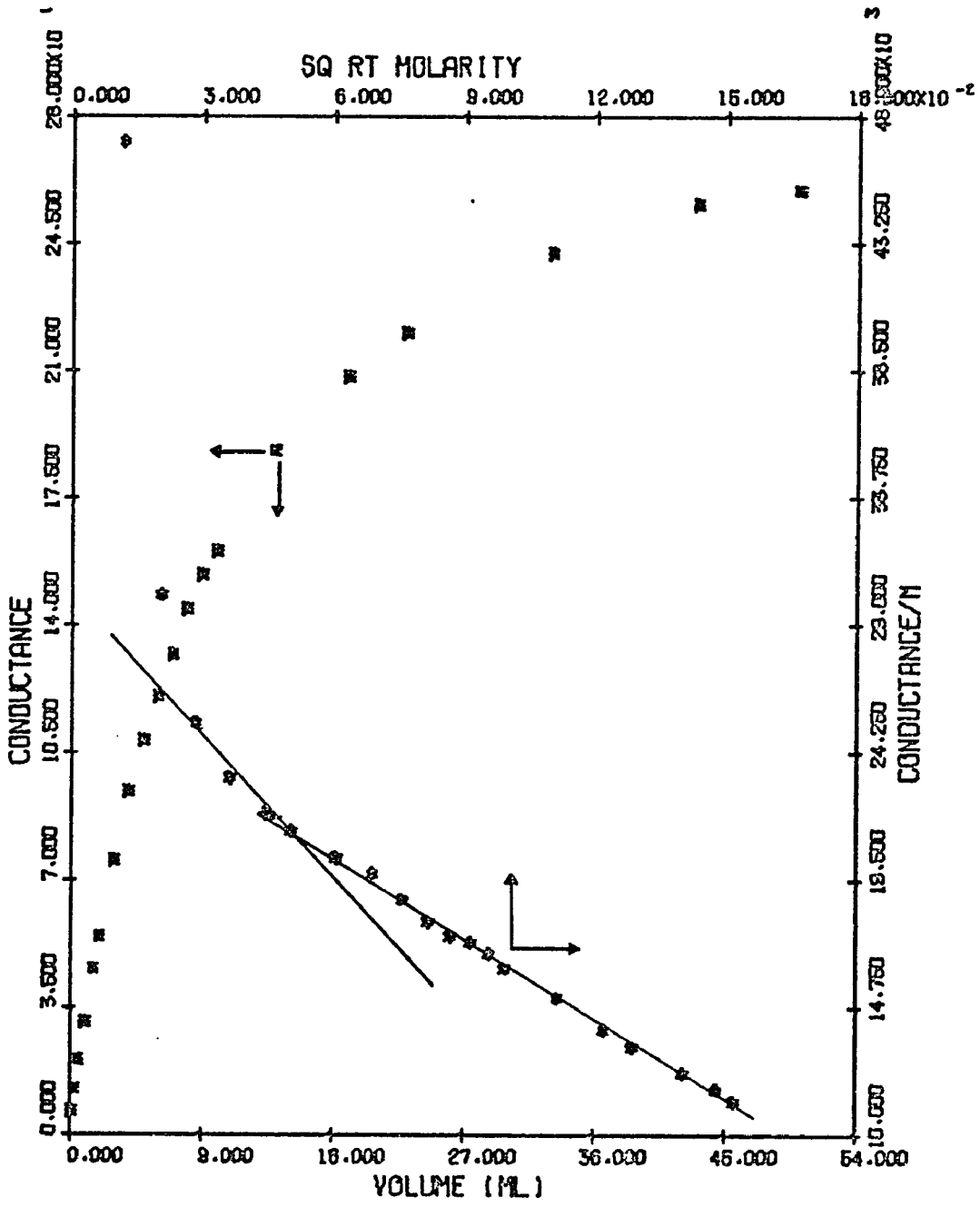

Figure 3-9 The comparison of two methods in finding the end point in terms of the concentration of the sodium dodecyl sulfate by titrating 1% sodium dodecyl sulfate solution against sample C.

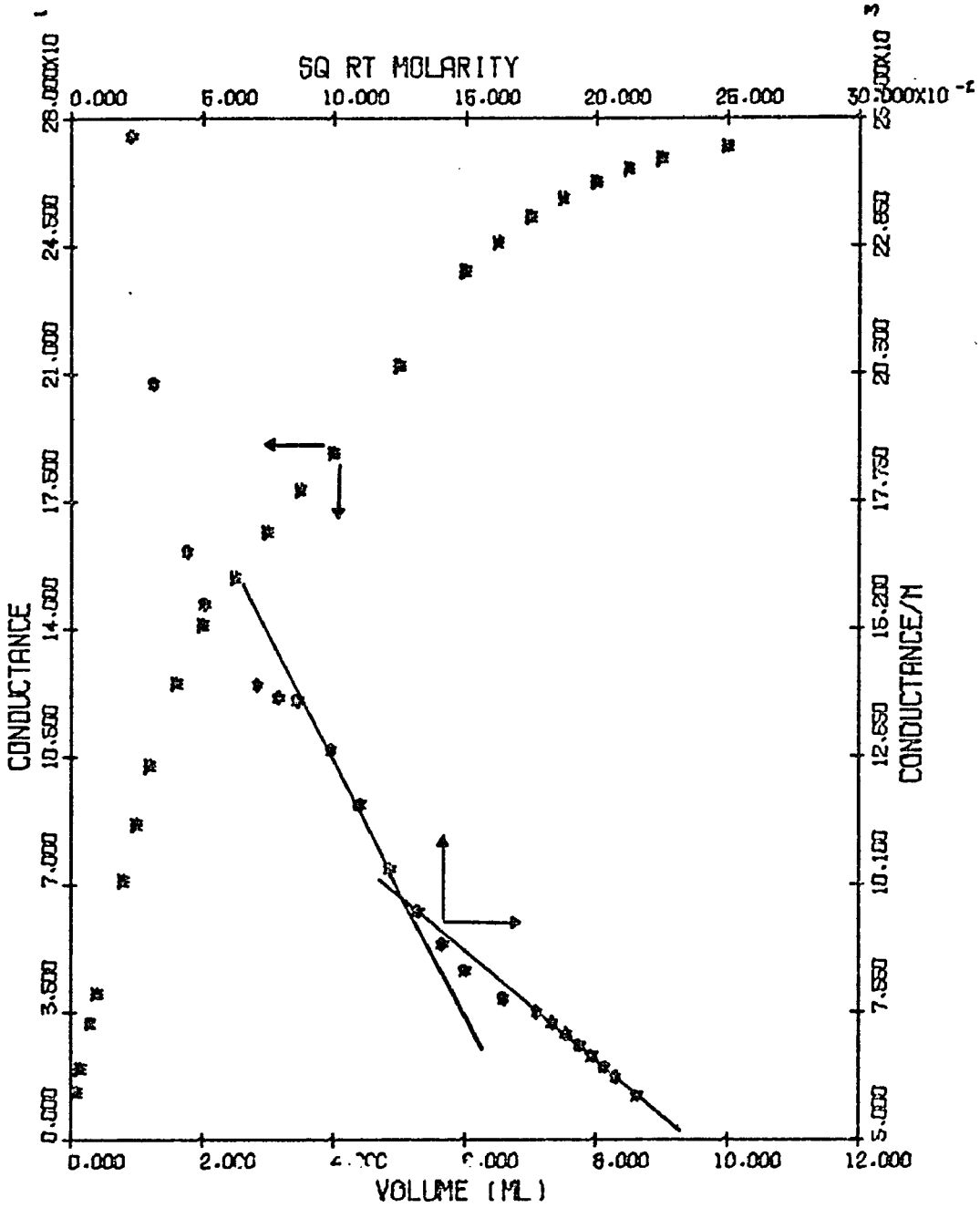

Figure 3-10 The comparison of two methods in finding the end point in terms of the concentration of the sodium dodecyl sulfate by titrating 4.694% sodium dodecyl sulfate solution against 25 cc deionized water.

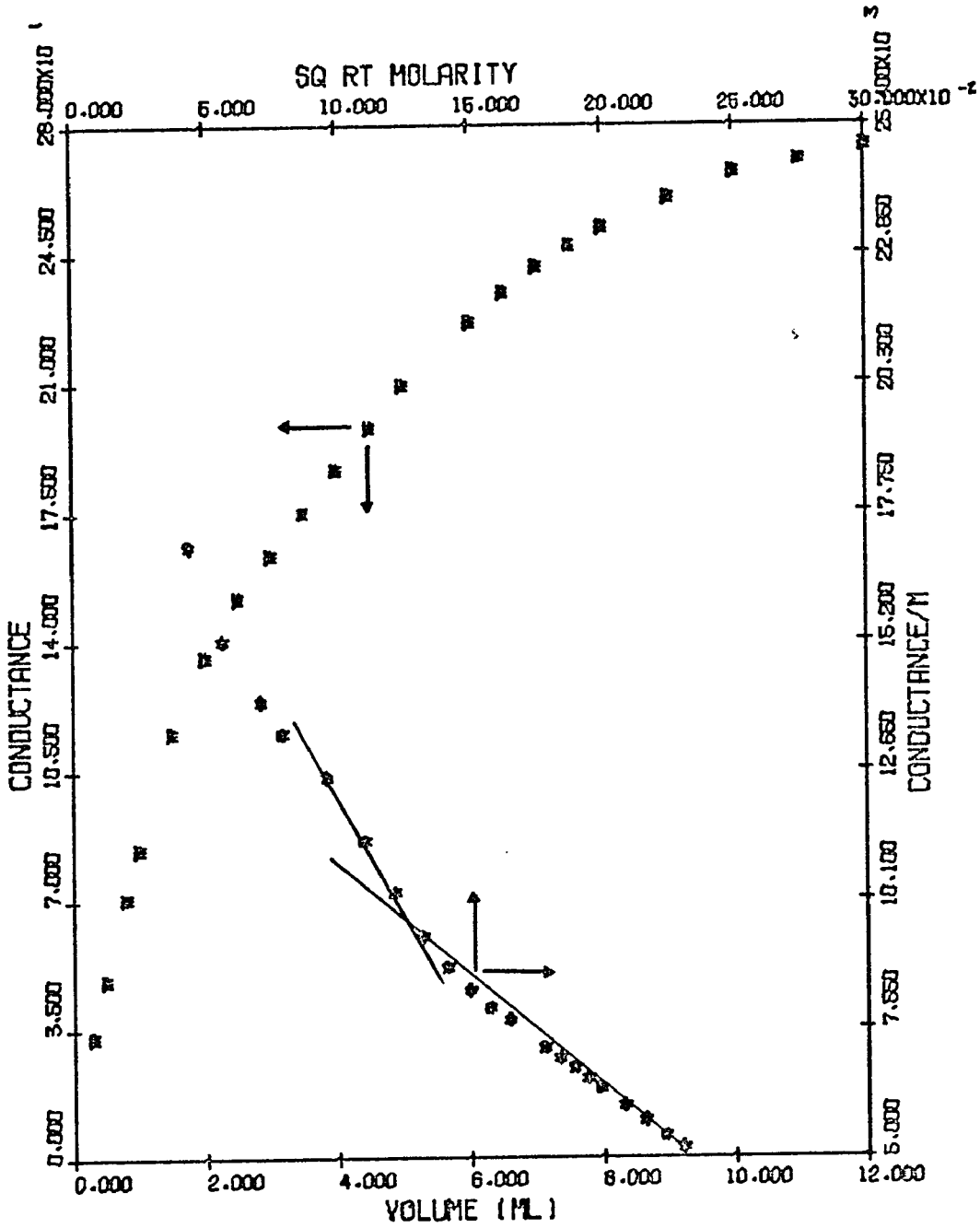

Figure 3-11 The comparison of two methods in finding the end point in terms of the concentration of the sodium dodecyl sulfate by titrating 4.694% sodium dodecyl sulfate solution against sample B.

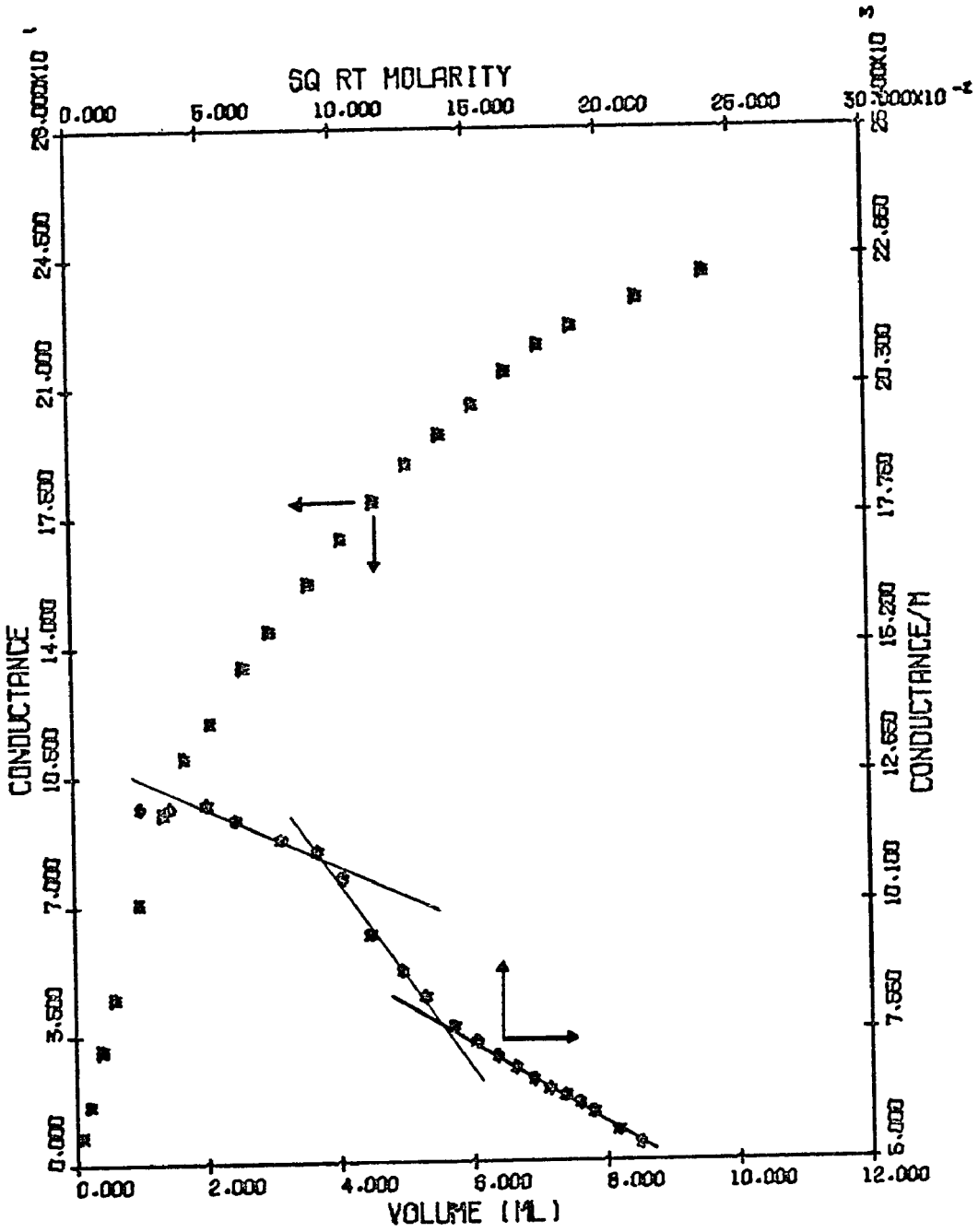

Figure 3-12 The comparison of two methods in finding the end point in terms of the concentration of the sodium dodecyl sulfate by titrating 5.0888% sodium dodecyl sulfate solution against sample C.

3-5 References

1. M. Okubo, S. Shibao and T. Matsumoto, Kohunsh Ron, 34 (8), 557 (1977).

2. S.H. Maron, M.E. Elder and I.N. Ulevich, J. Colloid Sci., 9, 89 (1954).

3. H.J. van den Hul and J.W. Vanderhoff "Clean monodisperse latexes as model colloids" from "Polymer Colloid", ed. by R. Fitch, 1 (1970).

4. E.A. Willson, J.R. Miller and E.H. Rowe, J. Phys. & Colloid Chem., 53, 357 (1949).

5. M. Morton, P.P. Salatiello and H. Landfield, J. Polymer Sci., 8, 270 (1952).

6. M. Cockbain, Trans. Faraday Soc., 50, 874 (1954).

7. W.M. Sawyer, and S.J. Rehfeld, J. Phys. Chem., 67, 1973 (1963).

8. S. Brunauer, L.S. Deming, W.E. Deming and E. Teller, J. Amer. Chem. Soc., 62, 1723 (1940).

9. I. Langmuir, J. Amer. Chem. Soc., 40, 1361 (1918).

10. S. Brunauer, P.H. Emmett and E. Teller, J. Amer. Chem. Soc., 60, 309 (1938).

11. S.H. Maron and M.E. Elder, J. Colloid Sci., 9, 351 (1954).

12. J.W. Vanderhoff, H.J. van den Hul, J. Colloid Interface Sci., 28, 336 (1968).

13. W.C. Wu, Ph.D. dissertation, Lehigh University, 150 (1977).

14. A.W. Adamson, "A Textbook of Physical Chemistry," New York, Academic Press, 489 (1973).

15. B.D. Flockhart, J. Colloid. Sci., 16, 484 (1961).

16. S.H. Herzfeld, M.L. Corrin and W.D. Harkins, J. Phys. and Colloid Chem., 54, 271 (1950).

17. S.H. Maron, M.E. Elder and C. Moore, J. Colloid Sci., 9, 104 (1954).

18. P. Mukerjee & K.J. Mysels, Critical Micelle Concentration of Aqueous Surfactant Systems, NSRDS-NB536, 51, (1971).

19. M.J. Schick and F.M. Fowkes, J. Phy. Chem. 61, 1063 (1957).

20. D.J.M. Robb, Ph.D. dissertation, University of Glasgow, 1964.

21. A.S.C. Lawrence and J.T. Pearson, Trans. Paraday Soc., 63, 499 (1967).

22. A.R.M. Azad, J. Ugelstad, R.M. Fitch and F.K. Hansen "Emulsification and Emulsion Polymerization of Styrene using Mixtures of Cationic surfactant and long chain fatty alcohol or Alkanes as Emulsifiers" from "Emulsion Polymerization," ed. by J. Piirma and J.L. Gardon, 1 (1976).

CHAPTER 4 ELECTRON MICROSCOPY

4-1 Introduction

4-1-1 Transmission Electron Microscopy: The transmission electron microscope reveals details of particles too small to be discerned with an optical microscope, which years ago could only be imagined. Electrons are of short wavelength and the resolution limit of the most powerful transmission electron microscope (TEM) is 0.5 nm. Therefore, the useful range for particle size studies lies with particles having diameters between 0.5 nm and 1×10^5 nm (the size which would block out the viewing area of the microscope) (1). The particle sizes of emulsions and latexes used for this study are within this range; therefore, TEM is employed for particle size measurement.

An electron microscope produces images by processes which are basically the same as those of the light microscope. An electron beam is employed instead of light, and electric or magnetic fields take the place of glass lenses. The final image, instead of being viewed directly, is observed on a screen coated with a phosphor which emits light under electron impact. A permanent record may be obtained by photographing the screen, or a photographic plate may be exposed directly to the electron beam.

The TEM technique was employed to compare the styrene monomer droplet size prepared in the presence of the mixed emulsifier systems that were studied in conductometric titration experiments. Styrene monomer droplets cannot be properly observed by TEM, because the styrene will evaporate while drying on the grid. Therefore, it was necessary to develop a staining method for hardening the styrene monomer prior to investigation by TEM (2).

4-1-2 Electron Diffraction

The electron microscope offers a number of high-resolution diffraction facilities which greatly increase the information that can be obtained from crystalline electron microscope specimens.

The diffraction effects which arise when a monochromatic beam of electrons of wavelength λ impinges on the surface of a crystal or passes through a crystal can be ascribed to the regular path difference between the wavelets elastically scattered by every atom.

To account for the diffraction of electrons by crystals, the electrons must be treated as waves. Thus, the initial problem is to consider the wavelike character of electrons and the scattering which is produced when they pass through a crystal.

When a crystal is bombarded with a beam of electrons, it is found that one or more strong and well-defined beams

of electrons are emitted from the bombarded area of the sample. Such a beam is analogous to the diffracted light rays from the grating or x-ray diffraction of crystals.

A particular advantage of diffraction in the electron microscope is that the area of the specimen contributing to the diffraction pattern can be selected and limited in size. Thus the identification or orientation determination of a small localized feature can be attempted.

To ensure that the diffraction pattern arises only from material within the aperture area, the correct operating procedure must be followed, as discussed by Agar (3) and Philips (4), with a scattering specimen in place, and the objective aperture withdrawn.

4-2 Theory and Background

The introduction of integers associated with the permissible state of electronic motion occurs quite naturally once the electron is given wave properties. The situation is analogous to the occurrence of stationary waves on a vibrating string. The necessary condition for a stable orbit of radius r_e is (5)

$$2\pi r_e = n\lambda \qquad (4\text{-}1)$$

In the case of a photon, there are two fundamental equations to be obeyed:

$$\mathcal{E} = h\nu \quad \text{and} \quad \mathcal{E} = mc^2$$

where

$\mathcal{E}$ = the quantum of energy

h = Planck's constant = 6.6263×10^{-34} Joule·sec

ν = frequency of the oscillator

m = mass of the particle

c = velocity of the light

When these are combined, we obtain $h\nu = mc^2$ or $\lambda = c/\nu = h/mc = h/p$,

where p is the momentum of the photon. De Broglie considered that a similar equation governed the wavelength of the electron wave. Thus

$$\lambda = \frac{h}{mv} = \frac{h}{p} \qquad (4\text{-}2)$$

If we eliminate λ between equations (4-1) and (4-2), we obtain $mv\, r_e = nh/2\pi$, which is simply the original Bohr condition for a stable orbit. Thus, the idea that electrons have wavelike properties suffices to give the rather mysterious Bohr condition directly.

The de Broglie equation (4-2) is a fundamental relation between the momentum of the electron considered as a particle and the wavelength of the electron considered as a wave.

The wavelength of the electron wave can be calculated by considering an electron that has been accelerated through a potential difference $\Delta\emptyset$. Then $\Delta\emptyset = 1/2\ mV^2$, and

the velocity of the electron (v) can be obtained if is known, where $\lambda = \frac{h}{mv} = \frac{h}{p}$

In the case where the speed of the electron is close to the speed of light, Einstein's relativity theory should be considered, where the momentum of the electron is given as:

$$P = \left\{ 2M_e \Delta\phi \left[1+(\Delta\phi/2)M_e c^2\right] \right\}^{\frac{1}{2}}$$

and M_e is the mass of the electron.

For example, $\Delta\phi$ = 100 kV = 10^5 V

$$\lambda = \frac{6.62\times10^{-34}}{\left\{2\times9.1\times10^{-31}\times10^{2}\times10^{3}\left[1+(10^5/2)\times9.1\times10^{-31}\times(3\times10^{8})\right]\right\}^{1/2}}$$

$$= 3.7\times10^{-12}\text{m} = 0.0037\times10^{-9}\text{m} = 0.0037 \text{ nm}$$

Table 4-1 lists the theoretical wavelengths associated with various particles.

Table 4-1 Wavelength of electron at various potential difference

Particle	Mass (kg)	Speed ($m.S^{-1}$)	Wavelength (nm)
1-V electron	9.1×10^{-31}	5.9×10^{5}	1.2
100-V electron	9.1×10^{-31}	5.9×10^{6}	0.12
10,000-V electron	9.1×10^{-31}	5.9×10^{7}	0.012
100,000-V electron	9.1×10^{31}	2.0×10^{8}	0.0037

Resolution is dependent upon the wavelength of illumination and the objective numberical aperture (NA). This is defined by NA = $\mu \sin\frac{\theta}{2}$ where μ is the refractive

index of the media in front of the lens and θ is the angle of acceptance of the oscillator. The most universally accepted expression for resolution is Rayleigh criterion.

$$R = \frac{1.22}{2\ NA}$$

where NA = numerical aperture

λ = wavelength of the oscillator

In air, the greatest NA available is 1.00 since

$\mu_{air} = 1.00$

The wavelength of light is in the range 350-750 nm, so the best resolution of an optical microscope is about 200 nm. The wavelength of the electron is dependent on the potential difference through which an electron that has been accelerated. Table 4-1 shows electron wavelengths at various potential differences. The best resolution of electron microscope at 100 KV is 0.0019 nm.

If electrons have wave properties, a 10^{-2} nm (5) electron wave should be diffracted by a crystal structure in much the same way as x-ray waves. Electron beams, owing to their negative charge, have one advantage over x-rays as a means of investigating the fine structure of matter in that the appropriate arrangements of electric and magnetic fields can be designed to act as lenses for electrons.

4-3 Preparation of Samples for Particle Size Measurement

The emulsion was prepared by titrating a quantity of styrene monomer into the mixed emulsifier system; with every addition of styrene monomer, a few drops of emulsion was placed on a Pyrex test plate; this emulsion was stained by slow dropwise addition of saturated solution of OsO_4 at a molar ratio 1:1.5. An immediate brown-blackening of the emulsion took place when an adequate amount of OsO_4 solution was added to the emulsion. Using a disposable pipet, the stained emulsion was removed and diluted with deionized water to translucence (10^{-3}-10^{-5} g/cc). One drop of this diluted solution was placed on a carbon and Formvar coated grid and allowed to dry. Because of the low penetrating power of electrons in the 50-100 KV range, it is necessary to mount objects for examination in the electron microscope on very thin films. These films must be made from materials with a high transparency to electrons and should not be more than about 200Å thick, consequently they are self-supporting with normal handling over only very small areas (about $0.1mm^2$) (6). The dried grids were shadowed with a 80/20 Pt/Pd alloy, to enhance the contrast and examined by transmission electron microscopy to ascertain that the particles were spherical.

4-4 Preparation of Osmium Tetroxide Saturated Solution

Osmium tetroxide vapors are poisonous, highly irritating, and damaging to the eyes, respiratory tract, and skin. Its solubility in water is 7.24 g/100 g at 25°C. All the preparation work was done in a hood in order to avoid the hazardous osmium tetroxide vapors. A specially designed apparatus which is a completely closed system for making osmium tetroxide solution is shown on Figure 4-1.

Part A is a top with a valve to adjust the pressure in order to titrate the osmium tetroxide solution easily. Part B is a container with a pyrex porous filter and a buret connection.

10 cc deionized water was placed in the container B. The top of a 0.5 g osmium tetroxide ampule was broken off. The osmium tetroxide and the broken ampule with the OsO_4 were quickly placed in container B, which was then capped with Top A. The whole apparatus was gently shaken until all the osmium tetroxide was dissolved and then it was clamped vertically on a stand which was in a hood.

4-5 Chemistry of Osmium Tetroxide

Osmium tetroxide has a molecular weight of 254.2, melts at 41°C and boils at 131°C. It exists as faintly yellow monoclinic crystals having an acid chlorine-like odor.

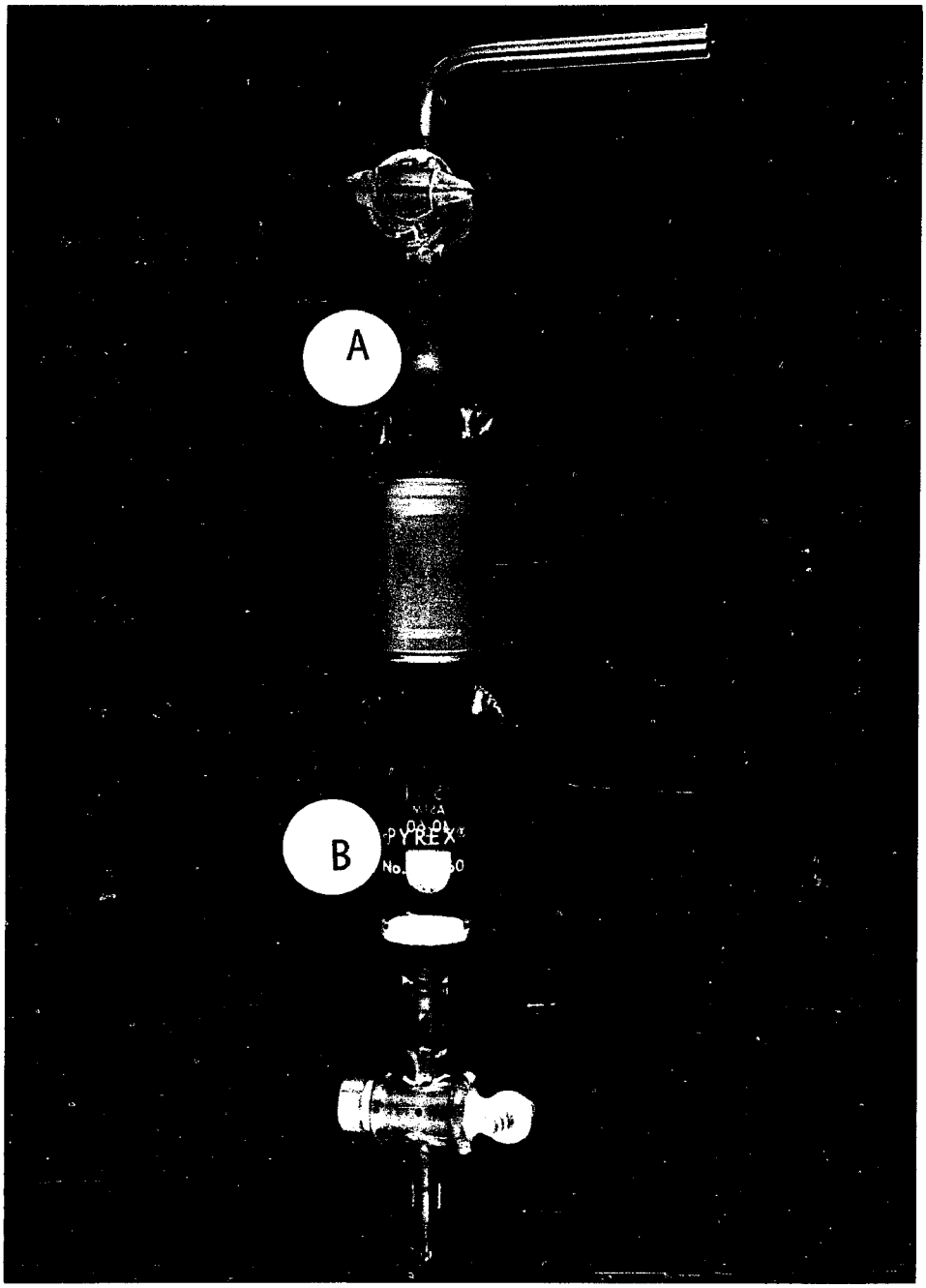

Figure 4-1 A specially designed apparatus for diluting osmium tetroxide solution. (A) Top , (B) Container with a porous filter and Teflon stopcock

Osmium tetroxide acts not only as a fixative, but also as an electron stain, which is its major advantage over most known fixatives. Osmium tetroxide is recognized to be the most versatile fixative known for preserving the cytoplastic details and is the most widely used fixative for electron microscopy of biological materials (7,8) as well as synthetic rubber latexes, such as polybutadiene, where the soft polymer particles show a tendency to flatten and merge upon drying on the support film, without first being stained.

Kato (10) has found that osmium tetroxide, when applied in vapor form, produces excellent fixing and staining of polybutadiene and other unsaturated polymer particles. This results in good electron micrographs for the measurement of particle size and distribution without requiring any additional treatment.

The oxidation of a double bond by osmium tetroxide, according to Criegee, would lead to the formation of a cyclic osmic acid monoester which, upon hydrolysis yields a diol and osmic acid. The scheme describing this reaction is shown below:

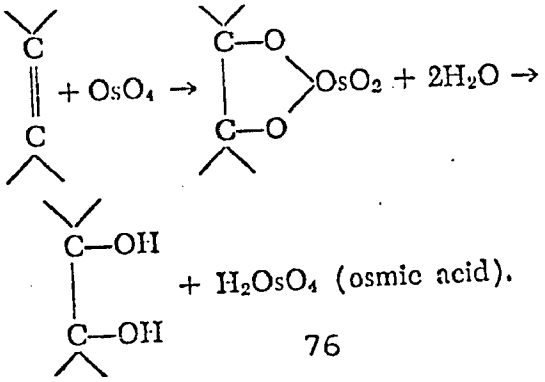

The monoester osmic acid is not very stable and is easily hydrolyzed, but it can react with diol, thus giving rise to a very stable diester as shown below:

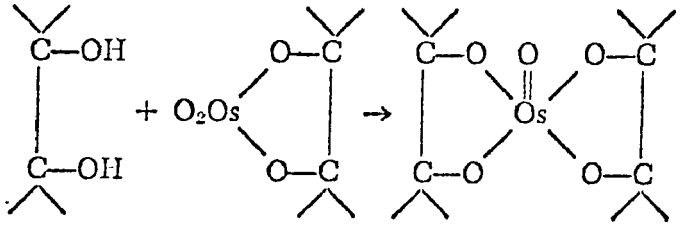

Since this diester constitutes a crosslinking of two molecules of olefin, the above reaction scheme is a satisfactory explanation of lipid fixation by osmium tetroxide.

As stated above, osmium tetroxide oxidizes olefins to glycols through the intermediate formation of cyclic osmic esters. The end product of this reaction is hard to identify; however, Korn (11) has isolated derivatives of methyl oleate, oleic acid, and a few other compounds. Methyl oleate, for instance, is oxidized and the product is the diester, bis (methyl 9, 10-dihydroxystearate) osmate, or upon hydrolysis the product is methyl 9, 10-dihydroxystearate. Dreher et al (12), have indicated that monolinolein and retinol formed solid films on osmium tetroxide substrates by crosslinking via diesters of osmic acid. It may be concluded from the above and other evidence that osmium tetroxide reacts with the double bonds of unsaturated lipids to form glycol osmates that are stable under the conditions of preparation of

of tissue for electron microscopy.

Ugelstad et al. (2) used osmium tetroxide solution to harden and stain the styrene monomer. This monomer is stained by a very rapid reaction. This reaction occurs within a few minutes and is apparently quantitative. The molar ratio of OsO_4 to double bonds must be carefully controlled in order to ensure complete reaction while leaving a minimum of excess OsO_4, which tends to darken the background of the micrographs.

It is reported (2), in the case of acrylate and methacrylate esters, that the stained electron microscope specimens of the emulsified monomer droplet were unsatisfactory. Presumably this results from a much more rapid hydrolysis of the more polar intermediate osmate esters.

4-6 Results and Discussion

4-6-1 The Particle Size Measurement

Table 4-2 shows that only rod-shaped formations exist in the styrene emulsion containing less than 0.3 cc styrene monomer in the 25 cc deionized water containing 0.15 g HTAB, and 0.1 g cetyl alcohol mixed emulsifier system. Therefore, this indicates that the 0.3 cc styrene may be solubilized in the micelles. This increment corresponds to the sharply decending leg of the

conductometric titration curve. (Figure 2-6)

The micrographs of the stained particles at various amount of styrene content, are shown in Figure 4-2.

One of the main problems in electron microscopy is the difficulty in obtaining a representative sample. For example, a dispersion at a concentration of 50 wt % made up of 2000Å particles can have over 10^{13} particles per cm^3. Since only 1000-2000 particles are generally counted the magnitude of the problem is apparent.

The temperature of the sample in a electron microscope is not well characterized, it is believed to be in the range of 100 to 275°C. Under these conditions a number of latexes will shrink and give diameters about 20% too low (13). Thus, the electron beam itself can introduce change in particle size.

Large particles were found in emulsions containing 0.3 and 0.4 cc styrene monomer in this mixed emulsifier system. These regions are located at the minimum positions of the conductometric titration curve. Also, a series of small droplets between 100 nm and 200 nm were measured in the range of 0.57 cc to 1.64 cc styrene monomer. This region corresponds to the ascending leg of the conductometric titration. If greater than 1.64 cc styrene was added to the mixed emulsifier system, the emulsion particle sizes were found to increase continuously. This region

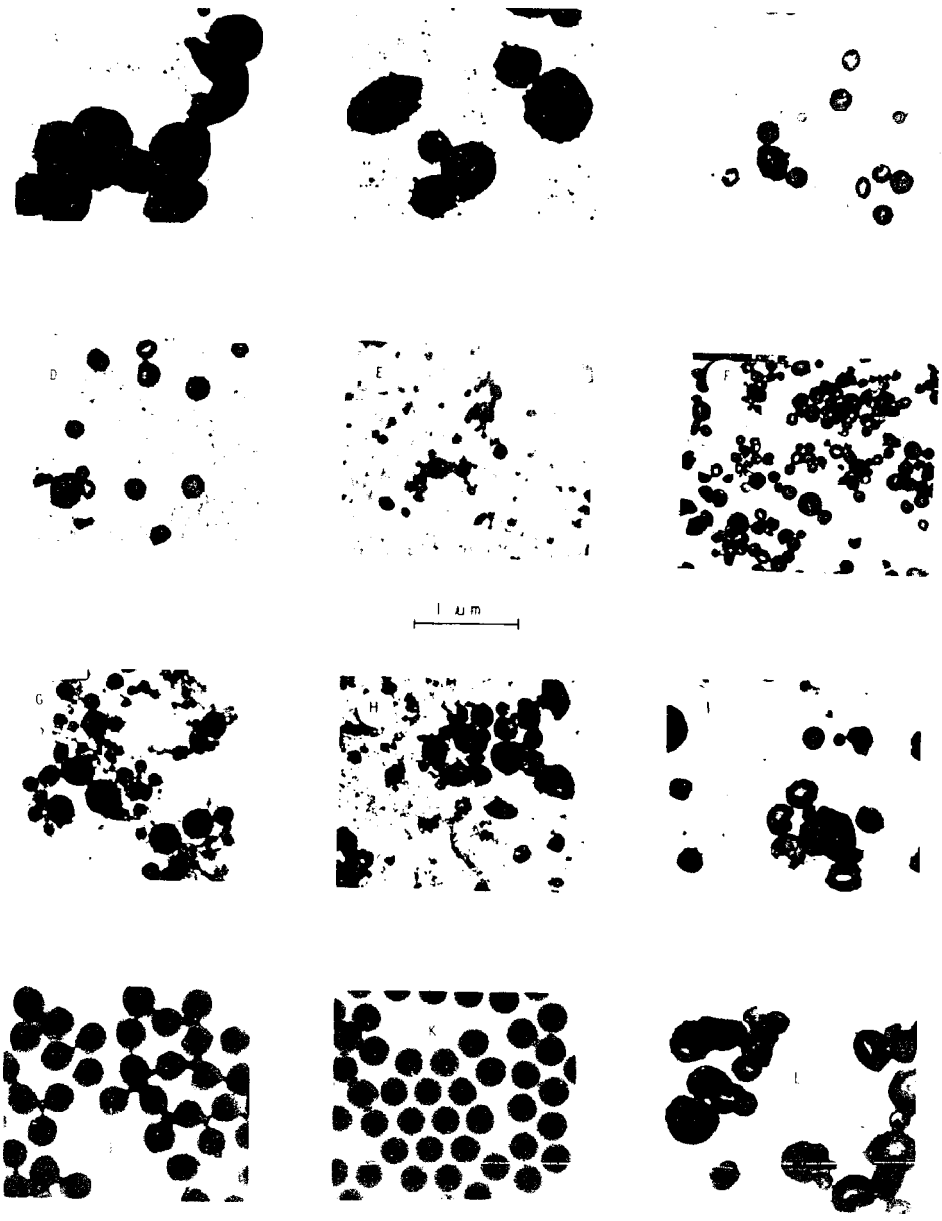

Figure 4-2 Electron mictrographs are of the stained particles containing various amounts of styrene : (A) 0.3 cc , (B) 0.4 cc (C) 0.57 cc , (D) 0.92 cc , (E) 1.12 cc , (F) 1.64 cc , (G) 2.33 cc , (H) 3.00 cc , (I) 5.74 cc , (J) 6.74 cc , (K) 7.74 cc , and (L) 8.3 cc

is located along the equilibrium portion of the conductometric titration curve.

Table 4-2 Stained Particle Size of Styrene Monomer Emulsion

cc of styrene /25 cc mixed emulsifier system*	Dn (nm)	Dw (nm)	Dmax (nm)	Dmin (nm)	Dw/Dn
0.3	539.5	606.5	737.2	344.9	1.124
0.4	542.7	639.3	742.3	248.7	1.178
0.57	175.9	238.5	285.6	89.3	1.358
0.92	139.8	181.5	228.2	63.1	1.298
1.12	129.5	171.0	211.9	56.6	1.320
1.64	127.9	154.9	183.5	80.8	1.211
2.33	206.4	293.8	348.3	33.9	1.423
3.0	212.1	296.5	310.6	110.0	1.398
5.74	282.1	342.6	476.9	133.1	1.214
6.74	308.7	384.3	485.3	142.1	1.245
7.74	323.7	325.8	342.9	264.7	1.007
8.3	355.3	374.9	434.5	243.7	1.055

* 25 cc deionized water + 0.15 g HTAB + 0.1 g cetyl alcohol

4-6-2 The Relationship Between Particle Size and Number of Particle as well as Surface Area

Table 4-3 shows the number average diameter of the monomer droplets, the average number of particles, the particle surface area and total area of the particles at certain volumes of styrene monomer in the mixed emulsifier system.

Figure 4-4 shows the plot of the number of particles against the added volume of styrene. It indicates a tremendous increase in the number of particles from 0.4 cc to 1.64 cc of styrene. A sharp decrease was found at

1.64 cc. After the sharp decrease at 1.64 cc the number of particles decreases steadily. In comparing the number of particles with the volume of added styrene in the conductometric titration curve (Figure 4-4), it was found that a tremendous increase in the number of particles corresponds to the ascending leg and a sudden decrease in number of particles corresponds to the second critical point (V2), which is followed by a steady decrease. This information suggests there is a particle break-down stage at the ascending leg period, which not only develops an increasing number of particles, but the average particle size also decreases. After this period a sudden coagulation occurs to minimize the total increased surface, and the number of particles continues to decrease steadily thereafter. The total surface area versus volume plot is shown in Figure 4-3. This curve shows the total surface area increase can be divided into two stages. The first stage corresponds to the ascending leg in the conductometric titration curve and shows a very sharp increase in total surface area. The second stage corresponds to a decrease in growth of the total surface area.

Table 4-3 The Relationship Between Particle Size and Number of Particles as Well as Surface Area

Volume of styrene (c c)	Dn (nm)	# of Particles	Surface Area/Par. (nm^2)	Total Surface Area (nm^2)
0.30	539.5	3.65×10^6	9.14×10^5	3.34×10^{12}
0.40	452.7	4.78×10^6	9.25×10^5	4.42×10^{12}
0.57	175.9	2.00×10^8	9.72×10^4	1.94×10^{13}
0.92	139.8	6.43×10^8	6.13×10^4	3.95×10^{13}
1.12	129.5	9.85×10^8	5.27×10^4	5.19×10^{13}
1.64	127.9	1.50×10^9	5.14×10^4	7.69×10^{13}
2.33	206.4	5.0×10^8	1.34×10^5	6.77×10^{13}
3.00	212.1	6.0×10^8	1.41×10^5	8.49×10^{13}
5.74	282.1	4.9×10^8	2.50×10^5	1.22×10^{14}
6.74	308.7	4.4×10^8	2.99×10^5	1.31×10^{14}
7.74	323.7	4.4×10^8	3.29×10^5	1.43×10^{14}
8.30	355.3	3.5×10^8	3.79×10^5	1.40×10^{14}

The results suggest the initial descending leg of the conductometric titration corresponds to the solubilization process that is, the styrene monomer is being solubilized in the micelles. The slightly decreased particle sizes along the ascending leg of the conductometric titration indicate the number of particles are increasing while the styrene monomer is increasing in the mixed emulsifier system. There is no particle growth process in this region. The particle sizes at the equilibrium portion of the conductometric titration curve increase continuously

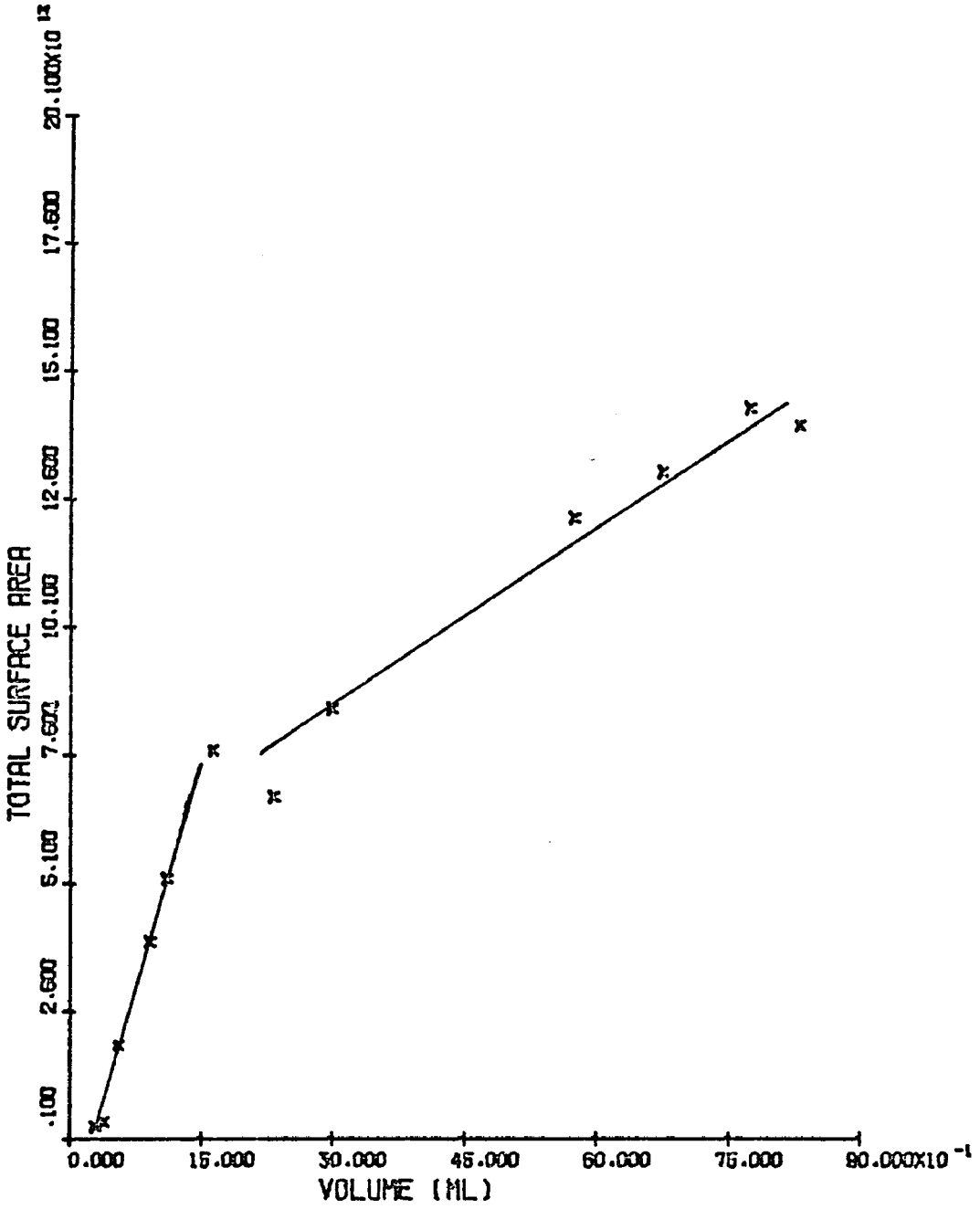

Figure 4-3 Variation of droplet surface area with added volume of styrene.

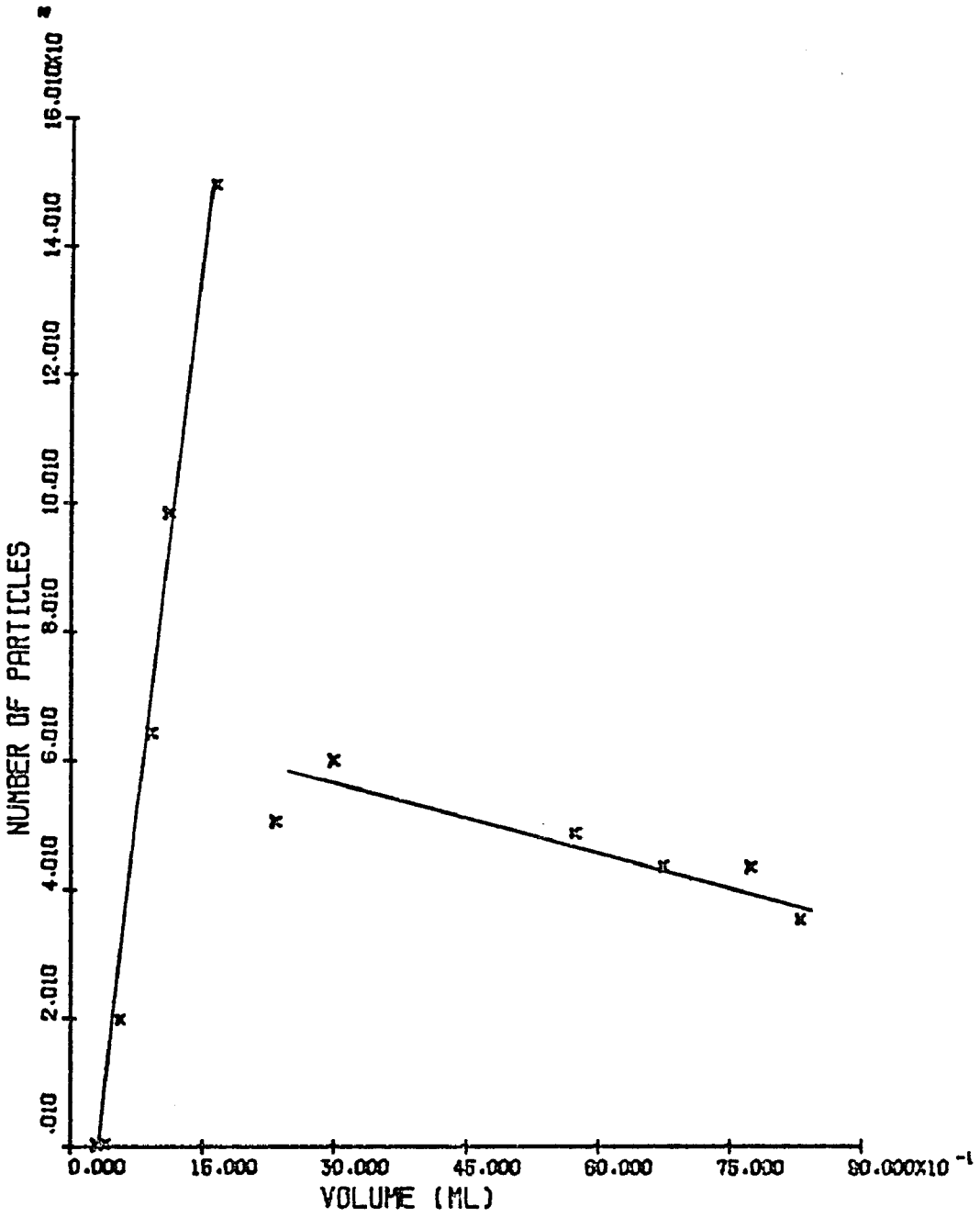

Figure 4-4 Variation of number of droplets with added volume of styrene.

while the amount of styrene monomer in the mixed emulsifier system is also increasing. This stage is the particle growth process, where the number of particles decreases slightly.

4-6-3 The Formation of Mixed Emulsifier System

The interesting phenomena in the emulsion prepared by using a mixed emulsifier system is the rod-shaped formation (Figure 4-5). This was never found in the single surfactant system. This rod-shaped formation could be due to OsO_4 or the presence of styrene monomer.

Therefore, mixed emulsifier solutions without styrene monomer and OsO_4 were examined by transmission electron microscopy and the rod-shaped formations were present here also (Figure 4-6). Furthermore, the cetyl alcohol could be suspected to form rods; a sample contains only cetyl alcohol was examined under TEM and no rod formation was observed as is illustrated in Figure 4-7. Therefore, this indicates these formations are a characteristic structure in the mixed emulsifier system.

In order to verify that the rods were not formed during sample preparation for TEM by drying at room temperature, a mixed emulsifier emulsion was prepared at 63°C, diluted by 63°C water, mounted on a 63°C grid, and oven dried at 63°C. Rod formations were still observed (Figure 4-8). This implies the rod formation existed in

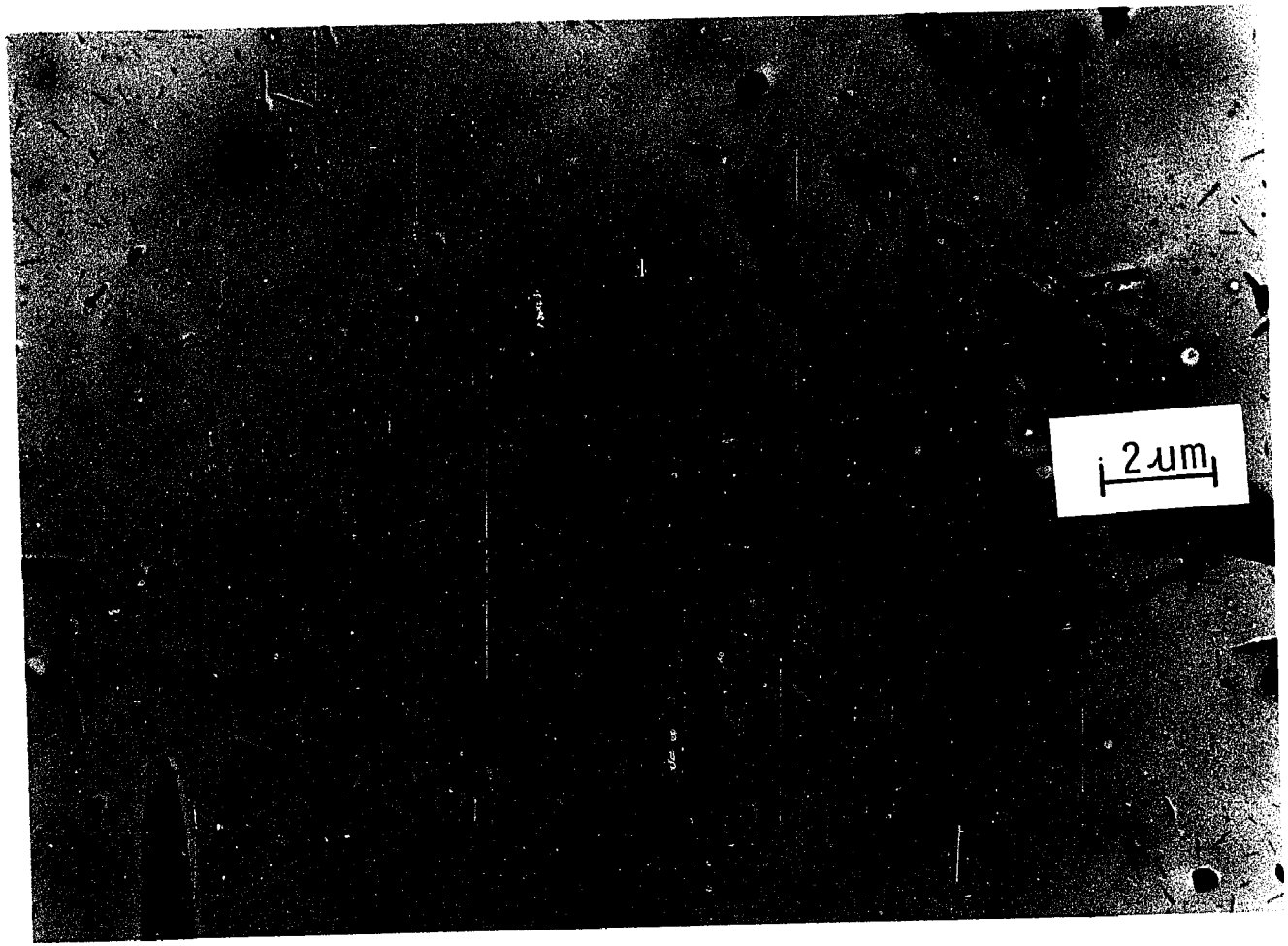

Figure 4-5 The rod-shaped formation of mixed emulsifier system in the presence of osmium tetroxide and styrene monomer

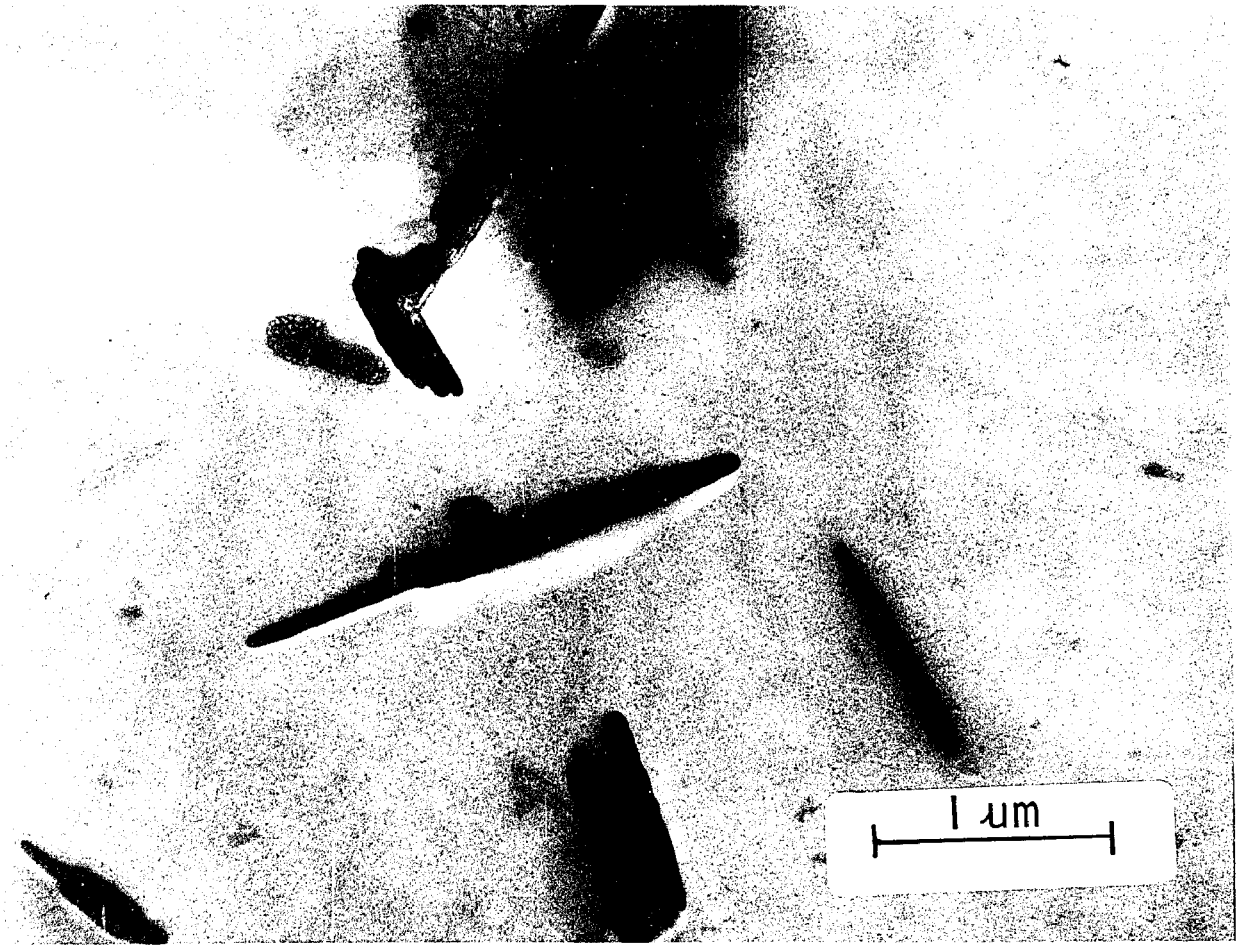

Figure 4-6 The rod-shaped formation of mixed emulsifier system without any additives

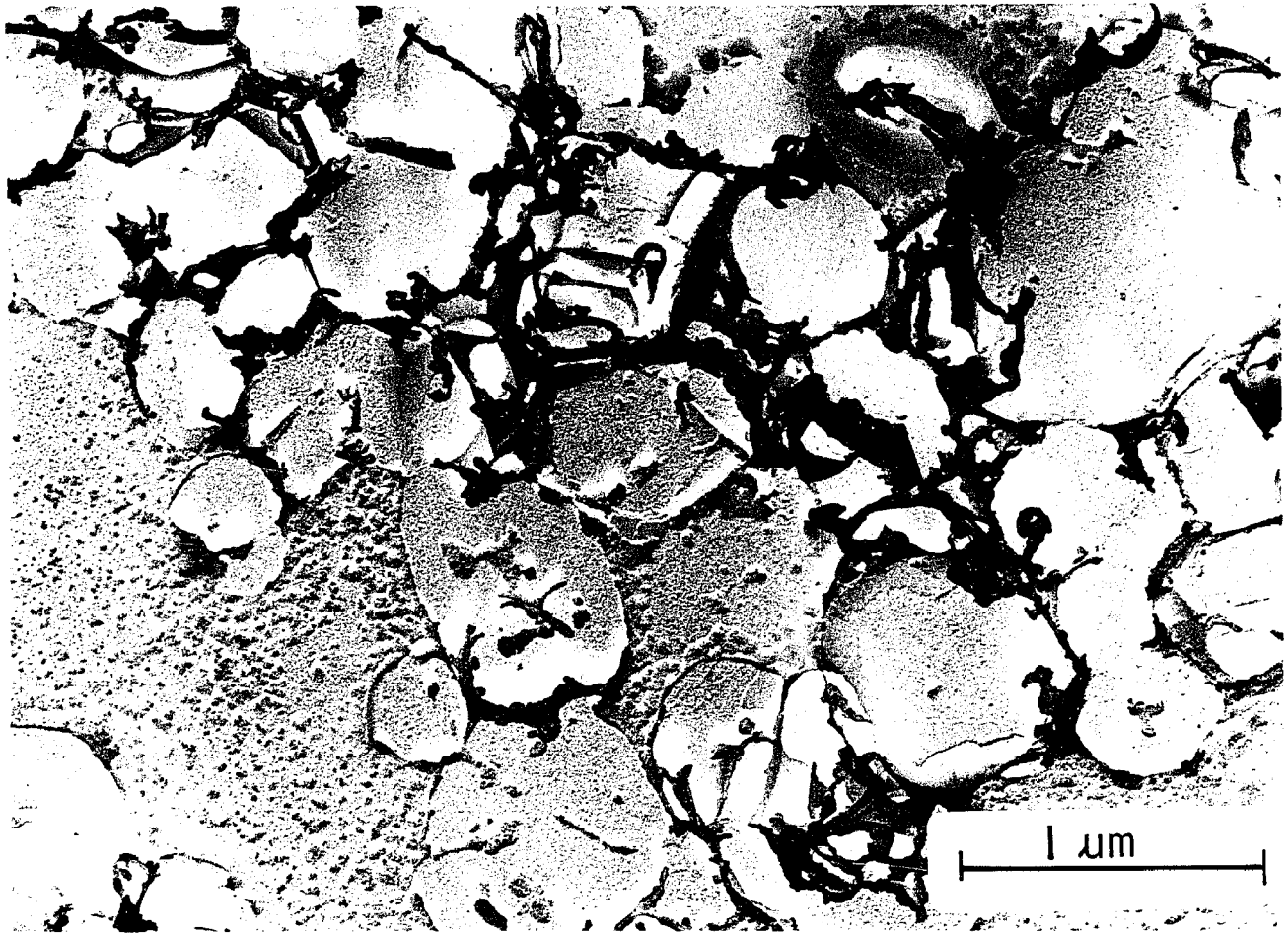

Figure 4-7 The transmission electron microscopy picture of cetyl alcohol alone

Figure 4-8 The rod-shaped formation of mixed emulsifier system prepared at 63° C

the mixed emulsifier system at 63°C while the emulsification take place.

4-6-4 Electron Diffraction Pattern

The selected area diffraction pattern shows the rod-shaped formations to be crystalline. Figure 4-9 indicates the spot patterns produced by a 100 KV electron beam of a mixed emulsifier system of HTAB and cetyl alcohol at a molar ratio 1:3.

The spot pattern of HTAB and cetyl alcohol combination at molar ratio 1:1 was seen on the screen of electron microscope but quickly disappeared while being exposed to the electron beam. This implies the crystallinity is easily destroyed by the 100 KV electron beam.

The above information indicates the rod-shaped crystal formed at molar ratio 1:3 of HTAB to cetyl alcohol has a higher melting point than the same mixed emulsifier system at molar ratio 1:1. In other words, the degree of crystallinity of the rod-shaped formation is higher at the molar ratio 1:3 of HTAB to cetyl alcohol than at the molar ratio of 1:1.

4-6-5 The Hot Stage Observation of the Rod-Shaped Crystal

The rod-shaped formation of HTAB and cetyl alcohol combination in the mixed emulsifier system is

Figure 4-9 The selected area diffraction pattern of rod-shaped formation of HTAB and cetyl alcohol mixed emulsifier system at molar ratio 1:3 produced by 100 KV electron beam

verified as crystalline in nature by electron diffraction patterns.

In order to investigate the melting point of the crystal, the hot stage of the transmission electron microscopy was employed.

The mixed emulsifier solution of HTAB and cetyl alcohol at a molar ratio 1:1 was placed on a carbon and Formvar coated grid and allowed to dry. The dried grid was not shadowed with a 80/20 Pt/Pd alloy, but was mounted on the heating holder directly. The sample was examined at various temperatures, this being controlled by varying the voltage of the heating unit. The micrographs are shown on Figure 4-10.

It is understood that the temperature of the sample in the electron microscope is not well characterized, and it is believed that the temperature there is much higher than room temperature when the examination is carried out at room temperature. Therefore, the temperature of the sample at hot stage is higher than indicated. Nevertheless, the results can be studied qualitatively.

The melting point of cetyl alcohol is 49^{o}C, the melting point of HTAB is 237-243^{o}C. The hot stage TEM showed some phase transformation occurring at 65.4^{o}C, and the melted area is not continuous. This suggests the melted area is formed by cetyl alcohol, in other words, the

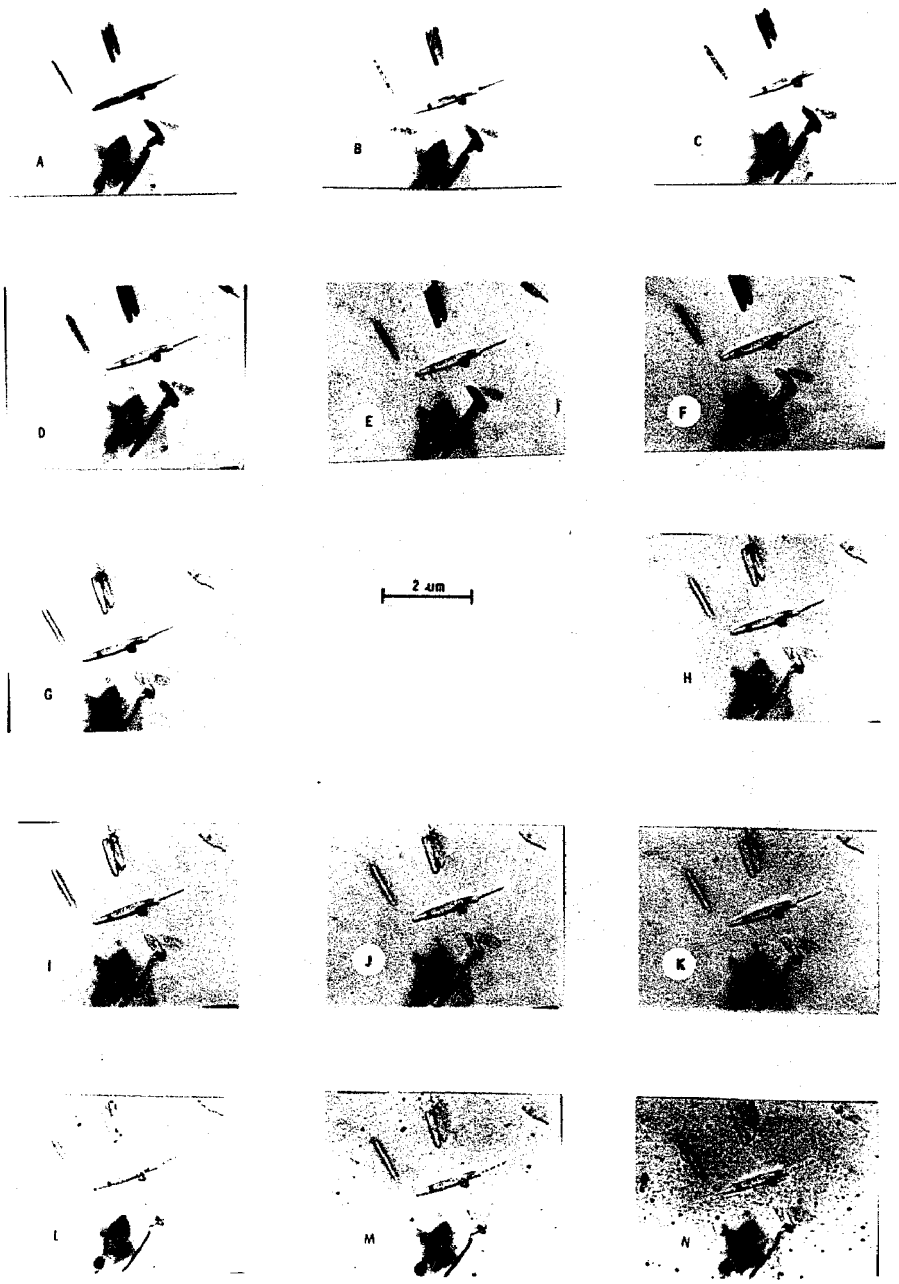

Figure 4-10 Electron micrographs are of rod-shaped crystals, examined under a hot stage TEM at various temperatures: (A) room temperature, (B) 65.4°C, (C) 105.1°C, (D) 159.5°C, (E) 207.8°C, (F) 265.1°C, (G) 320.0°C, (H) 373.5°C, (I) 426.0°C, (J) 477.7°C, (K) 528.1°C, (L) 626.2°C, (M) 674.3°C, and (N) 859.0°C.

rod-shaped formation is a regular and alternating arrangement between HTAB and cetyl alcohol. As the temperature increases, the melting area increases, due to the fact that the electron beam is concentrated at the center of the same. This center shows more phase transformation than other areas. A complete phase transformation of rod was observed at 265.1°C. Although the temperature continued to increase to 859°C, the shape of the rod formation remained.

4-7 References

1. C. Orr, Jr., and J.M. Dallavalle, "Fine Particle Measurement," 19, the Macmillan Co. (1959).
2. A.R.M. Azad, R.N. Fitch, and J. Ugelstad, ACS Symp. Series, No. 9, 135 (1975).
3. A.W. Agar, Brit. J. Appl. Phys., 11, 185 (1960).
4. R. Philips, Brit. J. Appl. Phys. 11, 504 (1960).
5. W.J. Moore, Physical Chemistry, 595, 4 ed., Prentice Hall (1972).
6. D.E. Bradley, Techniques for electron microscopy, 58, ed. by D. Ray, 2nd ed., Blackwell Scientific Publications (1965).
7. D.L. White, S.B. Andrews, J.W. Faller, R.J. Barrnett, Biochim. Biophys., Acta., 436 (3), 577 (1976).
8. P.C. Hydes, M.J. Cleare (Johnson, Matthey and Co. Ltd.), Ger. Offen. 2,630,823 (1977).
9. R. Criegee, Angew Chem., 51, 519 (1938).
10. K. Kato, Polymer Letters, 4, 35 (1966).

11. E.D. Korn, J. Cell Biol. 34 (2), 627 (1967).

12. K.D. Dreher, J.H. Schulman, O.R. Anderson and O.A. Roels, J. Ultratrust. Res., 19 (5b), 586 (1967).

13. E.A. Collins "Measurement of Particle Size" 8th Annual Short Course Advances in Emulsion Polymerization and Latex Technology Vol. 1, 48, ed. by G.W. Poehleim, Lehigh University (1977).

CHAPTER 5 ULTRAVIOLET ABSORBANCE

5-1 Introduction

Ultraviolet spectra were used to determine the concentration of benzene in the water layer after ultracentrifuge of emulsions prepared by using mixed emulsifier systems.

The visible and ultraviolet spectra of organic compounds are associated with transitions between electronic energy levels. The transitions are generally between a bonding or lone-pair orbital and an unfilled non-bonding or anti-bonding orbital. The wavelength of the absorption is then a measure of the separation of the energy levels of the orbitals concerned. Above 200 nm excitation of electrons from p-, d- and π-orbital and, particularly, π-conjugated system, gives rise to readily measured and informative spectra.

The fundamental equation is the Bohr equation:

$$\epsilon = h\nu$$

Where
ϵ is the energy per molecule, and the energy per mole (E) is ϵ N where N is Avogado's number; the values of the constants which are employed in the equation are as follows:

$$h = 6.6242 \times 10^{-27} \text{ erg sec}$$

$$1 \text{ kcal} = 4.1840 \times 10^{-10} \text{ ergs}$$

$$N = 6.023 \times 10^{23}$$

C = velocity of light = 2.9979×10^{10} cm sec^{-1}

The energy per mole (E) is related to wavelength by equation (5-1).

$$E \text{ (kcal/mole)} = \frac{hCN}{\lambda} = \frac{6.6242\times10^{-27}}{4.1840\times10^{10}} \times \frac{2.9979\times10^{10}}{\lambda^{(cm)}} \times 6.023\times10^{23}$$

$$= \frac{2.859\times10^{-3}}{\lambda^{(cm)}} = \frac{2.859\times10^{4}}{\lambda^{(nm)}} \qquad (5\text{-}1)$$

Two empirical laws have been formulated concerning the absorption intensity; Lambert's law which states that the fraction of the incident light absorbed is independent of the intensity of the source and Beer's law which states that the absorption is proportional to the number of absorbing molecules. From these laws, the remaining variables give the equation 5-2.

$$\log_{10}\frac{I_o}{I} = \varepsilon bc \qquad (5\text{-}2)$$

where I_o and I are the intensities of the incident and transmitted light respectively, b is the path length of the absorbing solution in centimeter, and c is the concentration in moles/liter. $\text{Log}_{10}\ (I_o/I)$ is called the absorbance or optical density, ε is known as the molar extinction coefficient and has units of 1000 cm^2/mole but the units are, by convention, never expressed.

Aromatic hydrocarbons show three main types of absorption bands which Clar (4) designated as α, P and β. The extinction coefficients of the α, P and β bands are of the order of 10^2, 10^4 and 10^5, respectively,

and the wavelengths are generally in the order $\alpha > P > \beta$. A weak band (T) due to triplet absorption is also found at longer wavelengths in aromatics. The β, P, α and T bands of benzene were reported (5) as 183 nm, 207 nm, 264 nm and 340 nm, respectively. In the aromatic molecule series, the ratio of β to α frequency (ν_β/ν_α) and the ν_T/ν_p are nearly constant ($\sim$1.35 and 0.6, respectively).

Platt and Klerens (6-8) reported benzene exhibits two intense absorption bands at 180 nm (ε max 47,000) and 200 nm (ε^2max $\sim$ 7000) and a weak absorption band around 260 nm (ε max $\sim$ 220). All three bands are associated with the electron system of benzene. The two intense bands may be ascribed to transitions dipole-excited states, while the weak 260 nm band is ascribed to the forbidden transition to a homopolar excited state. This explanation has been clearly verified (9,10,11) by studying crystalline hexamethylbenzene with polarized ultraviolet radiation. The results indicated that the electric vectors associated with the three bands lie in the plane of the benzene ring.

The low intensity α band centered around 260 nm exhibits a completely resolved vibrational structure and the mechanism of this absorption is explained in terms of the distortion of the benzene ring due to a bending vibration which allows the α band to borrow intensity

Table 5-1 The Figure Numbers, Sample Numbers and the Recipes for the Experiment

# of Fig.	Sample #	Sample	Reference
5-4	1	deionized water	deionized water
5-5	2	benzene solution at concentration 10^{-4}M	deionized water
5-6	3	benzene solution at concentration 10^{-3}M	deionized water
5-7	4	benzene solution at concentration 10^{-2}M	deionized water
5-8	5	0.048% HTAB	0.048% HTAB
5-9	6	0.006M benzene in 0.048% HTAB	deionized water
5-10	7	0.018M benzene in 0.048% HTAB	deionized water
5-11	8-a	0.048% HTAB	deionized water
	8-b	0.6% HTAB	deionized water
5-12	9	0.02M benzene in 0.6% HTAB	deionized water
5-13	10	0.01M benzene in 0.6% HTAB	deionized water
5-14	11-A	UV-2* diluted to 1/3	deionized water
5-15	11-B	UV-2* diluted to 1/3	0.6% HTAB
5-16	12	UV-2*	UV-1* diluted to 1/5

* UV-1 was prepared by emulsifying the mixed emulsifier system of 0.15 gm HTAB and 0.1 gm cetyl alcohol in 25 cc deionized water at 63°C. UV-2 was the water phase of the benzene in water emulsion after ultracentrifugzing at 25,000 rpm for 1 hour.

from the β band. The 260 nm band passing the fine structure is often referred to as "benzenoid absorption". The band is not sensitive to change in solvent (12).

The objectives of this study are to investigate the concentration of benzene in the water phase after ultracentrifuging the benzene-in-water emulsions in the presence of mixed emulsifier systems. Furthermore, to verify new methods in the interpretating of ultraviolet spectra data regardless of the base line adjustment.

5-2 Preparation of Samples for the Experiment

The list of experiments given in Table 5-1 were designed for analyzing the ultraviolet data systematically.

The sample number refers to the number of sample parts in the experiment.

Sample #4 was prepared by mixing benzene in water at the constant temperature of 22°C in a 50 cc separatory funnel. Phase separation between water and benzene was completed, and the water phase collected as sample #4. In order to determine the benzene concentration accurately, the first few cc of the benzene solution were drained and discarded in order to

(make sure no dilution occurs during the benzene removal.) The concentration should be 0.082%, as reported.

Sample #3 and #2 were prepared by diluting sample #4 to 1/10 and 1/50, respectively.

Sample #5 and #8-b were prepared by dissolving 0.048 gm and 0.6 gm HTAB in 100 cc deionized water, capping the bottles, and allowing to tumble in a water bath at 63°C for 1 hour, until the solution was homogeneous.

One drop of benzene (1/75 cc) was placed into 25 cc 0.048% HTAB solution to prepare sample #6 and three drops of benzene to prepare sample #7.

Sample calculation:

molecular weight of benzene = 78 g/mole

density of benzene = 0.884 at 22°C

Concentration of benzene:

$$\text{Sample \#6 } C_{\phi} = \frac{1}{75} \times \frac{0.884}{78} \times \frac{1000}{25} = 0.006 \text{ M}$$

$$\text{Sample \#7 } C_{\phi} = \frac{3}{75} \times \frac{0.884}{78} \times \frac{1000}{25} = 0.018 \text{ M}$$

Sample #9 and #10 were prepared by adding six drops and three drops of benzene, respectively to 25 cc 0.6% HTAB solution. These benzene concentration should be 0.02 M and 0.01 M, respectively. UV-1 was prepared by mixing the mixed emulsifier system of 0.15 gm HTAB and 0.1 gm cetyl alcohol in 25 cc deionized water at 63°C. UV-2 was the water phase of the benzene in water emulsion after

ultracentrifugzing at 25,000 rpm for 1 hour. The emulsion was prepared by adding 10 cc benzene to UV-1 for emulsification. This emulsification process was carried out at $63^{o}C$.

5-3 Experimental Process

The base-line adjustment is very important in the analysis of ultraviolet data. However, this is the most time-consuming stage in ultraviolet spectrophotometry. The base-line adjustment should adequately maintain the recording line level when the reference and sample (quartz) cells are filled with the same standard solution. The ultraviolet light is then scanned at various wavelengths.

For this study, two standard solutions were used, deionized water and an emulsifier solution. The samples prepared were analyzed using the same quartz cell.

5-4 Proposed New Methods for Ultraviolet Analysis

Ultraviolet spectroscopy offers several significant advantages as an analytical technique. First, the sensitivity is excellent. It is frequently possible to quantitatively determine less than 10^{-7} to 10^{-4} M concentrations of a molecular species. Moreover, it is relatively easy to automate spectrophotometric procedures, from sample introduction to the final calculation of the

concentrations of several constituents in a sample.

In order to minimize errors and achieve the highest possible analytical sensitivity, it is essential that the optimum wavelength be selected for an ultraviolet spectra determination. There are two important considerations in choosing this wavelength: the absorbance of the sample itself and the absorbance of interfering components. If a foreign component is present in the sample, and absorbs at the same band of frequencies or wavelengths as the desired species, there will be an error in the observed absorbance of the sample. Therefore, it is best to choose another absorption band of the sample for spectroscopy. This usually presents no problem, since most molecular species that absorb in the ultraviolet-visible region have several absorption bands suitable for analytical use.

Applying the Lambert-Beer Law ($A = \epsilon bc$) to the component and choosing a spectrophotometer with a sample path length, b, of 1.00 cm, the concentration, c, can then be obtained if the extinction coefficient, ϵ, is known. This method is a simple and fast method as long as the base line is well-calibrated.

Generally, the observed curve is obtained by substracting the reference curve from the sample curve, thus the base-line adjustment is very important.

In the multicomponent sample analysis using ultraviolet light the base-line might decline due to the interference between the components. Therefore, the absorbance measured will not equal the height from the maximum of the curve to the base-line. This might cause several percent error.

In order to overcome the base-line problem in analyzing the ultraviolet spectra, there are three new methods proposed and are described as follows:

1. Draw a line connecting the maxima of the peaks of interest, then draw another line parallel to the y-axis from the minimum point which lies between two maxima peaks (see Fig. 5-1). This distance, h_1, between the minimum and the intersection points should provide quantitative information in terms of sample concentration.
2. Draw a line parallel to x-axis from the minimum point b and intersect the height of absorbance at e and f (Fig. 5-1), the distance from the maximum point to the intersection point, i.e., h_2 and h_3 should provide quantitative information in terms of sample concentration.
3. Draw a line connecting the minima of the peaks of interest, then drawing another line parallel to the y-axis from the maximum point which lies

between two minima peaks (Fig. 5-3). This distance, h_4 between the maximum and the intersection points may provide quantitative information in terms of sample concentration.

5-5 Theory

Based on Beer-Lambert equation

$$A = \varepsilon bc$$

where A is absorbance, ε is the extinction coefficient at certain wavelength, b is the length of the cell for light passing through, and c is the concentration. The various absorption on the ultraviolet spectra can be expressed as $A_1 = \varepsilon_1 bc$, $A_2 = \varepsilon_2 bc$, $A_3 = \varepsilon_3 bc$ and so forth. A typical ultraviolet spectra is shown in Figure 5-3.
A_1 and A_2 represent absorptions of adjacent maxima while A_3 is the inter-peaks minimum.

Connect two adjacent maxima, a & c, and draw a fine parallel to absorbance A_1 from the minimum b, the intersection point to ac is denoted as d, bd is denoted as h_1, draw a line parallel to the base-line from b, and intersect A_1 and A_2 at e and f, be and bf are denoted as h_2 and h_3.

Since $A_1 = \varepsilon_1 bc$, $A_2 = \varepsilon_2 bc$ and $A_3 = \varepsilon_3 bc$ therefore,

$$(A_1 - A_3) = (\varepsilon_1 - \varepsilon_3)\, bc$$

$$h_2 = (\varepsilon_1 - \varepsilon_3)\, bc$$

for the same reason

$$h_3 = (\varepsilon_2 - \varepsilon_3)\, bc$$

If ε_1, ε_2, ε_3 are constants for a specific solution at a fixed wavelength and b is constant by using the same path length (quartz cell) in the system, then h_2 and h_3 should be a function of the solution concentration.

Let us focus on the trapezoid, aefc, as shown on Fig. 5-2, extend ac and ef and until they meet at g. Since Δgea, Δdgb, and Δcgf are similar, therefore

$$\frac{h_2}{ge} = \frac{h_1}{gb} = \frac{h_3}{gf}$$

$$\frac{h_2}{ge} = \frac{h_1}{gb}\ ,\ \frac{gb}{ge} = \frac{h_1}{h_2}\ ,\quad \frac{gb-ge}{ge} = \frac{h_1}{h_2-h_1} \qquad (5\text{-}3)$$

$$\frac{h_2}{ge} = \frac{h_3}{gf} \quad \frac{gf}{ge} = \frac{h_3}{h_2} \quad \frac{gf-ge}{ge} = \frac{h_3-h_2}{h_2} \qquad (5\text{-}4)$$

From equation (5-3), ge can be expressed as

$$ge = \frac{be}{h_1}\ (h_2-h_1) \qquad (5\text{-}5)$$

From equation (5-4), ge can be expressed as

$$ge = \frac{ef}{h_2}\ (h_3-h_2) \qquad (5\text{-}6)$$

Combine equations (5-5) and (5-6), we get

$$\frac{be}{h_1}\ (h_2-h_1) = \frac{ef}{h_2}\ (h_3-h_2)$$

Since be and ef are the constants for the same sample

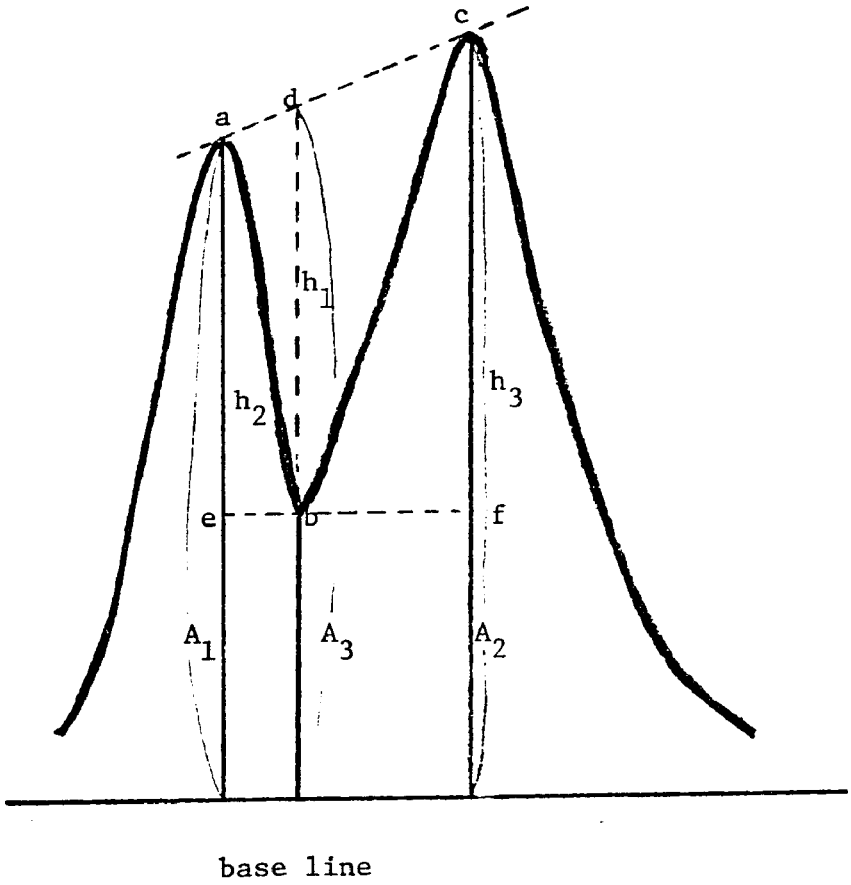

Figure 5-1 Analysis of absorption peaks by connecting maxima.

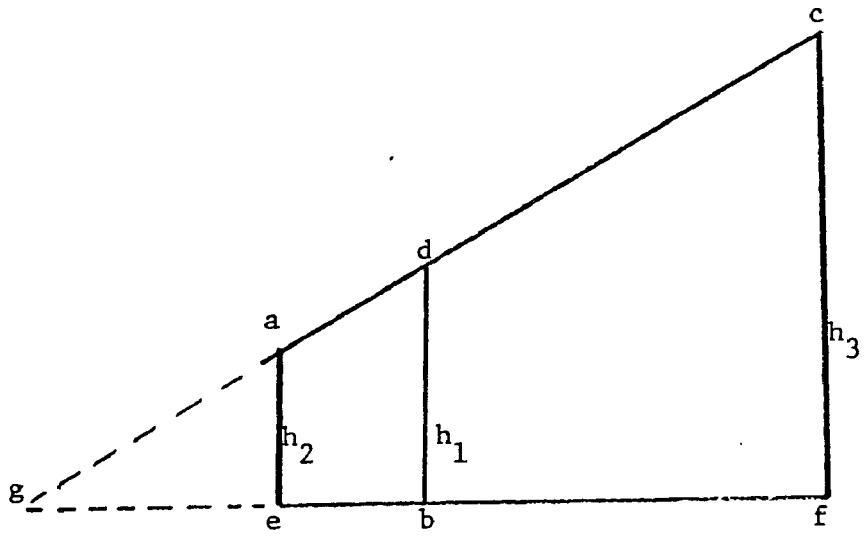

Figure 5-2 Mathematical analysis of Figure 5-1.

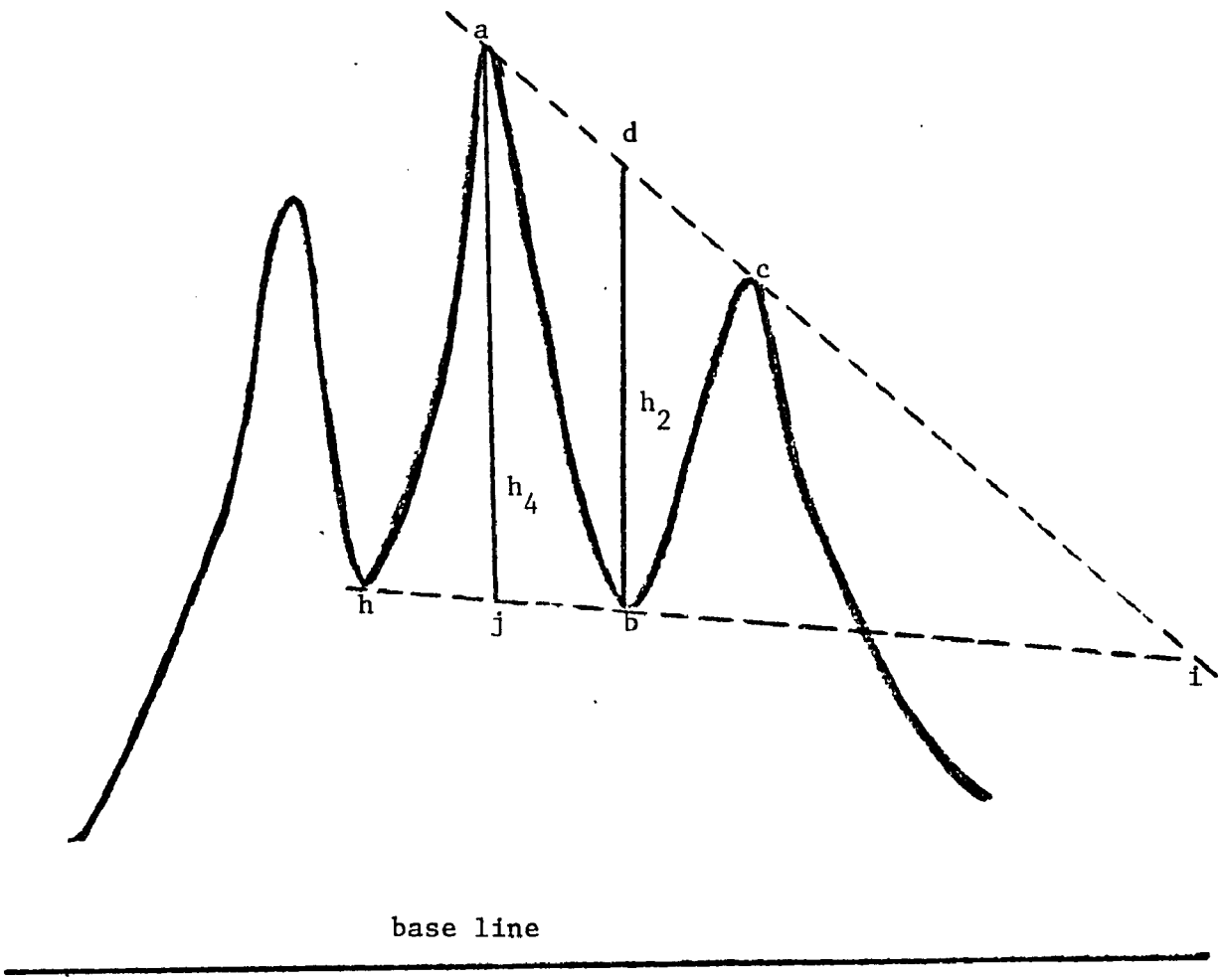

Figure 5-3 Analysis of absorption peaks by connecting minima.

solution, h_2 and h_3 are functions of sample concentration which has been proved above. Therefore, h_1 must be a function of the sample concentration.

Further, if one connects two adjacent minima h and b, extends hb and ac to meet at i, then draw a line parallel to h_2 from a; which intersects hb at j, then aj is denoted as h_4.

For two similar triangle $\triangle$idb and $\triangle$iaj

$$\frac{h_4}{h_2} = \frac{ij}{ib} \qquad (5-7)$$

If ij and ib are constant for the same solution, then h_4 will be a function of h_2. This means h_4 could be a function of the sample concentration.

Based on the theory derived, we can conclude h_1, h_2 and h_3 are functions of the sample concentration and h_4 may be related to the sample concentration.

The advantage of these new methods results is that the concentration can be obtained regardless of the base-line.

5-6 Results

The major difference between the Beckman DK-2A and the Cary 14 are the spectra, the wavelength axis on Beckman DK-2A, is non-linear a careful calibration being necessary; the Cary 14 has a linear wavelength axis (each division is 10 nm).

A well adjusted base-line spectrum of deionized water against deionized water is shown on Fig. 5-4.

Figures 5-5, 5-6 and 5-7 show the spectra of various concentrations of water-soluble benzene against deionized water. Table 5-2 correlates the height measurement of the absorbance from the maxima at wavelengths; 259-60 nm, 254-5 nm, 247-8 nm and 243-4 nm. The ratio of the absorbance at each maxima to sample #4 was calculated. The average absorbance ratio of sample #3 to sample #4 is 0.128, therefore the accurate benzene concentration of sample #3 should be 1.28×10^{-3}m. The average absorbance ratio of sample #2 to sample #4 is 0.028, therefore the accurate benzene concentration of sample #2 should be 2.8×10^{-4}M. Fig. 5-5 shows the absorbance of sample #2 is very weak and the maximum peak at wavelength 243-4 nm can hardly be measured; however, a very tiny peak can be observed. By connecting the maxima peaks between the wavelength of 261-252 nm, 252-246 nm and 249-242 nm, and drawing a line parallel to the y-axis from the minimum points between two maxima peaks (Fig. 5-1) it is possible to measure distances of the connecting line in terms of absorbance difference ($\bar{\Delta}A$). These are shown in Table 5-3. This method will be referred to as $\bar{\Delta}A$ between two maxima peaks. The ratio of sample #2 and sample #3 to sample #4 are also shown on Table 5-3. Sample #3 showed a reasonably good agreement

with the standard. The standard deviation is $\frac{0.128-(0.122+0.119+0.117)\div 3}{0.128}$ = 6.8%. Sample #2 seems to show relatively poor agreement to Table 5-2. This might be due to low solution concentration, the resolution sensitivity decreases, the standard deviation being $\frac{0.028-(0.022+0.023)\div 2}{0.028}$ = 19.64%. Generally, this new method correlates well with the standard. Further verification shown on Table 5-7 and Table 5-11.

By connecting two adjacent minima points on the ultraviolet spectra, and drawing a line parallel to y-axis (Fig. 5-3) it is possible to measure the absorbance difference ($\triangleq$A) from the maxima points to the connecting line. These are shown on Table 5-4. This method will be referred to as $\triangleq$A between two minima peaks. The ratio of sample #2 and sample #3 to sample #4 are also shown on Table 5-4. Sample #3 shows a reasonable agreement with Table 5-2. The standard deviation is $\frac{0.128-(0.121+0.117)\div 2}{0.128}$ = 7.0%. Sample #2 indicates a very poor agreement with this method. The standard deviation is $\frac{0.028-(0.01+0.01)\div 2}{0.028}$ = 64.3%. Presumably at low concentration not only the resolution sensitivity decreases, and also the ratio of $\frac{ij}{ib}$ varies in equation 5-7. (Fig. 5-3)

Equation 1 and 2 indicates h_1 and h_2 (Fig.5-1) are related to the sample solution concentration. This method

will be referred to as the relative absorbance (ΔA) at maximum peak. Table 5-5 shows the relative absorbance (ΔA) at maximum peak of sample #3 and sample #4, and the ratio of sample #3 to sample #4. The standard deviation is $\left|\frac{0.128-(0.1+0.12+0.1)\div 3}{0.128}\right| = 16.7\%$. The agreement is acceptable.

Figure 5-8 is a well adjusted base-line of 0.048% HTAB solution against 0.048% HTAB solution.

Figures 5-9 and 5-10 indicate the spectra of various benzene concentrations in 0.048% HTAB solution. Their concentrations are 0.006M and 0.018M, respectively.

Table 5-6 shows the absorbance of sample #6 and sample #7 against deionized water in the ultraviolet spectra. The ratios to sample #7 are also indicated.

The calculation of the benzene concentration of sample #7 was based on sample #4 at wavelength 259-60 nm. The benzene concentration of sample #7 is $0.01M \times \frac{1.66}{1.295}$ = 0.012M (which is slightly beyond the solubility of benzene in water at 22°C).

The benzene concentration of sample #6 is calculated as $0.012M(0.37+0.435+0.39+0.36)\div 3 = 0.012 \times 0.39 = 0.0047M$.

The $\bar{\Delta}A$ between two maxima peaks of sample #6 and sample #7 are shown on Table 5-7. In comparison with Table 5-2, the standard deviation of the ratio to sample #7 is $\left|\frac{0.39-(0.41+0.44+0.34)\div 3}{0.39}\right| = 1.7\%$. This agreement is

very good.

The Δ A between two minima peaks of sample #6 and sample #7 are shown on Table 5-8. In comparison with Table 5-2, the standard deviation of the ratio to sample #7 is $\left|\frac{0.39-(0.5+0.41)\div 2}{0.39}\right|$ = 16.7%. This agreement is acceptable.

The relative absorbance (Δ A) at the maximum peak of sample #6 and sample #7 are shown on Table 5-9. In comparison with Table 5-2, the standard deviation of the ratio to sample #7 is $\left|\frac{0.39-(0.37+0.53+0.43)\div 3}{0.39}\right|$ = 13.68%. This agreement is also acceptable.

Fig. 5-11 shows the ultraviolet spectra of various concentrations of HTAB solution against deionized water. There is a base-line shift as HTAB concentration changes. A strong absorption edge was also found in this system.

Figures 5-12 and 5-13 were obtained by dissolving benzene in 0.6% HTAB solution at concentration 0.02M and 0.01M respectively, deionized water was used as reference.

The absorbance of sample #10 at 259-60 nm, 253-4 nm and 247-8 nm were 1.37, 1.85 and 1.63 respectively. To compare sample #10 with sample #4, the concentration of sample #10 should be 0.011 M. This concentration is very close to the prepared concentration. Sample #9 has 0.02 M benzene concentration. It is too high for ultraviolet analysis and therefore the spectra was off scale at the

maxima peak shown on Fig. 5-13.

The ultraviolet spectra of sample #11 against deionized water was shown on Fig. 5-14 and against 0.6% HTAB solution was shown on Fig. 5-15.

Table 5-10 shows the absorbance of benzene at maximum peak of Fig. 5-14 and 5-15. The average absorbance ratio to sample #4 is 0.445. That means the benzene concentration in UV-2 is 0.01Mx0.445x3 = 0.0134 M.

Table 5-11 shows the absorbance difference between two maxima peaks of Fig. 5-14 and 5-15. The average absorbance ratio to sample #4 is 0.36. This information indicates the benzene concentration in UV-2 to be 0.0108 M.

Table 5-12 shows the absorbance difference between two minima peaks of Figure 5-14 and Figure 5-15. The average absorbance ratio to sample #4 is 0.372. Based on this information the benzene concentration in UV-2 is 0.0112 M. Although this average value is closer to the value obtained in Table 5-10, than the average value obtained from Table 5-11. The ratios of #4 to #11-A and 11-B in the two regions 260-247 nm and 254-243 nm are significantly different.

Table 5-13 shows the relative absorbance at maximum peak of Fig. 5-14 and 5-15. The average absorbance ratio to sample #4 is 0.333, therefore the benzene concentration in UV-2 is 0.01 M.

TABLE 5.2 The Absorbance (A) at Maximum Peak

Sample #	A (259-60nm)	Ratio to #4	A (253-4nm)	Ratio to #4	A (247-8nm)	Ratio to #4	A (243-4nm)	Ratio to #4
2	0.04	0.031	0.045	0.026	0.041	0.028	--	
3	0.162	0.125	0.22	0.128	0.19	0.13	0.12	0.13
4	1.295		1.71		1.47		0.93	

TABLE 5.3 $\bar{\Delta}$ A Between Two Maxima Peaks

Sample	$\bar{\Delta}$ A (261-252nm)	Ratio to #4	$\bar{\Delta}$ A (252-246nm)	Ratio to #4	$\bar{\Delta}$ A (249-242nm)	Ratio to #4
2	0.017	0.022	0.02	0.023	--	
3	0.095	0.122	0.1	0.119	0.062	0.117
4	0.78		0.84		0.53	

TABLE 5.4 $\underline{\Delta}$ A Between Two Minima Peaks

Sample #	$\underline{\Delta}$ A (260-247nm)	Ratio to #4	$\underline{\Delta}$ A (254-243nm)	Ratio to #4
2	0.01	0.01	0.008	0.01
3	0.115	0.121	0.09	0.117
4	0.95		0.78	

TABLE 5.5 The Relative Absorbance (ΔA) at Maximum Peak

Sample #	Δ A (259-60nm)	Ratio to #4	Δ A (253-4nm)	Ratio to #4	Δ A (247-8nm)	Ratio to #4
3	0.062	0.1	0.11	0.12	0.078	0.1
4	0.617		0.919		0.819	

TABLE 5.6 The Absorbance (A) at Maximum Peak

Sample #	A (259-60nm)	Ratio to #7	A (253-4nm)	Ratio to #7	A (247-8nm)	Ratio to #7	A (243-4nm)	Ratio to #7
6	0.611	0.37	0.87	0.435	0.715	0.39	0.469	0.36
7	1.66		2.0		1.83		1.29	

TABLE 5.7 $\bar{\Delta}$A Between Two Maxima Peaks

Sample #	$\bar{\Delta}$ A (261-252nm)	Ratio to #7	$\bar{\Delta}$ A (252-246nm)	Ratio to #7	$\bar{\Delta}$ A (249-242nm)	Ratio to #7
6	0.34	0.41	0.38	0.44	0.23	0.34
7	0.82		0.86		0.67	

TABLE 5.8 ΔA Between Two Minima Peaks

Sample #	Δ A (260-247nm)	Ratio to #7	Δ A (254-243nm)	Ratio to #7
6	0.49	0.5	0.355	0.41
7	0.98		0.86	

TABLE 5.9 The Relative Absorbance (ΔA) at Maximum Peak

Sample #	Δ A (259-60nm)	Ratio to #7	Δ A (253-4nm)	Ratio to #7	Δ A (247-8nm)	Ratio to #7
6	.26	0.37	.47	0.53	.32	0.43
7	.70		.89		.74	

TABLE 5.10 The Absorbance (A) at Maximum Peak

Sample #	A (259-60nm)	Ratio to #4	A (253-4nm)	Ratio to #4	A (247-8nm)	Ratio to #4	A (243-4nm)	Ratio to #4
11-A	0.588	0.45	0.77	0.45	0.635	0.44	0.43	0.46
11-B	0.575	0.44	0.76	0.44	0.625	0.43	0.43	0.46

TABLE 5.11 $\overline{\Delta}$ A Between Two Maxima Peaks

Sample #	$\overline{\Delta}$ A (261-252nm)	Ratio to #4	$\overline{\Delta}$ A (252-246nm)	Ratio to #4	$\overline{\Delta}$ A (249-242nm)	Ratio to #4
11-A	0.27	0.345	0.32	0.38	0.19	0.38
11-B	0.27	0.345	0.31	0.37	0.19	0.38

TABLE 5.12 $\underline{\Delta}$ A Between Two Minima Peaks

Sample #	$\underline{\Delta}$ A (260-247nm)	Ratio to #4	$\underline{\Delta}$ A (254-243nm)	Ratio to #4
11-A	0.387	0.405	0.265	0.34
11-B	0.388	0.41	0.26	0.335

TABLE 5.13 The Relative Absorbance (ΔA) at Maximum Peak

Sample #	Δ A (259-60nm)	Ratio to #4	Δ A (259-60nm)	Ratio to #4	Δ A (247-8nm)	Ratio to #4
11-A	0.19	0.31	0.37	0.4	0.24	0.295
11-B	0.19	0.31	0.37	0.4	0.23	0.28

Figure 5-14 and Figure 5-15 are quite similar, except for the absorption edge which was observed at low wavelength on Fig. 5-14 and not observed on Figure 5-15. This is caused by the presence of 0.6% HTAB solution as a reference in Fig. 5-15.

Figure 5-16 shows the spectra of UV-2 against UV-1, a very simplified curve was obtained, that means either cetyl alcohol interferes with the absorption band or the mixed emulsifier system interferes with the absorption band. Generally speaking aliphatic compounds have completely different absorption band than aromatic compounds (12), therefore the most probable interference is caused by the mixed emulsifier system.

5-7 Discussion

The base-line adjustment is very important in the analysis of ultraviolet data. However, this is the most time-consuming stage in the operation of ultraviolet spectrophotometer. Furthermore, Figure 5-11 indicates the base-line shift in 0.048% HTAB solution and 0.6% HTAB solution against deionized water. That implies that even with a well-calibrated base-line, various sample concentrations still interfere with the base-line. For similar reasons, various solutions serving as a reference line will also interfere with the base-line.

In order to minimize the error and achieve the highest possible analytical sensitivity, especially in the multicomponent sample analysis using ultraviolet light, the new methods regardless of base-line adjustment are necessary.

Based on the Beer-Lambert theory, there are three possible new methods proposed. They were described in the previous section.

Tables 5-3, 5-7 and 5-11 indicate the method of $\overline{\Delta}A$ between two maxima peaks has very consistant ratios to the standard sample, and the results have reasonably good agreement with those obtained by the traditional Beer-Lambert method.

Tables 5-4, 5-8, and 5-12 indicate that the method of A between two minima peaks gives a reasonable average ratio to the standard sample. The value scattered slightly at different regions. The agreement with those results obtained by traditional Beer-Lambert method is acceptable.

Tables 5-5, 5-9, and 5-13 indicate the method of the relative absorbance (ΔA) at maximum peak is the poorest method among the proposed three new methods. These are shown in a widely scattered data at different regions.

Figure 5-12 and Figure 5-13 indicate more benzene can solubilized in the HTAB solution than deionized water.

Figure 5-12 indicates the solubility of benzene in the presence of surfactant is much higher than the solubility of benzene in water.

The benzene concentration in the water phase of the ultracentrifuging emulsion which is prepared by emulsifying benzene in the mixed emulsifier system is calculated to be approximately 0.01M, that is the solubility of benzene which is soluble in water, all the solubilized benzene will be separated from the water phase by ultracentrifugation.

In comparison to Figure 5-14 and 5-15, Figure 5-16 indicates a significant change in the ultraviolet spectra of benzene. The maxima peaks at 259-60 nm and 242-3 nm disappeared, in Fig. 5-16 the absorbance also decrease appreciably. This is caused by using diluted mixed emulsifier system as a reference.

As mentioned before, there is a slight base-line shift by using various concentration of HTAB solution instead of deionized water as reference when examining the benzene concentration of the sample. The characteristic points are exactly the same. Therefore the change of the spectra must be due to the presence of cetyl alcohol in the reference cell.

There are two possible explanations for this phenomena:

1. Cetyl alcohol will disrupt the absorption band of benzene and cause a significant change. This assumption is not well supported, because aromatic compounds have very different absorption band from the aliphatic compound.

2. In the presence of cetyl alcohol that is in the HTAB solution, there may be a complex formed which could scatter the light or absorb the light at certain wavelengths. This will produce a very different ultraviolet spectra than observed.

5-8 References

1. H.M. Hershenson, Ultraviolet and Visible Absorption Spectra Academic Press, (1956).

2. R.A. Firiedel and M. Orchin, Ultraviolet Spectra of Aromatic Compound, Wiley, N.Y. (1951).

3. A.P.I. Research Project 44, Ultraviolet Spectra Data, Carnegie Institute and U.S. Bureau of Standards (1953).

4. E. Clar, Aromatische Kohlenwasserstoffe, Springer-Verlag, Berlin, (1952). (From C.N.R. Rao "Ultra-Violet and Visible Spectroscopy" Chapter 5 Aromatic Molecules, 60, 3rd ed.) Butterworths, (1975).

5. S.F. Mason, Quart Revs. (London), 15, 287 (1961).

6. J.R. Platt and H.B. Klevens, Chem. Rev., 41, 301 (1947).

7. J.R. Platt and H.B. Klevens, J. Chem. Phys., 16, 832 (1948).

8. J.R. Platt and H.B. Klevens, J. Chem. Phys, 17, 470, 481 (1949).

9. K. Nakamoto, J. Amer. Chem. Soc., 74, 390 (1952).

10. D.P. Craig and L.E. Lyons, Nature, 169, 1102 (1952).

11. C.N.R. Rao, Ultra-Violet and Visible Spectroscopy, 3rd ed., Butterworth, 60, (1975).

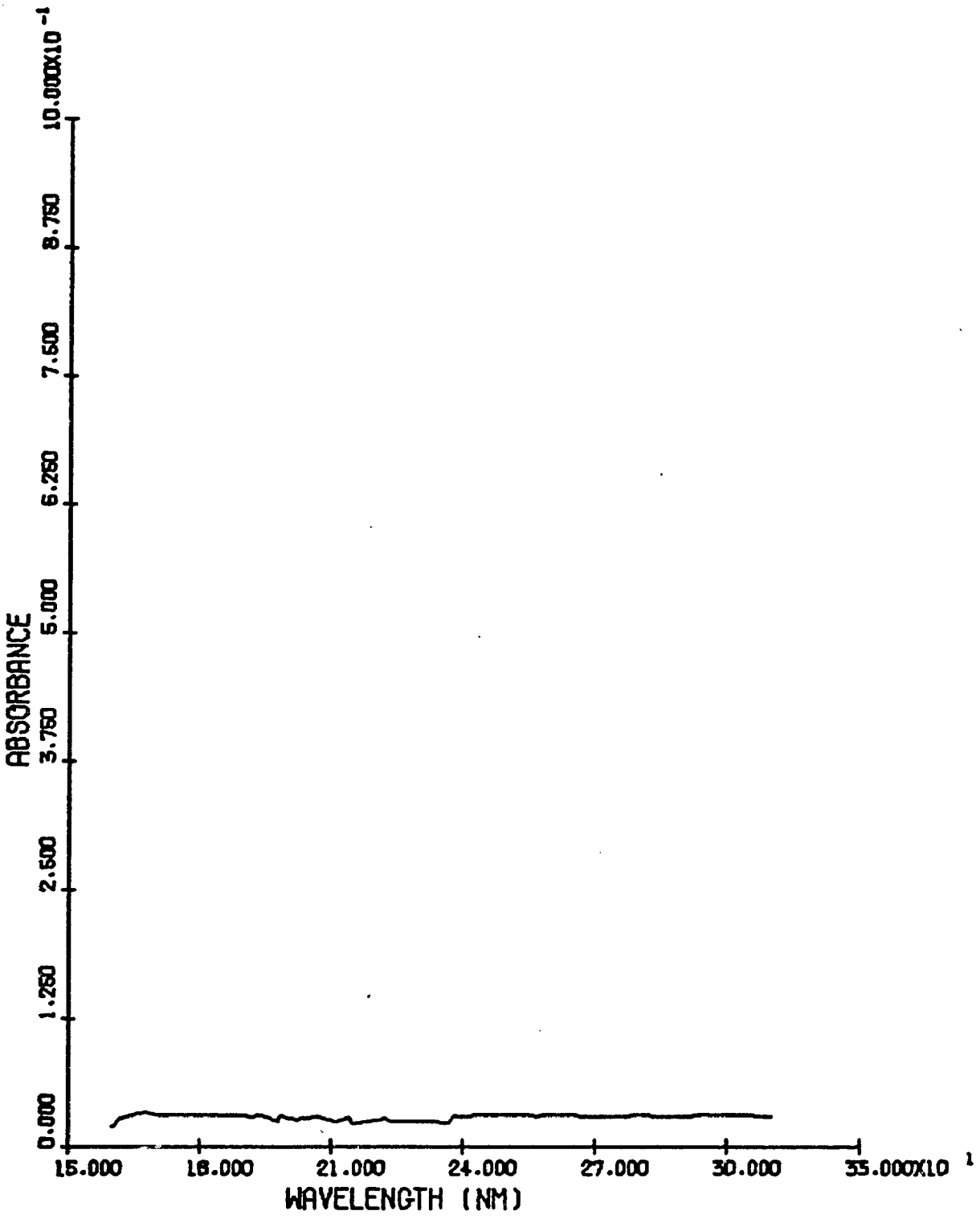

Figure 5-4 Absorption spectrum of deionized water

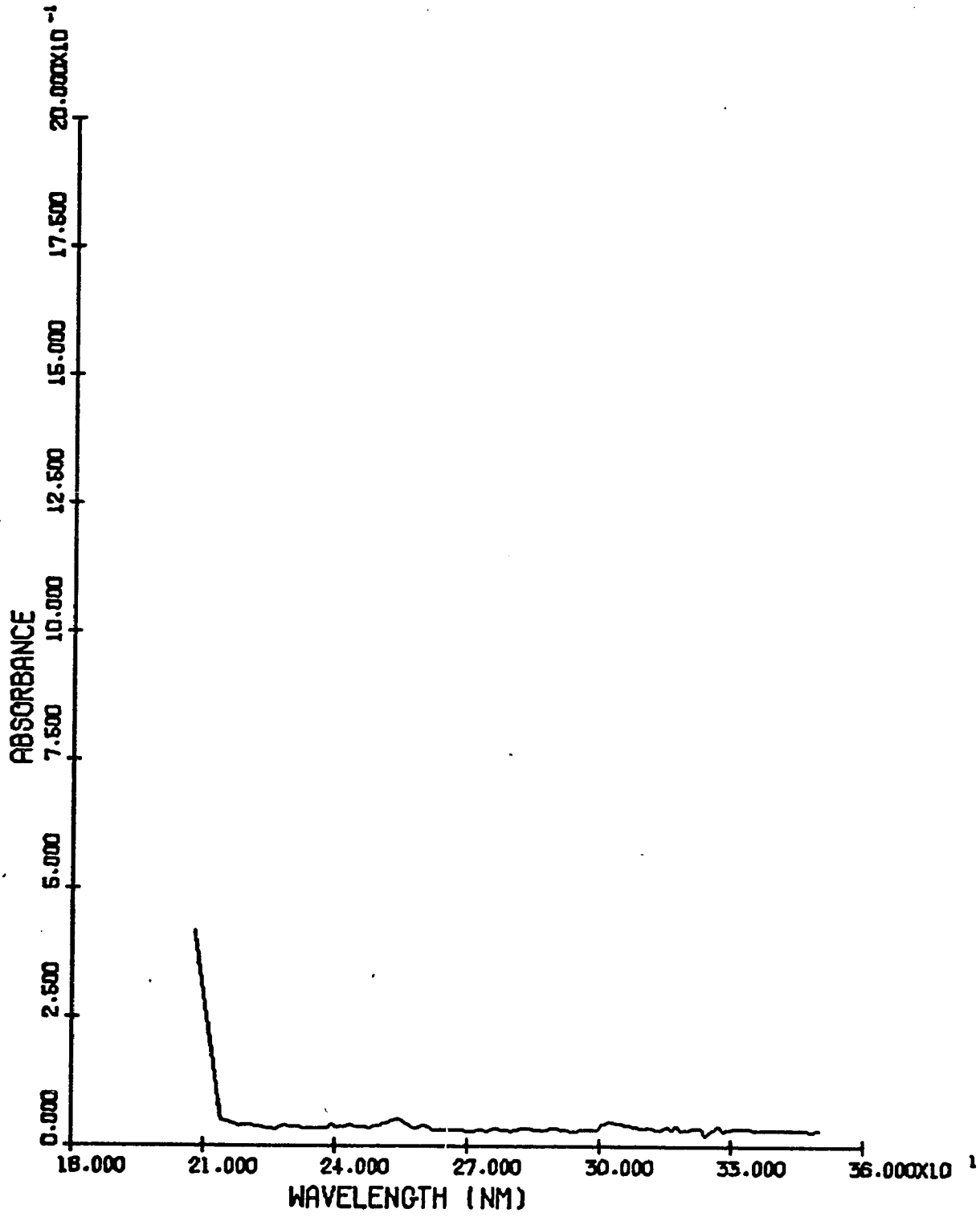

Figure 5-5 Absorption spectrum of 10^{-4} M benzene in deionized water.

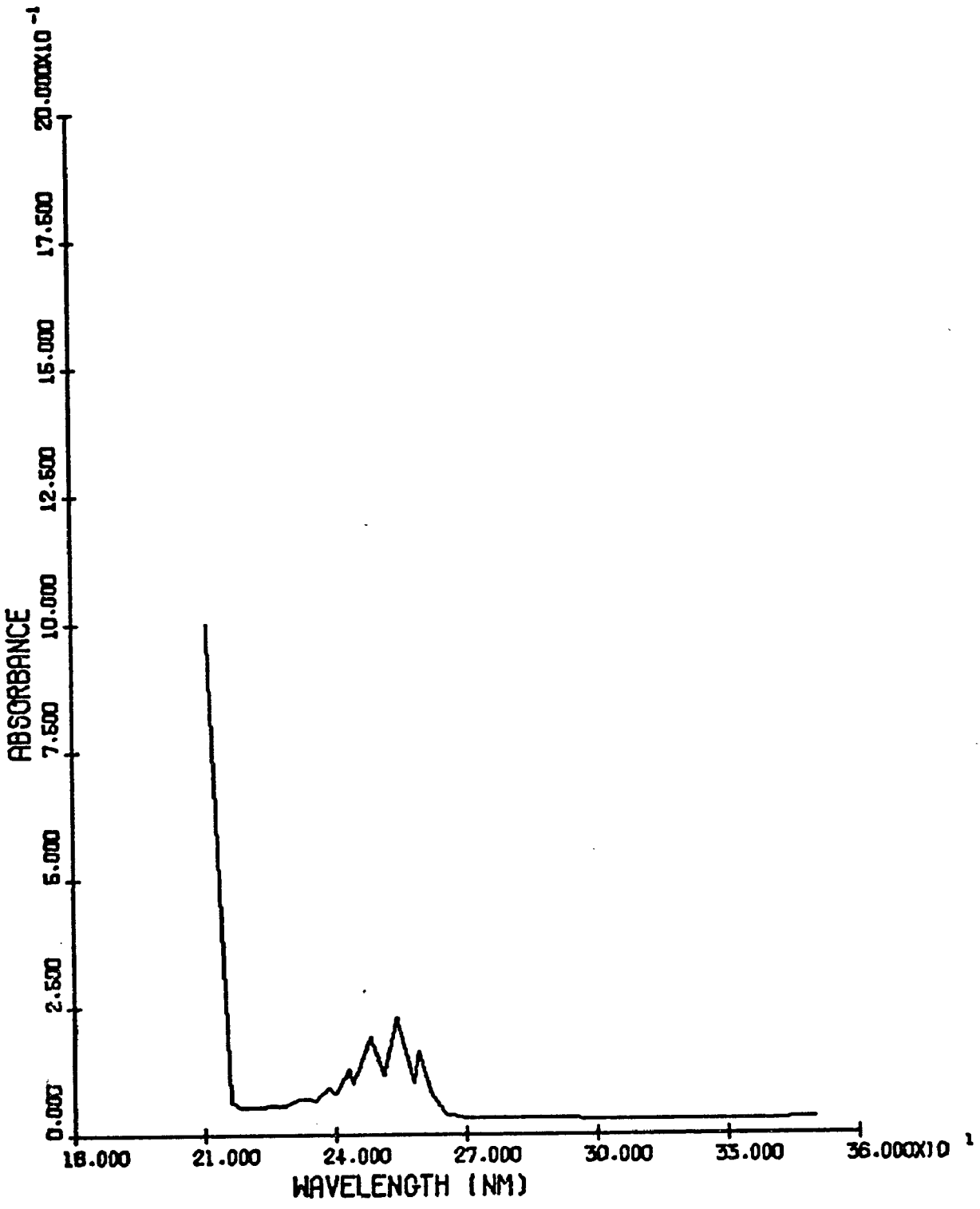

Figure 5-6 Absorption spectrum of 10^{-3} M benzene in deionized water.

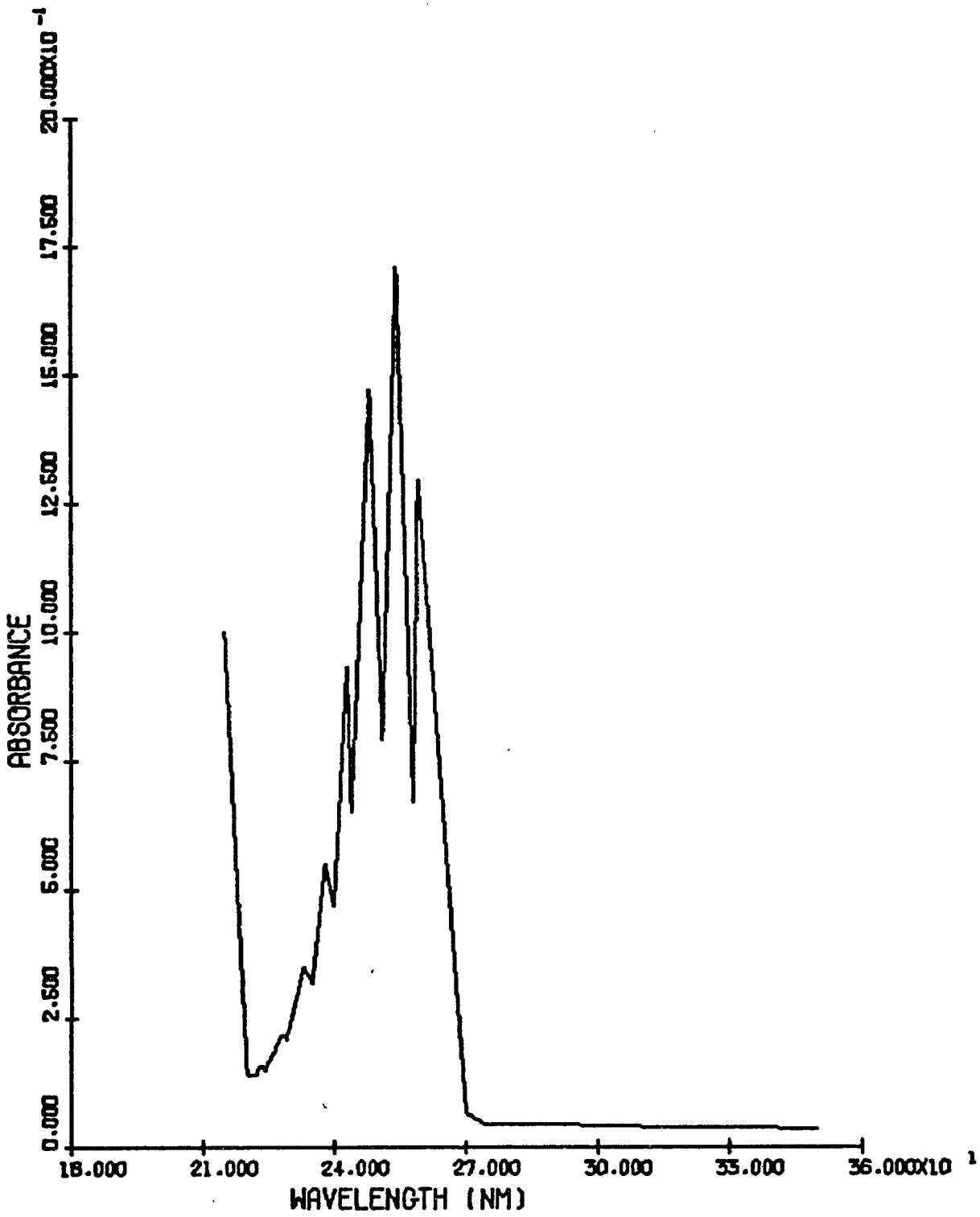

Figure 5-7 Absorption spectrum of 10^{-2} M benzene in deionized water.

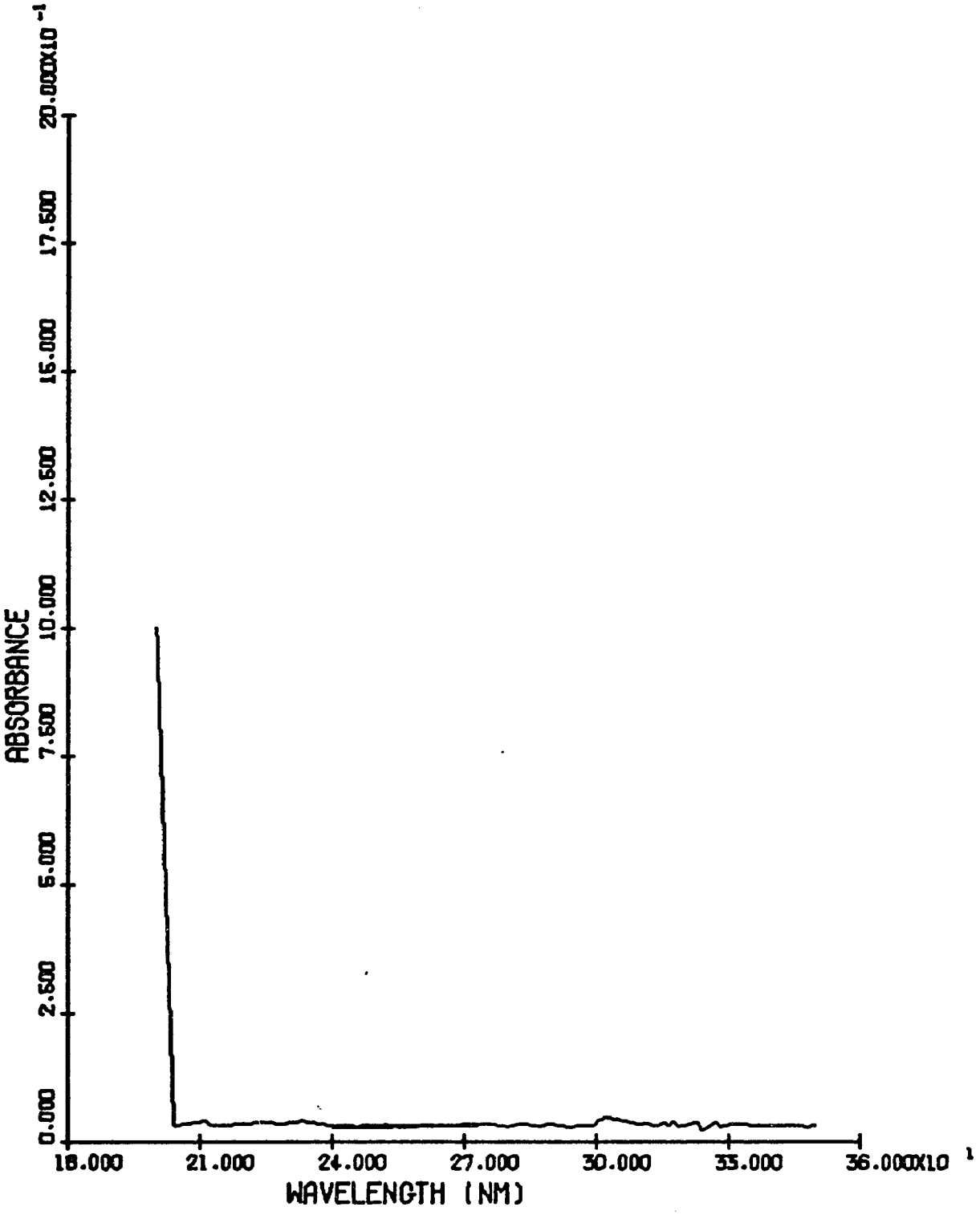

Figure 5-8 Absorption spectrum of 0.048% HTAB solution against 0.048% HTAB solution.

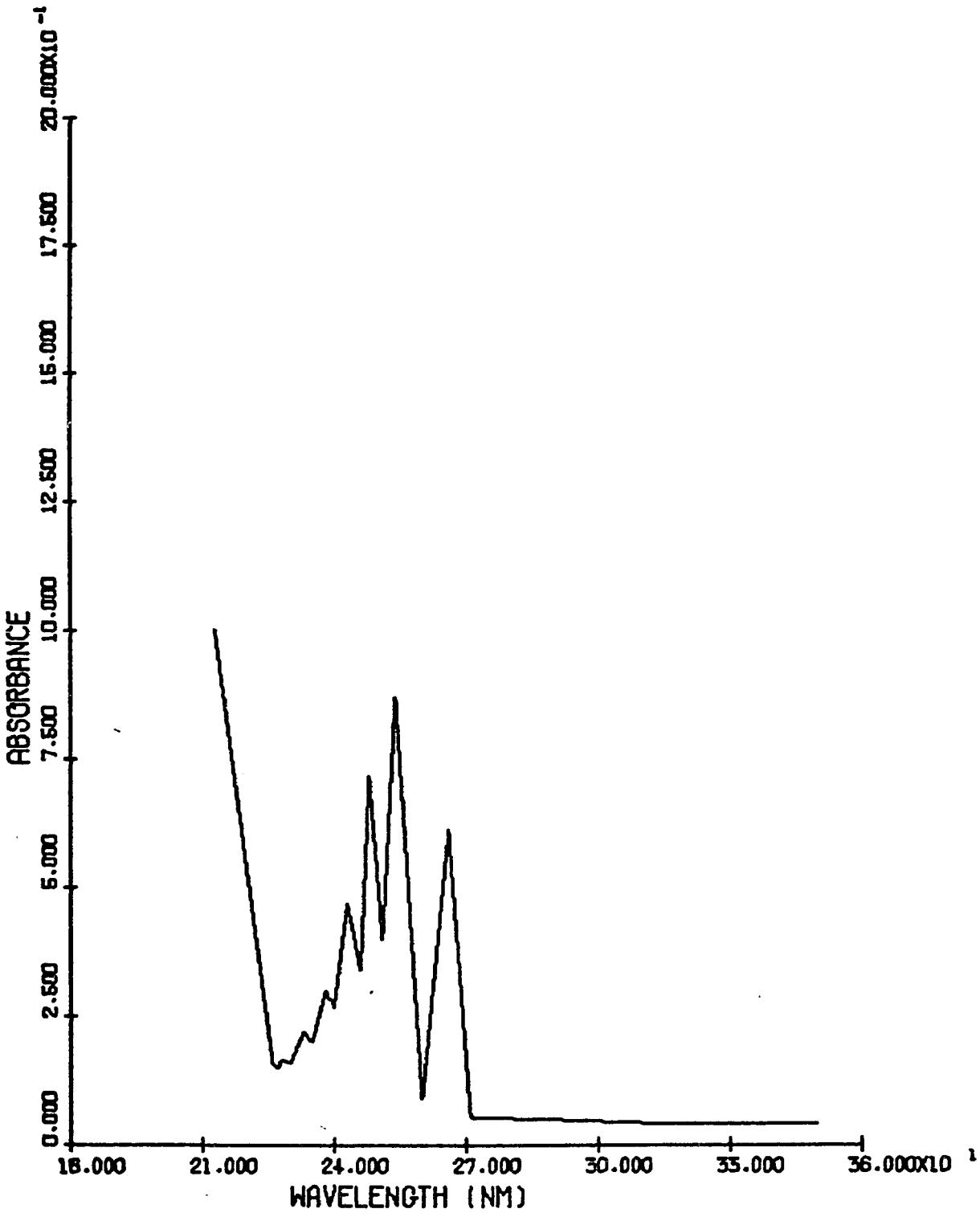

Figure 5-9 Absorption spectrum of 0.006 M benzene in 0.048% HTAB solution against deionized water.

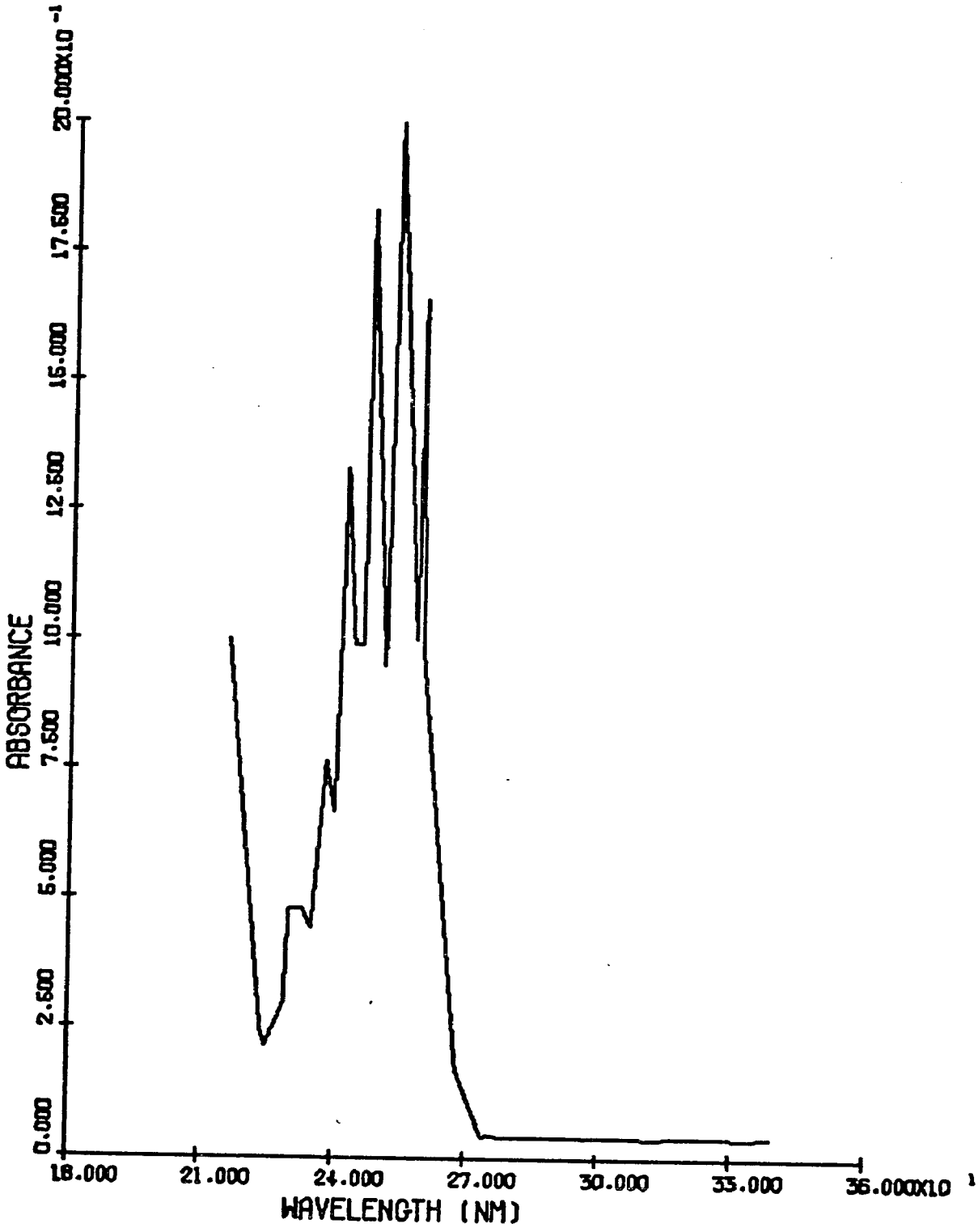

Figure 5-10 Absorption spectrum of 0.018 M benzene in 0.048% HTAB solution against deionized water.

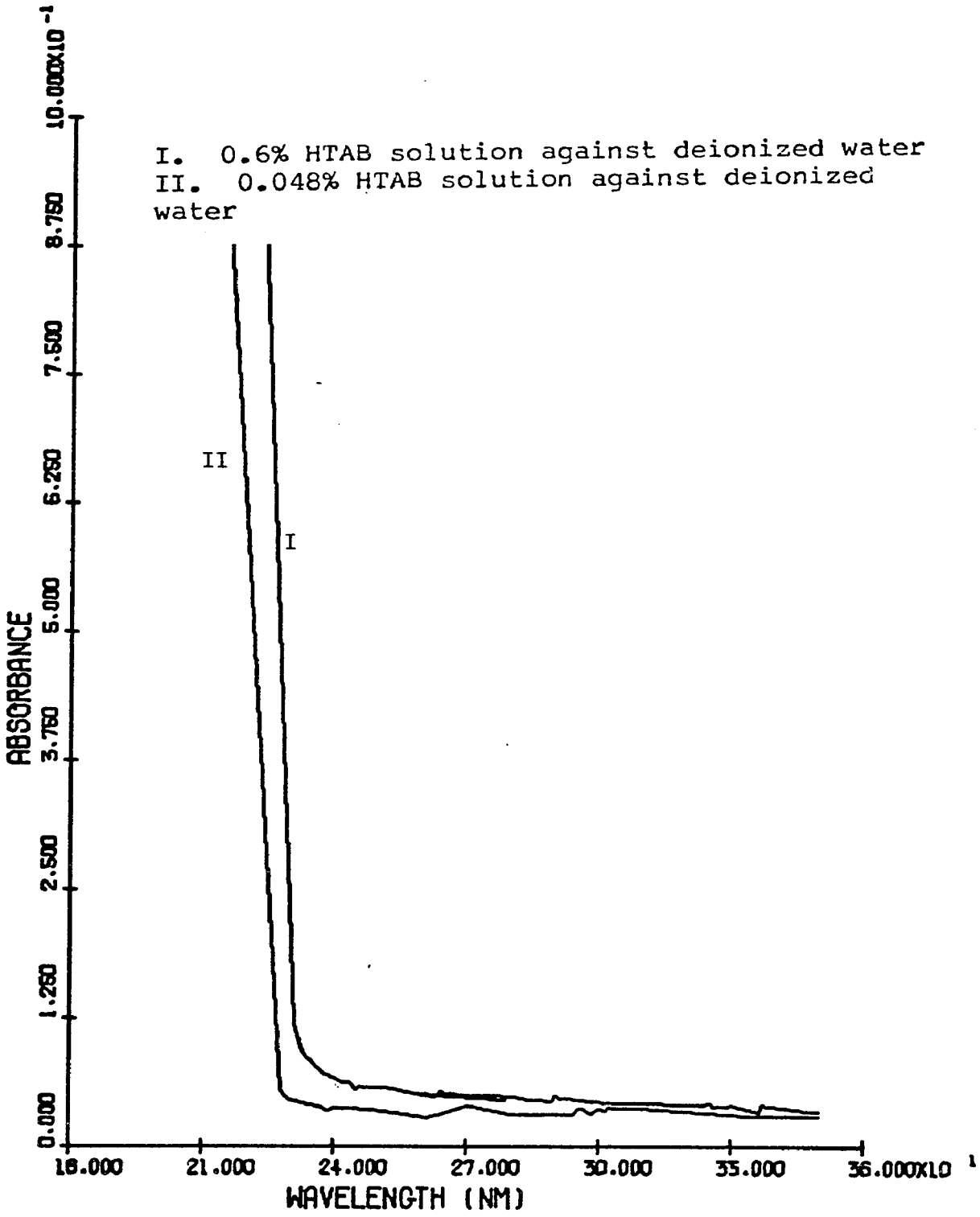

Figure 5-11 Absorption spectra of 0.048% HTAB solution and 0.6% HTAB solution against deionized water.

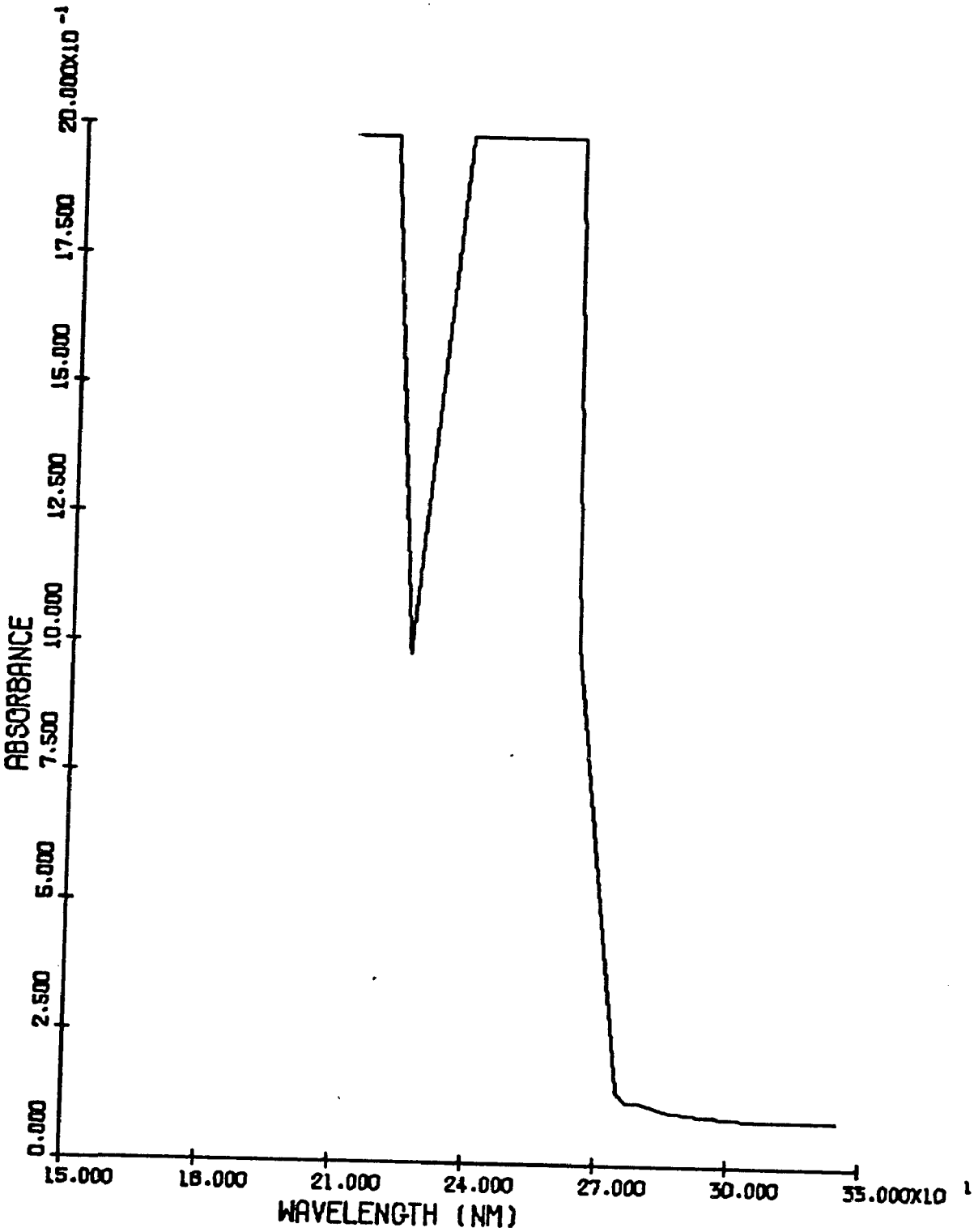

Figure 5-12 Absorption spectrum of 0.02 M benzene in 0.6% HTAB solution against deionized water.

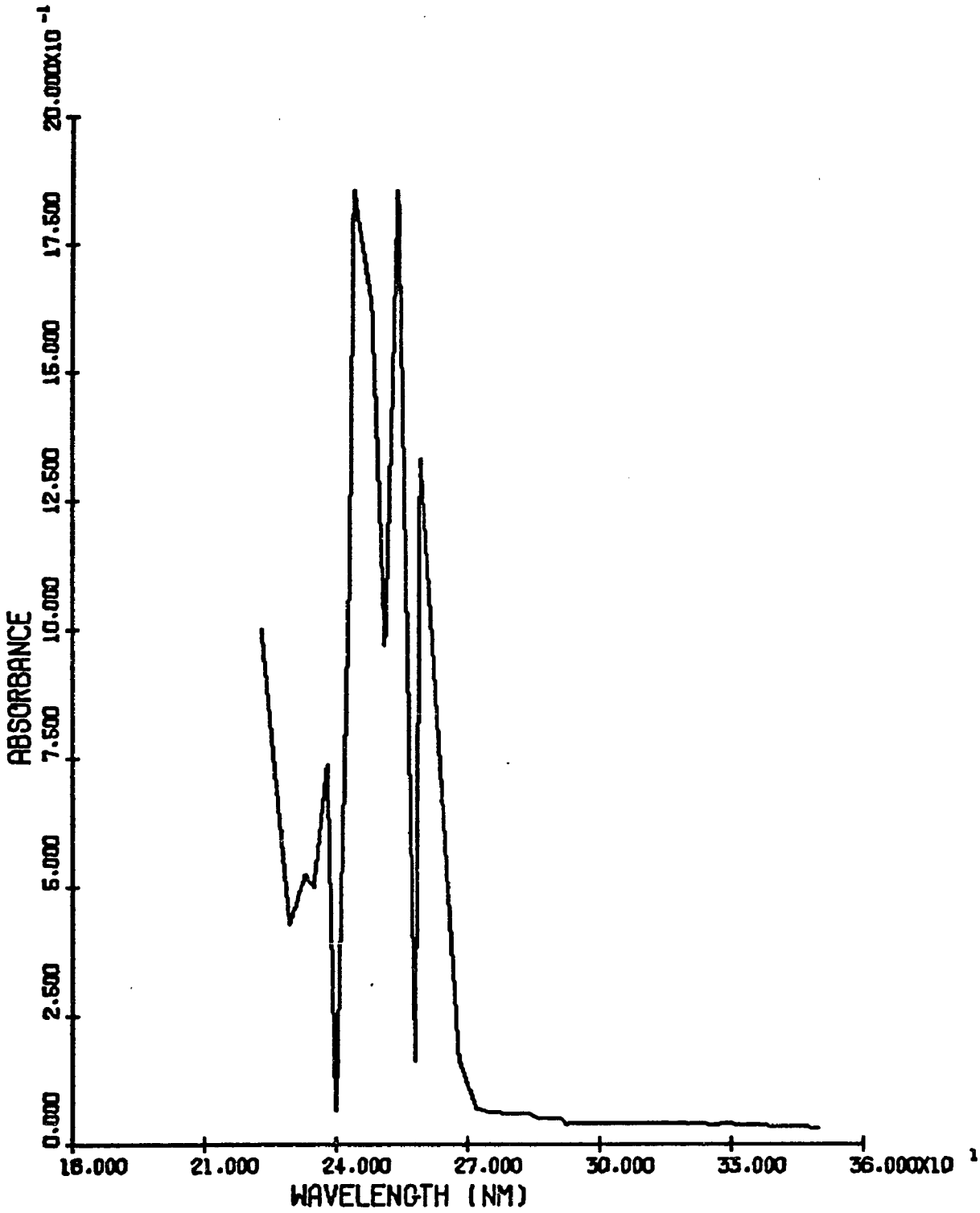

Figure 5-13 Absorption spectrum of 0.01 M benzene in 0.6% HTAB solution against deionized water.

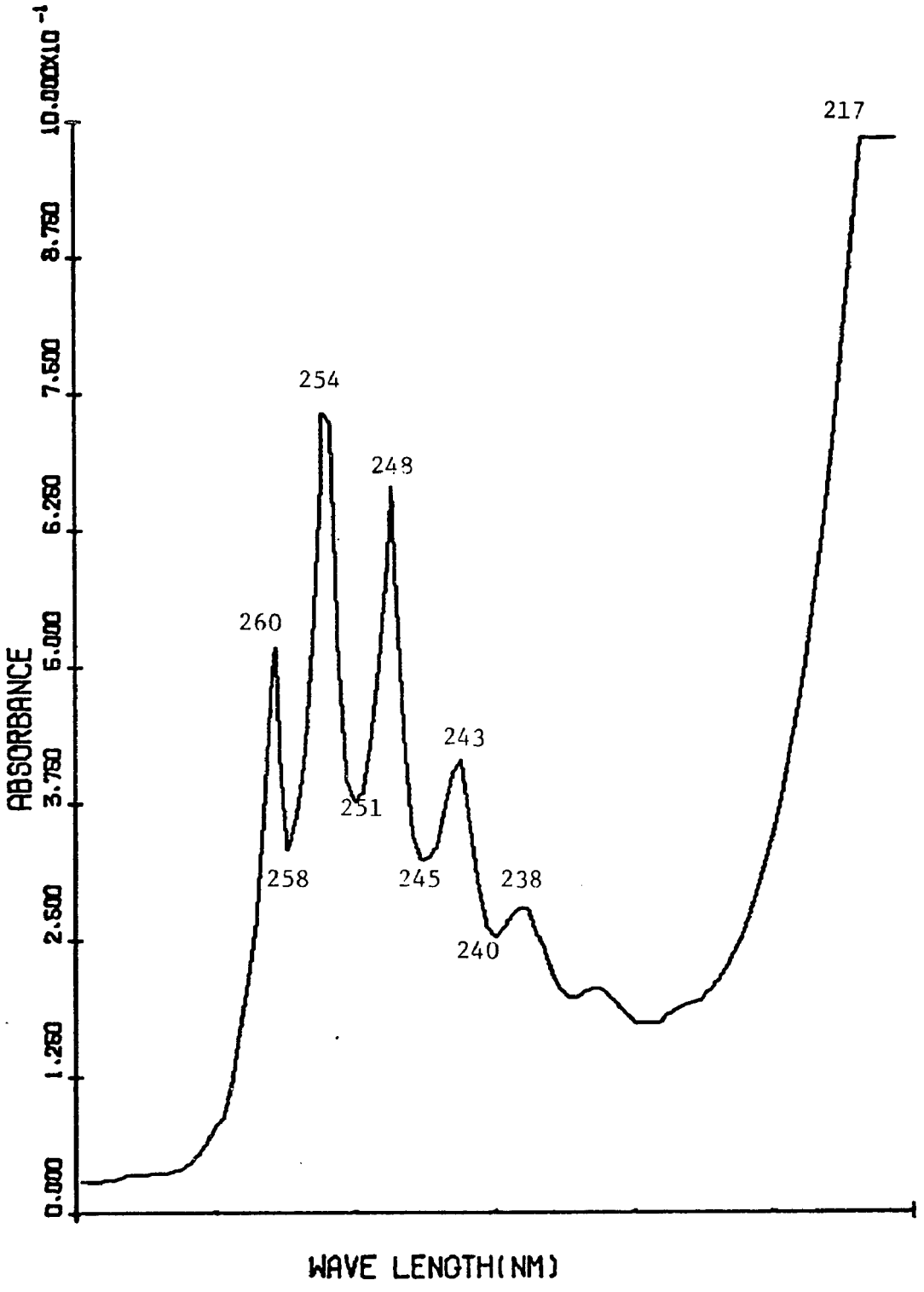

Figure 5-14 Absorption spectrum of sample UV-2 diluted to 1/3 against deionized water.

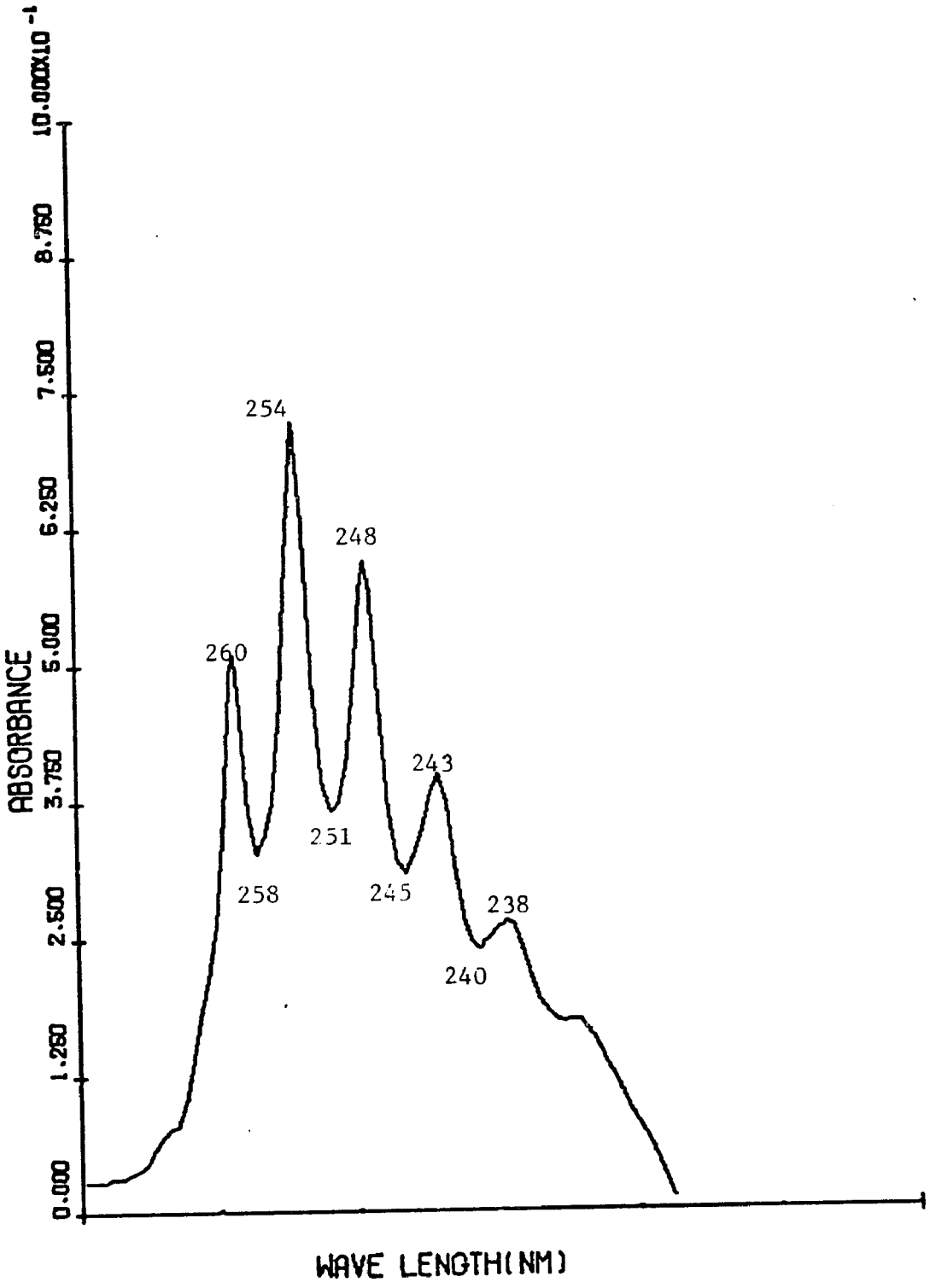

Figure 5-15 Absorption spectrum of sample UV-2 diluted to 1/3 against 0.6% HTAB.

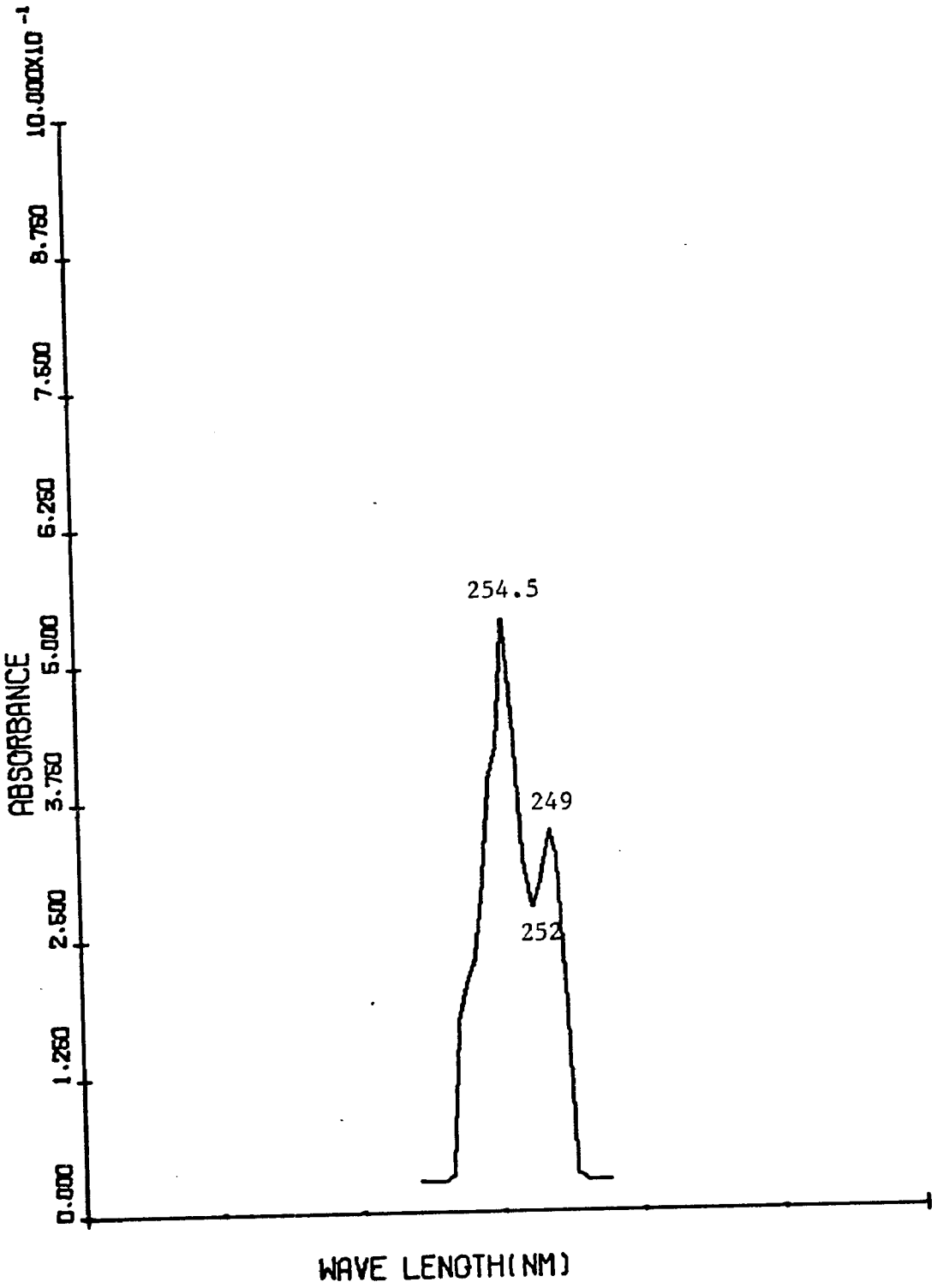

Figure 5-16 Absorption spectrum of sample UV-2 against sample UV-1 diluted to 1/5.

CAHPTER 6 ULTRACENTRIFUGATION

6-1 Introduction

The use of the ultracentrifuge in the study of emulsion stability has attracted considerable attention (1-5). Although the accelerated tests have their intrinsic value, one must be very careful in extrapolating information derived from such tests to predict the future stability behavior of emulsions, because the accelerated tests may modify the mechanism operative at normal condictions (6).

Separation of emulsions upon standing is expressed in the amount of the following parameters: cream, serum and oil. Creaming is measured by the amount of oil-rich layer (cream) and water-rich layer (serum) formed upon standing. The degree of instability is expressed as the percent of oil separated into free oil. As we know, a perfect emulsion system should be a homogeneous and a very unstable emulsion system should have most of the oil separated into free oil with the bottom layer as a serum. Many attempts have been made to measure the emulsion stability in terms of changes in size distribution (7-10), interfacial area (11-15), and otherwise (16-17). However, those based on counting techniques are tedious, time-consuming, and inaccurate. Merrill (18) used a

bucket type centrifuge to determine the emulsion stability, but for stable emulsions, did not separate free oil rapidly enough under these conditions.

Garrett (19) studied highly stable emulsions, measuring the rate of creaming and finding that the results obeyed the Svedberg equation relating distance from the center of rotation to time of centrifugation.

Vold and Groot (1) developed a method to determine the emulsion stability by using the ultracentrifuge to determine the rate of separation of Nujol from Nujol-water emulsions stabilized with sodium lauryl sulfate.

Vold and Mittal (20-24) studied the effect of various operative variables on the kinetics of separation of oil from a variety of oil-in-water emulsions. Rehfeld (25) determined the ultracentrifugal stability of oil-in-water emulsions. He found for C_8 to C_{17} straight chain hydrocarbon emulsions obeyed the empirical equation, $\phi = \phi_o t^{-n}$ where ϕ is the volume fraction of emulsion phase remaining uncoalesced after time t, ϕ_o is its initial volume, and n an empirical constant. Vold and Hahn (26, 27) showed that the kinetics of ultracentrifugal separation of oil from emulsion could be expressed in terms of classical rate equation for zero, first, or second order reactions.

Mittal (28) recently made a thorough review on ultracentrifugal studies.

Although all emulsions are thermodynamically unstable with respect to separation into their component phases, they may remain unchanged for a certain period depending on external conditions.

One accelerated test for studying emulsion stability is the measurement of the amount of continuous phase separated as a function of time when the emulsion is subjected to ultracentrifugal stress. Such a measurement is powerful in comparing the stability of different stabilizing agents with respect to the same oil-in-water system emulsions. As an emulsion deteriorates, it will undergo creaming, flocculation, coalescence, and finally cause phase separation.

Creaming is not a measurement of true stability since the discontinuous phase remains as drops, and can be redispersed by shaking, but it will result in phase separation.

Flocculation and coalescence are different terminologies. Flocculation is the aggregation of droplets; however, all droplets maintain their identity; it is a reversible process. Nevertheless, coalescence is an actual phase separation and irreversible process, the droplets losing their identity. In order to differentiate between coalescence and flocculation, Mittal (29) suggested using "micro-instability" and "macro-instability",

respectively.

In order to correlate the conductometric titration curve to the stability of the emulsion, as well as to the effect of a number of parameters on the stability of the emulsion, the ultracentrifugation method was used.

A mechanism for the stabilization/destabilization of these emulsions will be discussed based on both the theory and experimental data.

This study was carried out using the International Model B-35, and the International Equipment Company (IEC).

6-2 Effect of Operating Variables on Ultracentrifugal Stability

6-2-1 Surfactant Concentration Effect

Vold and Groot (1) investigated the effect of emulsifier concentration on the stability of Nujol-water-SLS emulsions. The results showed that the ultracentrifugal stability increased with increasing initial concentration of SLS until the equilibrium concentration in the aqueous phase reached the CMC. Thereafter, it is nearly independent of concentration. The increased stability is attributed to an increase in surface coverage of absorbed surfactant, the limiting value being due to attainment of saturation absorption.

Rehfeld (30) worked on benzene-in-water emulsions stabilized with SLS. It was also found that the

mechanical stability increased with increasing surfactant concentration until the CMC is reached. The relation between mechanical stability and time of ultracentrifugation was found to be non-linear for SLS concentrations below the CMC.

Mittal and Vold (20, 21) determined the effect of varying concentrations of non-ionic surfactants (Tween 20, Triton X-100) on the ultracentrifugal stability of Nujol-water emulsions, and of SLS on olive oil-water emulsions. In most cases the separation of oil with time was accurately represented by the empirical equation.

$$\frac{t}{x} = \frac{1}{ab} + \frac{t}{a}$$

where x = the percent oil separated at time t

a = extrapolated maximum amount of oil which would have separated after infinite time

b = experimental constant

When Vold and Hahn (26) replotted these data, they found the separation of oil from emulsions followed zero-, first-, and second-order kinetic expressions.

The stability increased continuously with increasing concentration of nonionic surfactant even though the equilibrium concentration of the emulsifier would have been above the CMC.

6-2-2 Effect of the Interfacial Area or Interfacial Effect

Published studies concerning the effect of drop size on the stability of emulsions is rather contradictory. Cockbain and McRoberts (31) reported that the stability increases with decreasing drop size. There are, likewise, some opposing conclusions (32-34), that is, stability decreases with decreasing size. Stanko (35) said there is no obvious relationship. Others have found a relationship that depends on both the nature of the oil and the surfactant. The decreasing average drop size will increase the surface absorption area of the emulsion.

6-3 The Preparation of Samples

The method of emulsion preparation should produce emulsions with identical drop size distributions from each preparation starting with systems of equal composition. This condition was difficult to produce even when a standardized procedure was followed, and therefore each emulsion was tested immediately after its preparation.

Table 6-1 shows the recipes of emulsions 1 to 18. Emulsions 1-4 were prepared at 63^{o}C by adding 10 cc benzene to the mixed emulsifier systems with the same molar ratio of HTAB to fatty alcohol but changing the chain length of the fatty alcohol. The molar ratio of HTAB to fatty alcohol is kept at 1:3. Emulsions 7-12

Table 6-1 Recipes of Sample 1 to Sample 18

25 ml deionized water plus:	molar ratio
1. 0.15 gm HTAB + 0.4784 gm cholesterol	1:3
2. 0.15 gm HTAB + 0.30gm cetyl alcohol	1:3
3. 0.15 gm HTAB + 0.195 cc n-octanol	1:3
4. 0.15 gm HTAB + 0.134 cc n-amyl alcohol	1:3
5. 0.15 gm HTAB + 0.30gm cetyl alcohol	1:3
6. 0.15 gm HTAB	
plus 10cc benzene at 63°C	
25 ml deionized water plus:	
7. 0.15 gm HTAB + 0.05 gm cetyl alcohol	1:0.5
8. 0.15 gm HTAB + 0.10gm cetyl alcohol	1:1
9. 0.15 gm HTAB + 0.20gm cetyl alcohol	1:2
10. 0.15 gm HTAB + 0.30gm cetyl alcohol	1:3
11. 0.15 gm HTAB + 0.40gm cetyl alcohol	1:4
12. 0.15 gm HTAB	
plus 10 cc styrene at 63°C	
25 ml deionized water plus:	
13. 0.15 gm HTAB + 0.033 gm cetyl alcohol	1:0.33
14. 0.15 gm HTAB + 0.50gm cetyl alcohol	1:0.5
15. 0.15 gm HTAB + 0.10gm cetyl alcohol	1:1
16. 0.15 gm HTAB + 0.30gm cetyl alcohol	1:3
17. 0.15 gm HTAB + 0.60gm cetyl alcohol	1:6
18. 0.15 gm HTAB	
plus 10 cc benzene at 63°C	

were prepared at 63°C by adding 10 cc styrene to mixed emulsifier systems (with varying ratios) of HTAB to cetyl alcohol. Emulsions 13-18 were prepared at 63°C by adding 10 cc benzene to the mixed emulsifier system of HTAB and cetyl alcohol while varying their molar ratios.

Emulsions 1-4, 7-12 and 13-18 were prepared in the following manner:

1. Together 0.15 gm HTAB and varying amounts of fatty alcohol at desired molar ratios were added to 2 oz bottles containing 25 cc deionized water. These mixed emulsifier solutions were placed in a vigorously stirred water bath at 63°C for 2 hours, and then tumbled for another 2 hours.

2. Then 10 cc benzene (or styrene) was added and the bottles were tumbled for another hour to make an emulsion.

Samples 5-6 were prepared by placing the mixed emulsifier solutions in a water bath and stirring for one half-hour. Then benzene was added and the system was emulsified for another half-hour as in 1-4.

Samples 2 and 5 have the same recipe, the duplication being made to check the effect of the emulsification process.

The stability of the emulsion was measured by ultracentrifugation in each of four methods. All the samples above which were centrifuged at 10,000 rpm for 10 minutes

are labeled "a"; samples centrifuged at 15,000 rpm for 20 minutes are labeled as "b"; and samples centrifuged at 20,000 rpm for 20 minutes, are labeled as "c". All the samples above contained about 9 cc of emulsion. As a check on the reliability of the measurements, 4.3 cc samples of the emulsions 7-18 were centrifuged at 15,000 rpm for 10 minutes. These samples are labeled "d".

6-4 Results and Discussion for IEC-35

In order to correlate the conductometric titration curve of oils in mixed emulsifier system to the stability of the emulsion, ultracentrifugation is used.

Tables 6-2 to 6-9 show the results for the three sets of recipes, with varying ultracentrifugal speeds and times as well as oil additives.

The stability criteria of emulsions is not well established for ultracentrifugation studies. By observation, the final solution could be divided into three parts, i.e., oil phase (A), cream phase (B), and water phase (C). Using these divisions, the observations can also be categorized in three ways as follows:

1. Part A, B, C were separated clearly.
2. Only Part B and Part C could be seen.
3. No separation.

Of course, the stability order for the categories is $3 > 2 > 1$. Comparison is also possible for emulsions in

Table 6-2 Ultracentrifugation Data of 1-a to 6-a

Sample #	1-a	2-a	3-a	4-a	5-a	6-a
h_1	0.8	4.0	5.1	5.1	4.4	4.97
h_2	5.9	6.1	6.2	6.0	6.2	5.6
h_3	5.9	6.1	6.9	6.7	6.2	6.6
oil phase h_3-h_2	0	0	0.7	0.7	0	1.0
cream phase h_2-h_1	5.1	2.1	1.1	0.9	1.8	0.63
water phase h_1	0.8	4.0	5.1	5.1	4.4	4.97
% of oil	0	0	10.15	10.45	0	15.15
% of cream	86.44	34.43	15.94	13.43	29.03	9.55
% of water	13.56	65.57	73.91	76.12	70.97	75.3

h_1 the height of the boundary between water phase and cream phase

h_2 the height of the boundary between cream phase and the oil phase

h_3 the total height of the sample

Table 6-3 Ultracentrifugation Data of 1-b to 6-b

Sample #	1-b	2-b	3-b	4-b	5-b	6-b
h_1	4.2	4.3	4.55	4.3	3.8	4.5
h_2	6.4	6.4	5.7	5.7	5.0	4.8
h_3	6.4	6.4	6.4	7.1	5.0	6.35
oil phase h_3-h_2	0	0	0.7	1.4	0	1.55
cream phase h_2-h_1	2.2	2.1	1.15	1.4	1.2	0.3
water phase h_1	4.2	4.3	4.55	4.3	3.8	4.5
% of oil	0	0	10.94	19.72	0	24.41
% of cream	34.38	32.81	17.97	19.72	24.0	4.72
% of water	65.62	67.19	71.09	60.56	76.0	70.87

h_1 the height of the boundary between water phase and cream phase

h_2 the height of the boundary between cream phase and the oil phase

h_3 the total height of the sample

Table 6-4 Ultracentrifugation Data of 7-a to 12-a

Sample #	7-a	8-a	9-a	10-a	11-a	12-a
h_1	5.2	4.1	3.93	3.75	4.05	4.97
h_2	6.25	6.3	6.3	6.3	6.3	5.6
h_3	6.25	6.3	6.3	6.3	6.3	6.6
oil phase h_3-h_2	0	0	0	0	0	1.0
cream phase h_2-h_1	1.05	2.2	2.37	2.55	2.25	0.63
water phase h_1	5.2	4.1	3.93	3.75	4.05	4.97
% of oil	0	0	0	0	0	15.15
% of cream	16.8	34.92	37.62	40.48	35.71	9.55
% of water	83.2	65.08	62.38	59.52	64.29	75.3

h_1 the height of the boundary between water phase and cream phase

h_2 the height of the boundary between cream phase and the oil phase

h_3 the total height of the sample

Table 6-5 Ultracentrifugation Data of 7-c to 12-c

Sample #	7-c	8-c	9-c	10-c	11-c	12-c
h_1	4.45	4.15	4.3	4.25	4.28	4.30
h_2	6.1	6.15	6.2	6.3	6.1	4.35
h_3	6.35	6.3	6.2	6.3	6.2	6.2
oil phase h_3-h_2	0.25	0.15	0	0	0.1	1.85
cream phase h_2-h_1	1.65	2.0	1.9	2.05	1.82	0.05
water phase h_1	4.45	4.15	4.3	4.25	4.28	4.3
% of oil	3.94	2.38	0	0	1.61	29.84
% of cream	25.98	31.75	30.65	32.54	29.55	0.806
% of water	70.08	65.87	69.35	67.57	69.03	69.35

h_1 the height of the boundary between water phase and cream phase

h_2 the height of the boundary between cream phase and the oil phase

h_3 the total height of the sample

Table 6-6 Ultracentrifugation Data of 7-d to 12-d

Sample #	7-d	8-d	9-d	10-d	11-d	12-d
h_1	1.62	1.45	2.1	1.95	1.85	2.10
h_2	2.9	2.83	3.05	3.1	3.0	2.15
h_3	3.2	3.1	3.05	3.1	3.2	3.1
oil phase h_3-h_2	0.3	0.27	0	0	0.2	0.95
cream phase h_2-h_1	1.28	1.38	1.05	1.15	1.15	0.05
water phase h_1	1.62	1.45	2.0	1.95	1.85	2.10
% of oil	9.38	8.71	0	0	6.25	30.65
% of cream	40	47.52	34.43	37.10	35.94	16.13
% of water	50.63	46.77	65.57	62.90	57.81	67.74

h_1 the height of the boundary between water phase and cream phase

h_2 the height of the boundary between cream phase and the oil phase

h_3 the total height of the sample

Table 6-7 Ultracentrifugation Data of 13-b to 18-b

Sample #	13-b	14-b	15-b	16-b	17-b	18-b
h_1	3.2	4.35	4.3	4.2	4.1	4.5
h_2	5.4	6.1*	6.1	6.2	6.0*	4.8
h_3	5.5	6.1	6.1	6.2	6.0	6.35
oil phase h_3-h_2	0.1	little	0	0	little	1.55
cream phase h_2-h_1	2.2	1.75	1.8	2.0	1.9	0.3
water phase h_1	3.2	4.35	4.3	4.2	4.1	4.5
% of oil	1.82	little	0	0	little	24.41
% of cream	40	28.69	29.51	32.26	31.67	4.72
% of water	58.18	71.31	70.49	67.74	67.23	70.87

* oil layer is not clear

h_1 the height of the boundary between water phase and cream phase

h_2 the height of the boundary between cream phase and the oil phase

h_3 the total height of the sample

Table 6-8 Ultracentrifugation Data of 13-c to 18-c

Sample #	13-c	14-c	15-c	16-c	17-c	18-c
h_1	4.0	4.3	4.2	4.3	4.1	4.30
h_2	5.7	6.1*	6.15*	6.1	5.9	4.35
h_3	6.0	6.1	6.15	6.1	6.2	6.2
oil phase h_3-h_2	0.3	little	little	0	0.3	1.85
cream phase h_2-h_1	1.7	1.8	1.95	1.8	1.8	0.05
water phase h_1	4.0	4.3	4.2	4.3	4.1	4.4
% of oil	5.0	little	little	0	4.84	29.84
% of cream	28.33	29.59	31.71	29.51	29.03	0.806
% of water	66.67	70.5	68.29	70.49	66.13	69.35

* oil layer is not clear

h_1 the height of the boundary between water phase and cream phase

h_2 the height of the boundary between cream phase and the oil phase

h_3 the total height of the sample

Table 6-9 Ultracentrifugation Data of 13-d to 18-d

Sample #	13-d	14-d	15-d	16-d	17-d	18-d
h_1	3.95	4.4	4.3	4.2	4.2	4.4
h_2	5.5	6.05	6.15*	6.2*	5.9	4.45
h_3	5.85	6.2	6.15	6.2	6.3	6.2
oil phase h_3-h_2	0.35	0.15	little	little	0.4	1.75
cream phase h_2-h_1	1.55	1.65	1.85	2.0	1.7	0.05
water phase h_1	3.95	4.4	4.3	4.2	4.2	4.4
% of oil	5.98	2.42	little	little	6.35	28.23
% of cream	26.5	26.6	30.08	32.26	26.98	0.806
% of water	67.52	70.97	69.92	67.74	66.67	70.97

* oil layer is not clear

h_1 the height of the boundary between water phase and cream phase

h_2 the height of the boundary between cream phase and the oil phase

h_3 the total height of the sample

the same category.

For number 1, more oil phase (A) means the sample emulsion is less stable. For number 2, the more cream phase (B) means the sample emulsion is more stable.

According to these criteria, the stability order of samples 1-6 at conditions "a" and "b" are 1> 2 >5 > 3> 4 > 6. The stability of 2 and 5 are similar as expected.

If the same criteria are applied to sample 7-12, the stability order at condition "a" is 10> 9> 8 >11 > 7 >12, at condition "c" is 10> 9> 8 >11 > 7 >12, and at condition "d" is 10> 9 >11 > 8 > 7 >12. That means that an optimum amount of cetyl alcohol in the mixed emulsifier system will give maximum stability of the emulsion. More or less cetyl alcohol than the optimum amount will decrease the stability of the emulsion. The data shows the most stable emulsion is obtained at the 1:3 molar ratio of HTAB to cetyl alcohol. The stability of the emulsion using HTAB and cetyl alcohol in the molar ratio 1:1 and 1:4 are similar.

By applying the same criteria to samples 13-18, the stability order varied depending on the ultracentrifuge conditions. For conditions "b," the stability order is 16 > 15 > 17 > 14 > 13 > 18. For condition "c," the stability order is 16 > 15 >14 > 17 > 13 > 18. For condition "d," the

stability order is 16 > 15 > 13 > 17 > 18. It is observed that the stability of sample 17 varied as a function of ultracentrifugal speed and time. It is found that in the mixed emulsifier system containing 0.15 gm HTAB and 0.60 gm cetyl alcohol, a molar ratio 1:6, there is no observed descending leg when benzene is titrated into this mixed emulsifier system and the conductance is followed.

An interesting phenomenon is that for a stable emulsion, while increasing ultracentrifugal rate and time, the cream phase will decrease and the water phase will increase. For an unstable emulsion, while increasing ultracentrifugal rate and time, the cream phase will increase, the water phase decrease, and the oil phase increase. This suggests that for stable emulsions the water will be separated before the oil during ultracentrifugation. For unstable emulsions, the water will go back to the cream phase while the oil goes out.

The conductometric titration of benzene or styrene into aqueous solutions containing a mixed emulsifier system gives the characteristic curve as Figure 6-1.

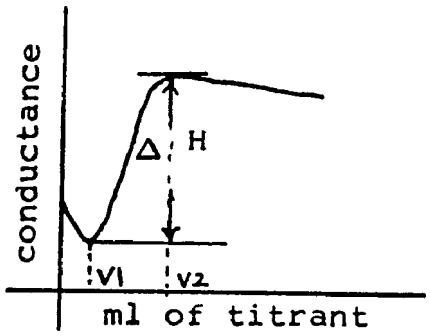

Figure 6-1 Characteristic Conductometric Titration Curve

Differences in these characteristic curves are a function of the mixed emulsifier molar ratio as well as the chain length of fatty alcohol in the systems. It is believed that a certain portion of the characteristic curve will relate to the stability of the emulsion. In order to check this hypothesis, ultracentrifugation is employed to study the emulsion stability.

Table 6-10 shows the conductivity difference between two critical volumes V1 and V2 (ΔH). The stability obtained from ultracentrifugation is also shown.

The results show that ΔH of the characteristic conductometric titration curve is strongly correlated to the stability of the emulsion.

For samples 1-6 and 7-12, the order of increasing stability from ultracentrifugation and ΔH agree reasonally well. The only exception is sample 11 which has a higher ΔH (27.5) than sample 9 (25.0) with less stability but the difference may not be significant.

In the series 13-18, it is found for sample 17 that

Table 6-10 Correlating the ΔH from conductometric titration curve to ultracentrifugation stability

No.	ΔH	No.	ΔH	No.	ΔH
1	41.56	7	7.5	13	5.0
2	32.5	8	17.5	14	10.63
3	13.75	9	25.0	15	27.5
4	--	10	32.5	16	32.5
6	--	11	27.5	17	31.9
		12	--	18	--

Stability from Ultracentrifugation 1>2>3>4>6

Stability from Ultracentrifugation 10>9>11>8>7>12

Stability from Ultracentrifugation at condition

b: 16>15>17>14>13>18

c: 16>15>14>17>13>18

d: 16>15>14>13>17>18

the ultracentrifugation stability is a function of ultracentrifugal speed. The stability of sample 17 decreases as the ultracentrifugal speed increases. Note, however, that the conductometric titration curve of sample 17 does not have an initial descending leg, which means that there is no solubilization process. Presumbly, the solubilization process is correlated with ultracentrifugal stability.

6-5 Model of Ultracentrifugation Instability

Based on the data obtained from ultracentrifugation, a proposed mechanism of coagulation is made. A schematic diagram is shown Figure 6-2.

There are three phases that can be observed in the ultracentrifuged emulsion, the oil phase, the cream phase and the water phase.

A phase separation occurs in the homogeneous emulsion when ultracentrifugal force is applied. The oil droplets will float upward while the water is forced downward. A water phase will be observed as soon as the ultracentrifugal force is applied. The concentrated emulsion layer is called the cream phase.

The oil concentration in the cream phase is higher than the oil concentration in the homogeneous oil in water emulsion. A critical force is needed to condense the oil

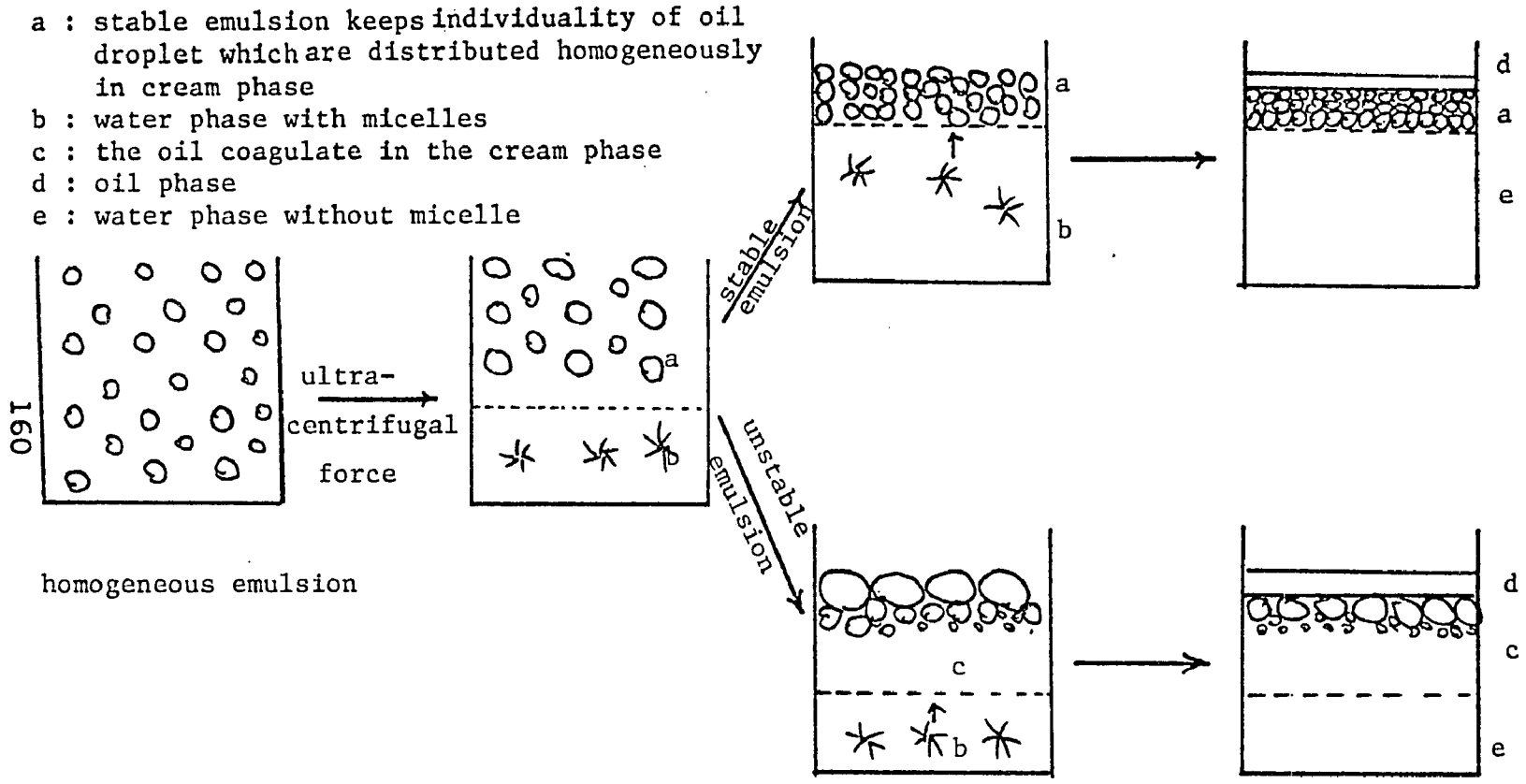

Figure 6.2 A schematic diagram of the proposed stability mechanism of emulsion

droplets in the cream layer. Ultracentrifugal speed is directly related to this phase separation force.

It is found that for stable emulsions, the size of water layer will increase with increasing ultracentrifugal speed. But, an opposite phenomenon is observed in unstable emulsions. Presumably, the oil in the cream phase plays a very important role. For stable emulsions the oil droplet tries to maintain its individuality, and therefore the oil droplets are homogeneously dispersed within the cream phase. The water can always be kept between the particles. While the ultracentrifugal speed increases, the oil droplets will be pressed closer together until the critical force reached, and the oil droplets will coagulate to form an oil phase. Meanwhile the amount of water in water layer will continue increasing. For unstable emulsions, the oil droplets will coagulate in the cream layer under the ultracentrifugal force. An oil concentration gradient occurs in the cream layer and to a certain extent, the lower portion of the cream phase will contain condensed mixed emulsifier and water. It is possible that this bottom portion of the cream phase might be pressed downward into the water phase with increasing ultracentrifugal speed.

Initially, the water layer must contain many micelles in which oil is solubilized. The ultraviolet data shows

that the concentration of benzene in the water layer of ultracentrifuged emulsion is 0.01M. This is the solubility of benzene in water. The micelles that exist in the water phase can be separated by ultracentrifugation but only the molecular scale species are able to exist in the water phase under ultracentrifugal forces.

The stability mechanism of the emulsion can be divided into two categories: a stable emulsion and an unstable emulsion.

For a stable emulsion the oil droplets have a tendency to keep their individualty until the oil phase separation occurs. In other words the oil droplet exists individually in the cream phase.

For an unstable emulsion the oil droplets begin to float upwards and no longer have a tendency to maintain their individualty, with coagulation occurring in the cream phase. A little force is needed to cause oil phase separation.

In order to check the coagulation mechanism using ultracentrifugation, the SPINCO-E analytical ultracentrifuge was employed. A characteristic picture of layer location obtained from a photograph of an emulsion during ultracentrifuge and the analysis is shown in appendix 9.

SPINCO-E analytical ultracentrifuge has been widely employed by Vold et al (1,20-27) in studying the effect of various operative variables on the kinetics of separation

TABLE 6-11 The percentage of oil in cream phase at various ultracentrifugal speeds for sample 16

Time	Pct. of oil in cream phase at various rpm 25,980 rpm	31410 rpm	34600 rpm	39460 rpm
2.4	98.88	101.05	88.12	56.38
4.0	101.33	99.54	87.77	55.88
6.0	100.82	99.66	86.58	55.39
8.0	100.64	99.11	84.93	55.05
16.0	101.67	98.63	64.87	53.16
24.0	101.04	98.54	52.53	52.96
32.0	101.88	97.90	47.39	52.77
40.0	102.55	95.46	44.68	52.59
48.0	101.47	89.08	43.90	52.04
56.0	98.33	85.79	44.20	51.64
64.0	94.94	79.90	44.10	51.05
72.0	93.60	77.95	42.95	50.60
80.0	90.37	77.08	38.23	48.34
88.0	89.28	76.70	42.81	48.16

of oil from a variety of oil in water emulsions. Several attempts (21,27,36) have been made to identify all the processes involved in the separation of oil from oil in water emulsions under ultracentrifugal conditions. Interest has centered on the dynamic properties involving the rate of draining of an aqueous solution from oil drops.

Assuming the oil exists only in the oil phase and the cream phase, the volume of oil phase subtracted from the volume of the total oil should be the volume of oil in the cream phase. The percentage of oil in the cream phase can be now calculated.

Table 6-11 shows the percentage of oil in the cream phase (OC) at various ultracentrifugal speeds for sample 16. It is found that at lower ultracentrifugal speeds, i.e., 25,980 and 31,410 rpm, the OC values obtained were greater than 100%; this supports the possible argument that the solubilized oil in the water phase will be centrifuged to the cream phase. At higher ultracentrifugal apeeds, the OC values are lower; this indicates that the ultracentrifugal force is sufficiently large to separate the solubilized oil from the water phase initially. All this information supports the coagulation mechanism.

6-6 References

1. R.D. Vold and R.C. Groot, J. Phys. Chem. 66. 1969 (1962).
2. K.L. Mittal, J. Soc. Cosmet. Chem. 22, 815 (1971).
3. E.R. Garrett, J. Pharm. Sci. 54, 1557 (1965).

4. R.C. Groot, "The Ultracentrifugation of Oil in Water Emulsions," Ph.D. Dissertation, U. of Utrecht (1965).

5. S.J. Rehfeld, J. Phys. Chem. 66, 168 (1962).

6. K.L. Mittal and A.U. Hahn, ABS PAP ACS, 172 (1976).

7. S. Berkman, J. Phys. Chem. 39, 527 (1935).

8. P. Sherman, Proc. 4th Int. Congr. Surface Active Substances, Vol. 2, 1199 (1967).

9. H.H.G. Jellinek, J. Soc. Chem. Ind., 69, 225 (1950).

10. J. Boyd, C. Parkinson and P. Sherman, J. Colloid & Inter. Sci. 41, 359 (1972).

11. A. King and L.N. Mukerjee, J. Soc. Chem. Inc. 57, 431 (1938).

12. A. King and L.N. Mukerjee, J. Soc. Chem. Ind. 58, 243 (1939).

13. L.N. Mukerjee and S.N. Srivastava, Kolloid Z. , 147, 146 (1956).

14. H. Lotzkar and D. Maclay, Ind. Eng. Chem., 35, 1294 (1943).

15. N.E. Lloyd, J. Colloid Sci., 14, 441 (1959).

16. P. Becher, "Emulsions: Theory and Practice" 2nd ed., Reinhold Publishing Corp., New York 172 (1965).

17. K.J. Lissant, "Emulsions and Emulsion Technology" Part I, Marcel Dekker, New York (1974).

18. R.C. Merrill, Ind. Eng. Chem. (Anal. Ed.) 15, 743 (1943).

19. E.R. Garrett, J. Pharm. Sci. 51, 35 (1962).

20. K.L. Mittal and R.D. Vold, J. American Oil Chem. Soc., 49, 527 (1972).

21. R.D. Vold and K.L. Mittal, J. Soc. Comet. Chem., 23, 171 (1972).

22. R.D. Vold and K.L. Mittal, J. Pharm. Sci., 61, 869 (1972).

23. R.D. Vold and K.L. Mittal, J. Colloid & Int. Sci., 38, 451 (1972).

24. R.D. Vold and K.L. Mittal, J. Colloid & Int. Sci., 42, 436 (1973).

25. S.J. Rehfeld, J. Colloid & Int. Sci., 46, 448 (1974).

26. R.D. Vold and A.U. Hahn, "Colloidal Dispersions and Micellar Behavior," ACS Symposium Series No. 9, 64-75 (1975).

27. A.U. Hahn and R.D. Vold, J. Colloid & Int. Sci., 51, 133 (1975).

28. K.L. Mittal, "Colloidal Dispersions and Micellar Behavior," ACS Symposium Series No. 9, 76-96 (1975).

29. K.L. Mittal, J. Soc. Cosmet, Chem., 22 815 (1971).

30. S.J. Rehfeld, J. Phys. Chem., 66, 1966 (1962).

31. E.G. Cockbain and T.S. McRoberts J. Colloid Sci., 8, 440 (1953).

32. T. Gillespie and E.K. Rideal, Trans. Famday Soc., 52, 173 (1956).

33. A. King and LN. Makerjee, J. Soc. Chem. Ind., 58, 243 (1953).

34. L.N. Mukerjee and S.N. Srivastava, Kolloid 2., 147, 146 (1956).

35. G.L. Stanko, J. Soc. Cosmet. Chem., 5, 39 (1954).

36. R.D. Vold and R.C. Groot, J. Colloid Sci., 19, 384 (1964).

CHAPTER 7

MATHEMATICAL MODEL

7-1 Introduction:

It is found that the conductometric titration curves resulting from the titration of benzene (or styrene) in water containing a single or mixed emulsifier system, are very different as shown in Figure 2-3. Based on the information obtained from previous chapters, a mathematical model is developed to help in a quantitative understanding of the difference between the two emulsifier systems and to predict the behavior of other systems.

7-2 Titrating Oil Into The Single Surfactant (HTAB) System (Case A)

Two models have been proposed to explain this system.

7-2-1 Model 1: This model has been derived based on the following assumptions.

1. The conductivity is attributed to the soluble surfactant (solute) and the dissociated counterion only.

$$\Lambda = (\Lambda_- + \Lambda_+) + KG$$

2. The conductivity of the cation part of the emulsifier molecule $[C_{16}H_{33}N^+(CH_3)_3]$ is 0.1 of the anion $[Br^-]$ (1).

3. The retardation effect occurs during particle growth stage after the solubilization limit has been

reached.

Based on the above assumptions, the conductivity equation could be written as:

$$F=\underbrace{\left[(\Lambda_+ +\Lambda_-)(1-XV)\right.}_{A}+\underbrace{\left.KG(1+YV)\right]}_{B}\left[U(V)-U(V-V0)\right]\ \underbrace{-Z(V-V0)}_{C}\ \left[U(V-V0)\right] \qquad (7\text{-}1)$$

where F = conductivity

Λ_+ = conductivity of cation

Λ_- = conductivity of anion

V = volume of benzene

V0 = the volume of benzene at critical point (in Figure 2-3)

G = the conductivity of the counterions of the micelles

K = dissociation constant of counterion in the micelle

X = CMC decrease constant

Y = micelle concentration increase constant

Z = retardation constant

U(V-V0) = step function, occurs when V is more than V0C.C

U(V)-U(V-V0)= step function, occurs when V is less than V0C.C

The above equation can be divided into three parts, A, B, and C. Part A accounts for the solute concentration decrease as the volume of benzene increases; Part B represents the increase of the micelle concentration as the volume of benzene increases; Part C accounts for the retardation effect of benzene.

7-2-1-1 Calculations

a) CMC of HTAB at 63°C.

In order to evaluate the CMC of HTAB at 63°C, a plot of log T (temperature) versus log CMC has been made using values reported in the literature (Table 7-1) (2). By extrapolating the CMC of HTAB at 63°C was determined to be 1.38×10^{-3}M.

Table 7-1 CMC of HTAB at Various Temperature

T (°C)	log T	CMC (W*)	log CMC
25	1.40	9.2×10^{-4}	-3.04
45	1.65	1.155×10^{-3}	-2.94
55	1.74	1.32×10^{-3}	-2.88
63	1.80	1.38×10^{-3}	-2.863

* at low concentration $W \doteq M$

b) The distribution of surfactant molecules between the solute form and the micelle form.

0.15 g HTAB is equivalent to $\frac{0.15}{364.46} \times 6.023 \times 10^{23} = 2.479 \times 10^{20}$ molecules.

The molecules in the solute molecules form is

$1.38 \times 10^{-3} \times 6.023 \times 10^{23} \times \frac{25}{1000} = 2.078 \times 10^{19}$ molecules.

the molecules in the micelle form is

$2.479 \times 10^{20} - 2.078 \times 10^{19} = 2.271 \times 10^{20}$ molecules.

c) The conductivity.

It is found that the equivalent ionic conductivity of bromide ion at infinite dilution (25°C) is

$78.4 \times 10^4 \frac{m^2}{ohm\ mole}$ (3)

$\Lambda_- = 78.4 \times 10^4 \frac{m^2}{ohm\ mole} \times 10^{-4} \frac{cm^2}{m^2} \times 1.38.10^{-3}$ mole/1x0.001 $1/cm^3$

$= 1.082 \times 10^{-4} ohm^{-1}\ cm^{-1} = 1.082 \times 10^{-4} / 1.74 \times 10^{-6} = 62.18$ read out.

$\Lambda_+ = \frac{\Lambda_{Br^-}}{10} = 1.082 \times 10^{-5} ohm^{-1} cm^{-1} = 1.082 \times 10^{-5} / 1.74 \times 10^{-6} = 6.218$

read out.

$G = 78.4 \times 10^4 \frac{m^2}{ohm\ mole} \times 10^{-4} \frac{cm^2}{m^2} \times \frac{2.271 \times 10^{20}}{6.023 \times 10^{23}} \times \frac{1000}{25} \frac{mole}{1} \times 0.001\ 1/cm^3$

$= 1.182 \times 10^{-3} ohm^{-1} = 1.182 \times 10^{-3} / 1.74 \times 10^{-6} = 679.6$ read out.

d) the dissociation constant.

The cell constant was determined to be 1.74×10^{-6} $ohm^{-1}\ cm^{-1}$ (4).

At the beginning of the titration (V = 0)

$$132 = (\Lambda_- + \Lambda_+ + KG)/1.74 \times 10^{-6}$$

$$132 = 62.18 + 6.218 + 679.6K$$

K = 0.0936 or 9.36% of the micellar counter ions dissociates.

7-2-1-2 Process and Results

In order to fit the proposed equation (7-1) to the experimental data, a computer program using a trial and error method to determine the constant X, Y, and Z has been written (BMDO7R, Lehigh University Computer Center).

The best fit to the data is determined by Nonlinear Least Square (NLS) method. The variables X, Y, and Z are assigned initial guess values. These values should be independent of the initial guess. The results are shown in Table 7-2.

Table 7-2 The Results of Equation 7-1

	X	Y	Z
Initial guess	0.1	0.1	0.1
NLS fit	0.74843	0.1	2.7999
Initial guess	1.0	1.0	1.0
NLS fit	1.5854	1.0	2.7999
Initial guess	100.0	100.0	100.0
NLS fit	93.656	100.0	2.7999

It is found that X and Y are dependent on the initial guess values implying that these are not two independent variables but rather they are related. Therefore, the original equation should be modified by assuming X = Y, then the equation becomes:

$$F= \left[(\Lambda_+ + \Lambda_-)(1-XV)+KG(1+XV)\right]\left[U(V)-U(V-V0)\right] -Z(V-V0)\left[U(V-V0)\right] \quad (7\text{-}2)$$

The results are shown in Table 7-3.

Table 7-3 The Results of Equation 7-2

	X = Y	Z
Initial value	0.1	0.1
NLS fit	9.3642	2.7999
Initial value	100.0	100.0
NLS fit	9.3642	2.7999

Table 7-3 shows the final calculated values for the constants, X and Z,are now independent of the initial values guessed.

Z is considered to be the retardation constant while X is the CMC decrease constant.

The comparison of this model with the experimental data is shown on Figure 7-1. A good agreement is observed between them.

7-2-2 Model 2: Model 1 did not account for the distribution of surfactant between the solute form and the micelle form (n_1/n_2). This model attempts to do so by assuming that the ratio of their molar concentrations is a function of the volume of titrant in the range of $0 \leq V \leq V0$ This relation is given by:

$$n_1/n_2 = A + Be^{-\alpha V} \qquad (7\text{-}3)$$

where:

n_1 = the molar concentration of surfactant in the solute form

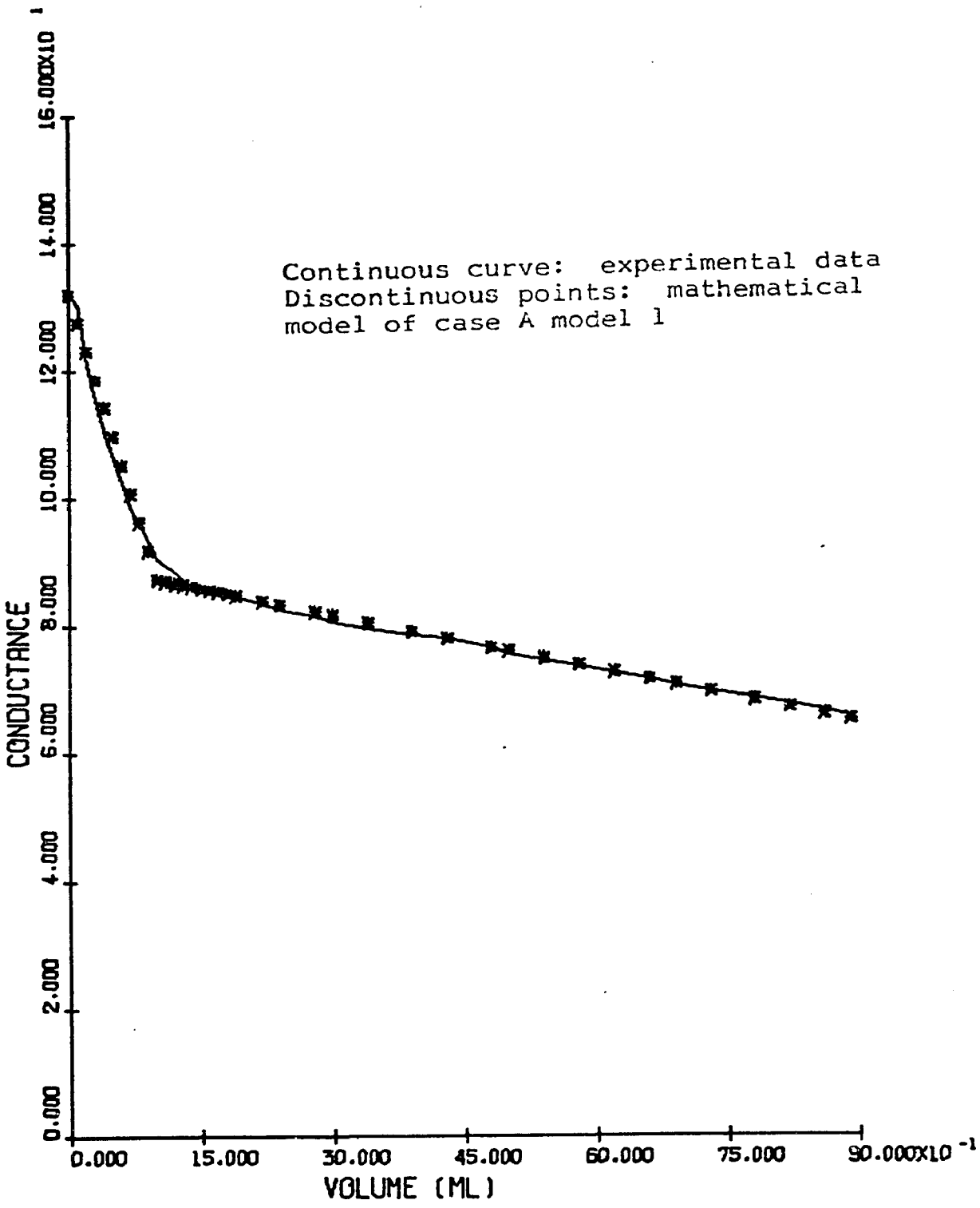

Figure 7-1 Comparison of conductometric titration curve to theoretical prediction for titrating benzene at constant rate of 1 c c /minute into 25 c c. of 0.6% HTAB solution for model I.

n_2 = the molar concentration of surfactant in the micelle form

A, B, α = constants

V = the volume of benzene

V0 = the volume of benzene at critical point

Assume that n_1 decreases and n_2 increases as the volume of benzene increases until the critical point reached. The ratio, n_1/n_2 becomes constant when the volume of benzene exceeds the critical point.

The sum of the surfactant concentrations in solute form and micelle form should be constant.

$$N = n_1 + n_2 \qquad (7\text{-}4)$$

Solve (7-3) (7-4) in the range of $0 \leq V \leq V0$

$$n_1 = N(A + Be^{-\alpha V})/(1.0 + A + Be^{-\alpha V})$$

$$n_2 = N/(1.0 + A + Be^{-\alpha V})$$

The conductance F can be expressed as

$$F = C_1 n_1 + C_2 e^{-\beta(V-V0)}\, n_2\, [U(V-V0)] \qquad (7\text{-}5)$$

where:

F = conductance

C_1 = molar conductance of solute

C_2 = molar conductance of micelle

β = the retardation effect constant

The term $C_2 e^{-\beta(V-V0)}$ represents the decreased mobility of swollen micelle, the retardation effect caused by the growing of particles. In other words, it occurred after the critical point V0.

7-2-2-1 Calculations

$$N = \frac{0.15}{364.46} \times \frac{1000}{25} = 0.01646M$$

$$C_{1+} = 78.4 \times 10^4 \frac{m^2}{ohm\ mole} \times 10^{-4} \frac{cm^2}{m^2} \times .001\ 1/cm^3 \div 1.74 \times 10^{-6}$$

read out

$$= 45057.5 \frac{\text{read out}}{M}$$

$$C_{1-} = 45057.5/10 = 4505.75 \frac{\text{read out}}{M}$$

$$C_1 = C_{1+} + C_{1-} = 45057.5 + 4505.75 = 49363.25 \frac{\text{read out}}{M}$$

By using NLS method, the best fit constants are as follows:

$\alpha = -0.063295$

$\beta = 0.057846$

$A = 1.0649$

$B = -0.96543$

$C_2 = 3725.9$

The identical results were obtained by using different initial guess values, that means all the parameters are independent, and the results are the only answer for the proposed mathematical model.

Based on model two, the ratio of surfactant in the solute

form and the micelle form is:

$$n_1/n_2=1.0649-0.96543\ e^{0.063293V}\left[U(V)\ -\ U(V\ -\ V0)\right]$$

The comparison of this model with the experimental data is shown on Figure 7-2.

7-2-3 Discussion

For case A (single surfactant system), model 1 reveals that X (a constant related to the solute concentration), and Y (a constant related to the micelle concentration), are mutually dependent variables, meaning that the decrease in the CMC corresponds to the increase in the number of micelles. A good agreement was obtained by comparison of this model to experimental data. Model 1 did not account for the distribution of surfactant between the solute form and the micelle form as a function of titrant volume. Model 2 shows that the ratio of surfactant in the solute form to the micelle form (n_1/n_2) is a function of the volume of benzene before the critical point. This ratio becomes constant when the volume of benzene exceeds the critical point. This ratio is given by the following equation:

$$n_1/n_2=1.0649-0.96543\ e^{0.063293V}\left[U(V)-U(V-V0)\right]$$

When $V = 0, n_1/n_2=1.0649-0.96543=0.099$

Model 1 shows $n_1/n_2 = \frac{2.078\times10^{19}}{2.271\times10^{20}} = 0.0915$

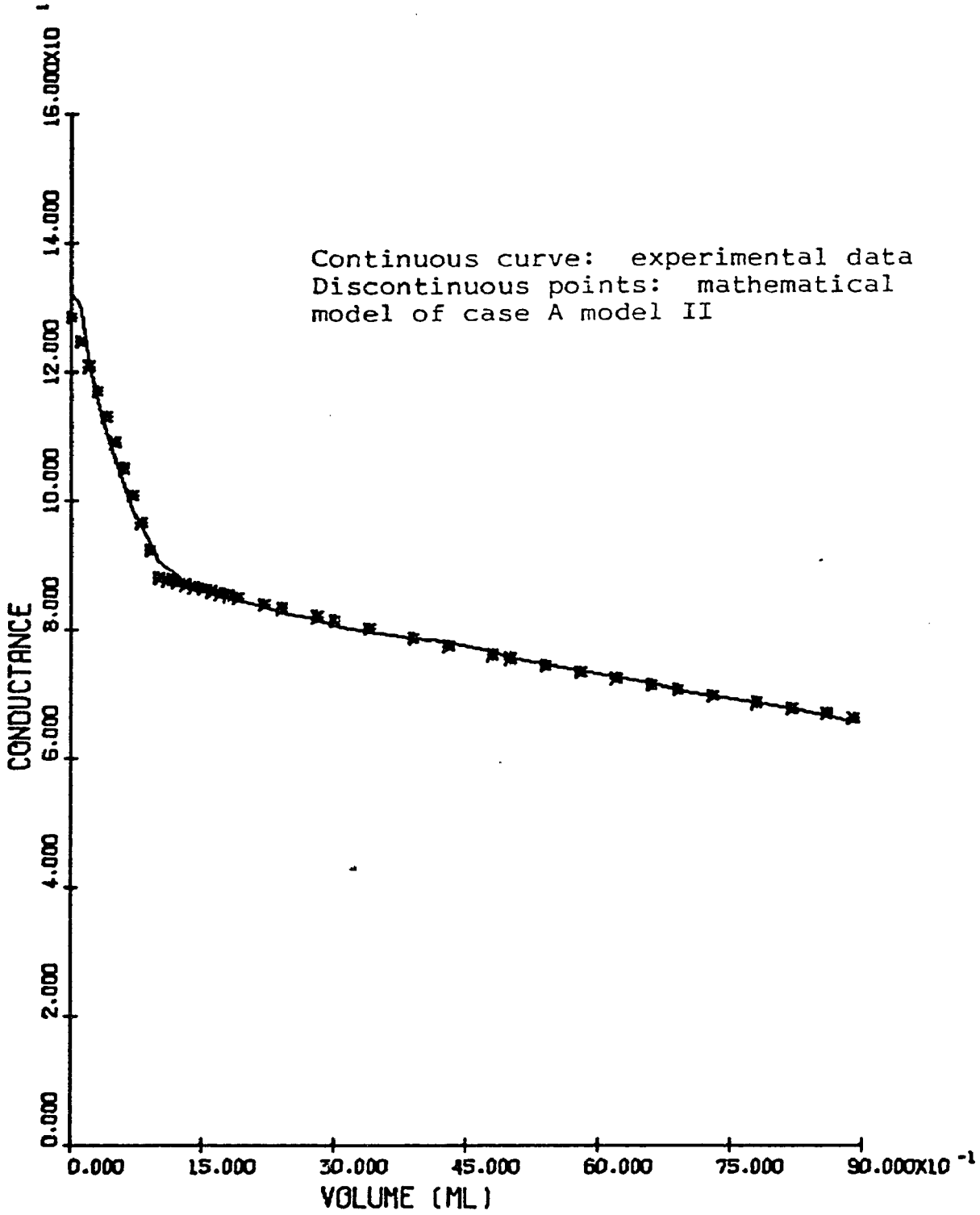

Figure 7-2 Comparison of conductometric titration curve to theoretical prediction for titrating benzene at constant rate of 1 c c /minute into 25 c c of 0.6% HTAB solution for model II.

The agreement is good.

7-3 Titration of Oil in The Mixed Emulsifier Systems (Case B)

The characteristic conductometric titration curve of titrating oil into mixed emulsifier system can be divided into three parts (See Figure 2-3).

I. the initial descending leg

II. the ascending leg

III. the equilibrium part

Examination by Transmission Electron Microscope (TEM), showed the presence of a rod shaped complex formation in the mixed emulsifier systems, which does not exist in a single surfactant system or cetyl alcohol alone.

The diffraction pattern shows that the rods are crystalline. This is an important difference between single surfactant and mixed emulsifier systems. The rods are complex formations of cetyl alcohol and HTAB in an ordered and alternating arrangement.

For Case B, (the mixed emulsifier systems), the ionic surfactant can exist in the aqueous phase in one of three forms: solute, micelle and complex formation of ionic surfactant and fatty alcohol (rod formation). The conductivity of these different forms should decrease in the following order: solute > micelle > rod formation. With cetyl alcohol present with the HTAB system, the solute

HTAB concentration is assumed constant and independent of cetyl alcohol content in the mixed emulsifier system. By varying the amount of cetyl alcohol and/or HTAB, the only change should be the distribution of HTAB molecules between micelles and rod formations. If the amount of cetyl alcohol is increased and since the concentration of HTAB being constant, the number of micelles will decrease, and as a result the conductance should decrease.

Since solubilization of styrene or benzene occurs in the micelles, if there are no micelles then the solubilization process will not occur. Furthermore, the composition of the rods is directly proportional to the molar ratio of HTAB to cetyl alcohol. The highest degree of crystallinity will occur at an optimum ratio of HTAB to cetyl alcohol, above or below which, the excess or deficiency in the amount of HTAB in the rod formation will result in defects in the crystallinity. Because HTAB is an ionic surfactant, it is more hydrophilic compared to cetyl alcohol and the change can be detected by conductometric titration.

Part I of the titration curves in Figure 2-3 can be explained by the solubilization process. The ascending leg of Part II can be attributed to breaking up of the complex formation and the kicking out of the ionic surfactant into the aqueous solution as swollen micelles. Meanwhile the large droplets begin to break up into

small droplets due to the absorption of cetyl alcohol on the surface of the oil droplets. Part III can be explained by a particle growth stage.

V_1, V_2 are two critical volumes on the characteristic curve, the values at different molar ratio of HTAB to cetyl alcohol are shown on Table 7-4.

Table 7-4 The Value of V1, V2 on the Characteristic Titration Curve at Different Molar Ratio of HTAB to Cetyl Alcohol

Molar Ratio HTAB: Cetyl Alcohol	V1 (cc)	V2 (cc)
1:6	0	3.1
1:3	0.3	3.5
1:1	1.2	4.2
1:0.5	2.5	6.4
1:0.33	5.8	7.7

7-3-1 Model: Based on the above picture, a mathematical expression is constructed as given in the following equation:

$$F=P(1)e^{-P(2)V}\left[U(V) - U(V-V1)\right] + P(3)e^{P(4)(V-V1)}\left[U(V-V1) - U(V-V2)\right] + P(5)e^{P(6)(V - V2)}\left[U(V - V2)\right] \quad (7-6)$$

where

P(1) : initial conductance

P(2) : solubilization constant

P(3) : the conductance at V1

P(4) : emulsification constant

P(5) : the conductance at V2

P(6) : particle size growing constant

V1, V2 : the volume at critical points land 2

7-3-2 Results

In order to fit the proposed equation (7-6) to the experimental data, a computer program using a trial and error method to determine the constants P(1) to P(6) has been written. The best fit to the data is determined by Nonlinear Least Square (NLS) method. The best fit is shown on Table 7-5.

Table 7-5 The Results of Equation 7-6

Molar Ratio HTAB:cetyl alcohol	P(1)	P(2)	P(3)	P(4)	P(5)	P(6)
1:6	—	—	39.798	0.21056	74.189	-0.0090745
1:3	53.879	0.38526	49.864	0.16087	80.309	-0.0072375
1:1	86.701	0.34437	60.637	0.09420	75.257	-0.0039782
1:0.5	107.87	0.16148	73.300	0.024818	79.877	0.0011059
1:0.33	114.40	0.072949	76.840	0.00637	78.742	0.017278

The comparison of this model with the experimental data are shown on Figures 7-3 to 7-7.

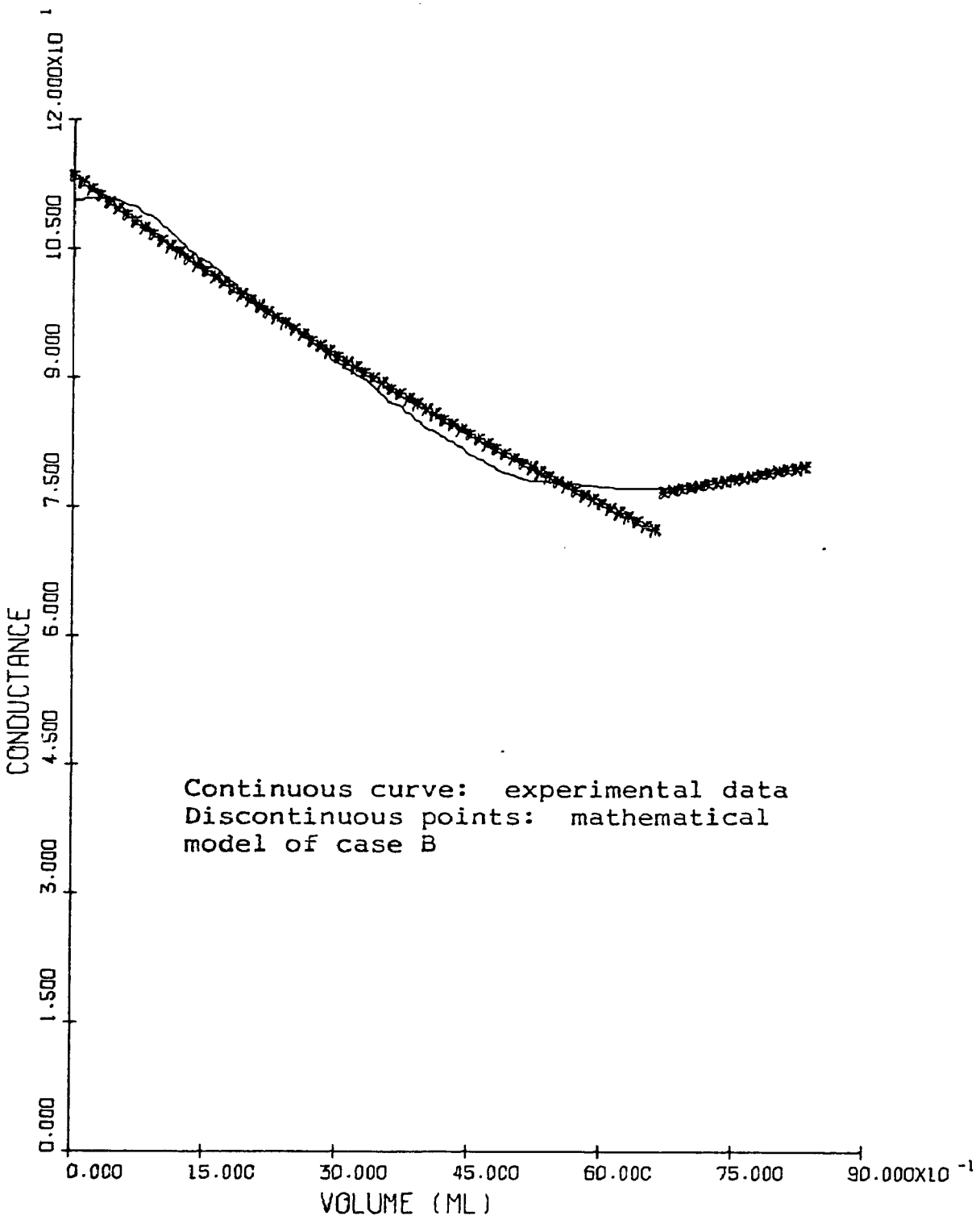

Figure 7-3 Conductometric titration curve for titrating benzene at constant rate of 1 c c /minute into 25 c c solution of 0.6% HTAB plus cetyl alcohol at a molar ratio 1:0.33.

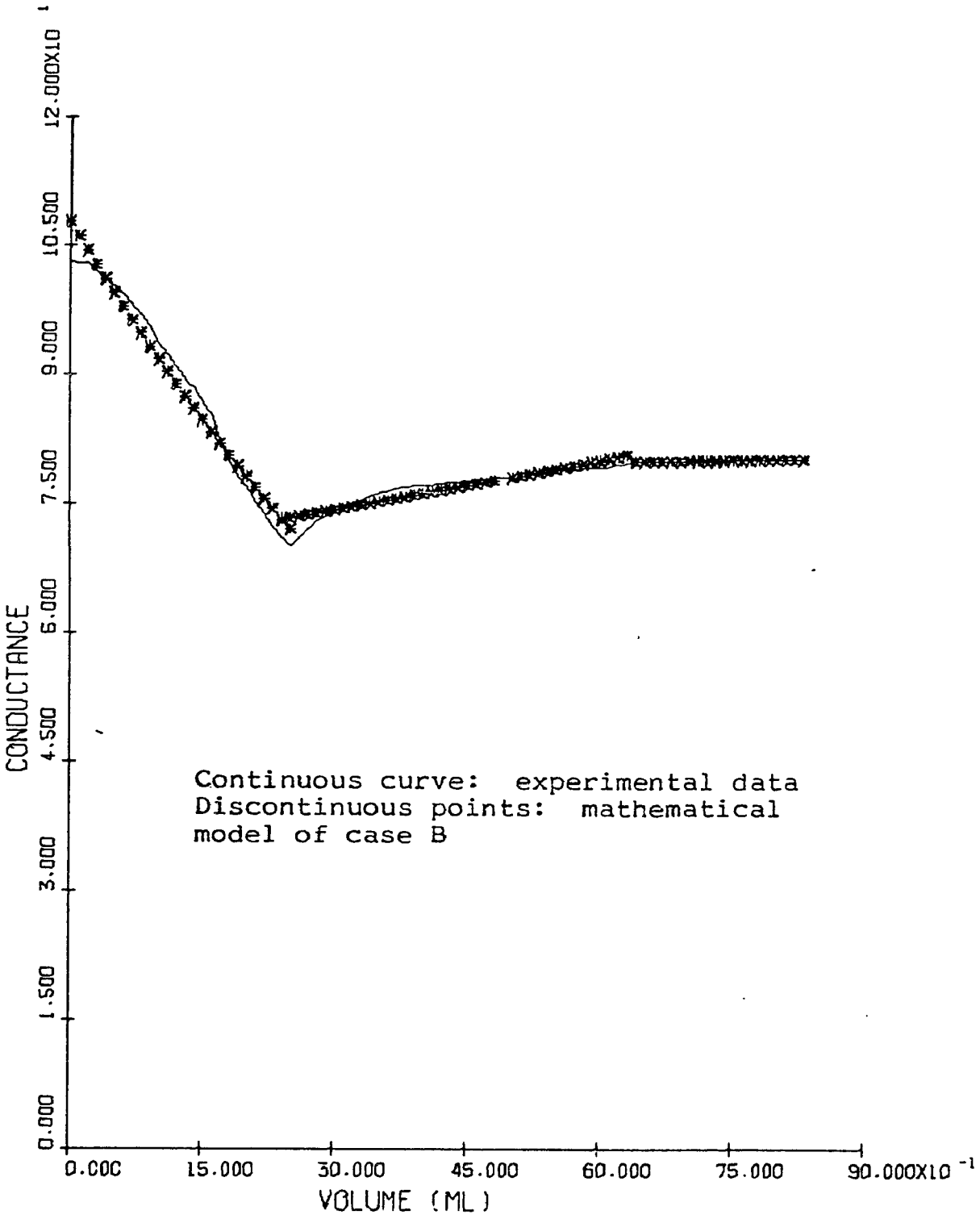

Figure 7-4 Conductometric titration curve for titrating benzene at constant rate of 1 c c /minute into 25 c c solution of 0.6% HTAB plus cetyl alcohol at a molar ratio 1:0.5.

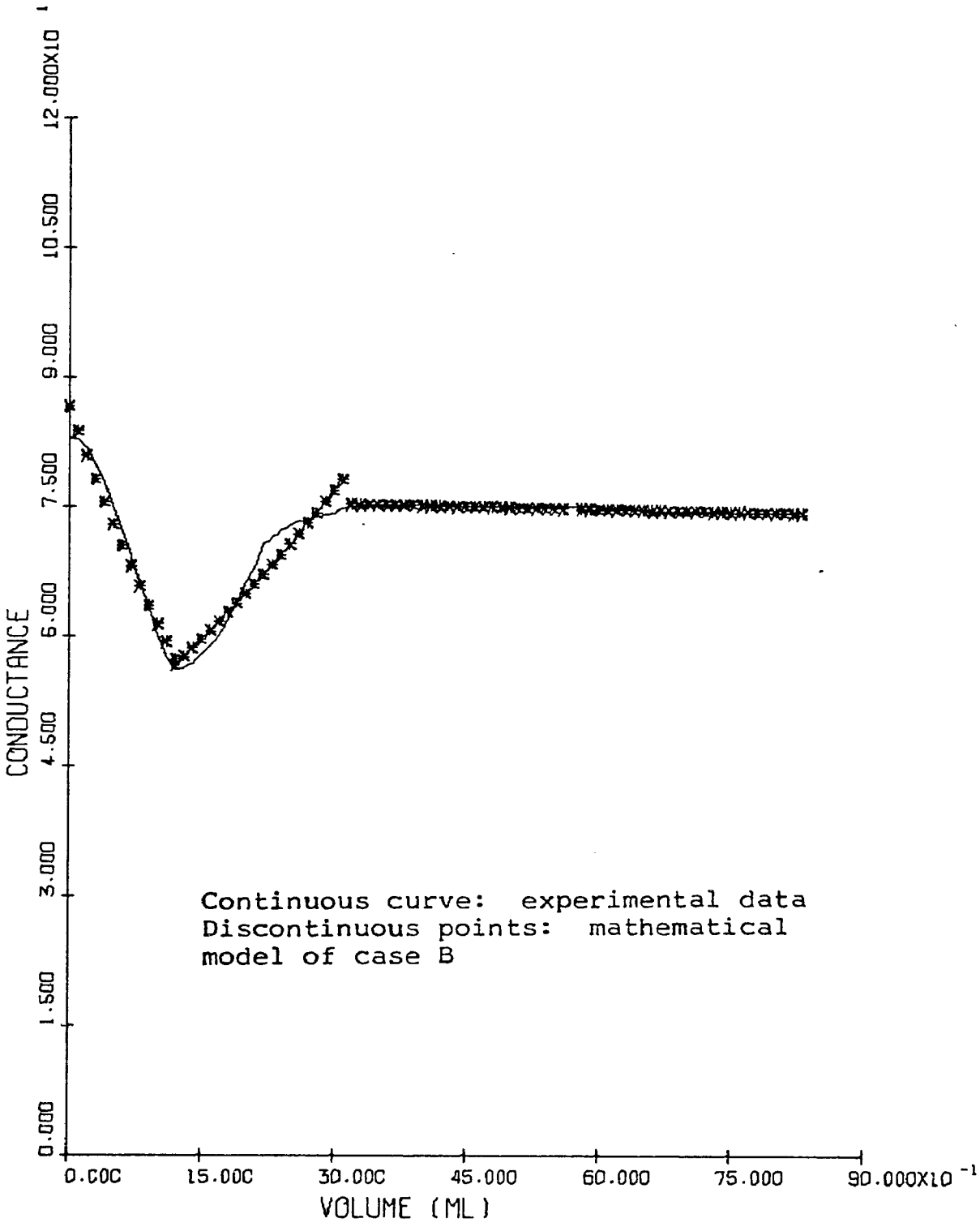

Figure 7-5 Conductometric titration curve for titrating benzene at constant rate of 1 c c /minute into 25 c c solution of 0.6% HTAB plus cetyl alcohol at a molar ratio 1:1.

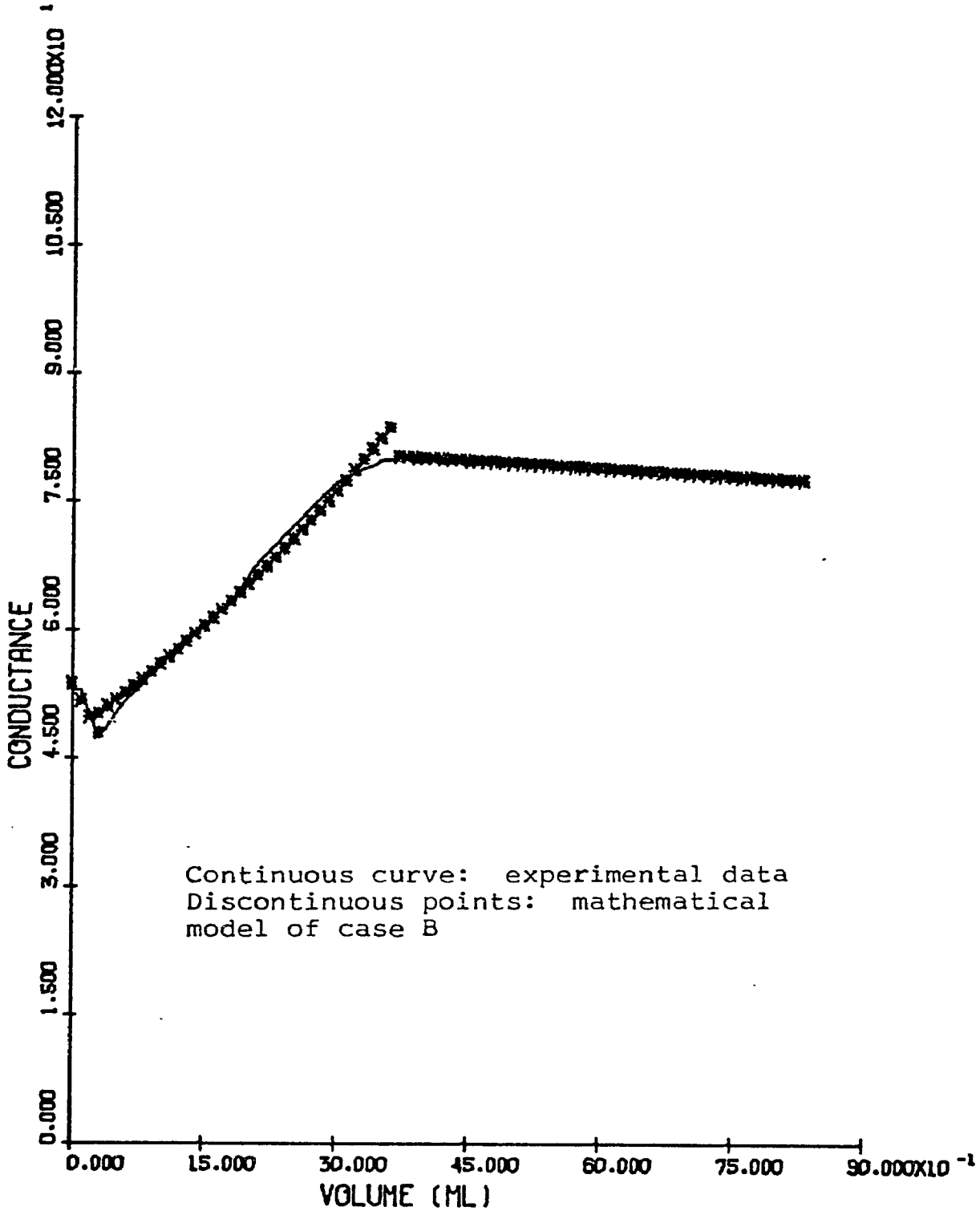

Figure 7-6 Conductometric titration curve for titrating benzene at constant rate of 1 c c /minute into 25 c c solution of 0.6% HTAB plus cetyl alcohol at a molar ratio 1:3.

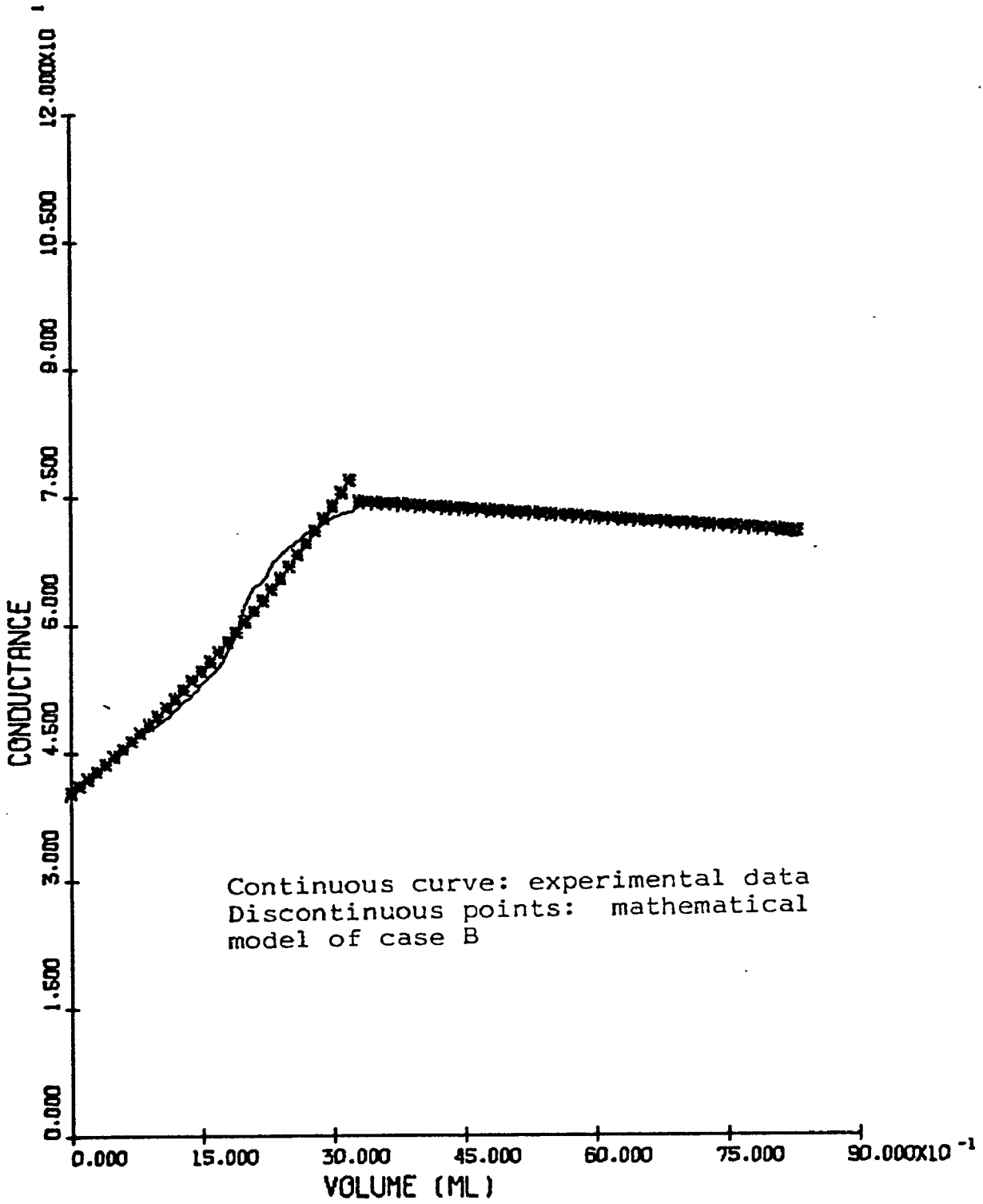

Figure 7-7 Conductometric titration curve for titrating benzene at constant rate of 1 c c /minute into 25 c c solution of 0.6% HTAB plus cetyl alcohol at a molar ratio 1:6.

7-3-3 Discussion: P(1), the initial conductance, is a function of the alcohol content as well as a function of the ionic surfactant concentration, therefore, P(1) will decrease as the alcohol content increases for fixed amounts of ionic surfactant. P(2), solubilization constant, being related to the solubilization process, is a function of the crystallinity of the complex rod formation. P(3) is an indication of the conductance at the start of the emulsification process, and is a function of alcohol content. P(3) decreases as the alcohol content increases. P(4), the emulsification constant, is a function of the amounts of the crystal rods in the aqueous phase. The more complex rod formations existing, the larger this constant. P(5) is the conductance at the beginning of the retardation process, and is nearly constant. P(6) is the droplet growth constant. It decreases as the alcohol content increases, since the number of particles at higher alcohol content is larger.

7-3-3-1 The distribution of ionic surfactant in the mixed emulsifier system

The initial conductance for various alcohol contents are listed on Table 7-6.

Table 7-6 The Initial Conductance at Various Molar Ratio of HTAB to Cetyl Alcohol

Molar ratio of HTAB to Cetyl Alcohol	Initial Conductance
1:6	41.0
1:3	53.1
1:1	83.0
1:0.5	103.1
1:0.33	110.5

According to the proposed model, the descending leg of the conductometric titration curve is caused by a solubilization process. The descending leg disappears from the conductometric titration curve and thus indicates that all the conductance is caused by the solute molecules (assuming rod formation is non-conducting species) at the beginning of the titration. The alcohol content decreased in the mixed emulsifier system and the initial conductance increased. The initial conductance difference between with and without descending leg is contributed by micelle. Since the total amount of ionic surfactant in the mixed emulsifier system is known, the ionic surfactant in the rod formation can be obtained by substracting the amount of solute molecules and micelle molecules from the total amount of ionic surfactant.

The conductivity Λ_- can be calculated as:

$$\Lambda_- = 78.4\times10^{4}\ m^2/ohm\text{-}mole \times 10^{-4}\ cm^2/m^2 \times 10^{-3}\ 1/cm^3$$

$$= 7.84\times10^{-2}\ cm^{-1}\ ohm^{-1}\ mole^{-1}$$

divide by cell constant $1.74\times10^{-6}\ cm^{-1}\ ohm^{-1}$

$$7.84\times10^{-2} cm^{-1}\ ohm^{-1}\ mole^{-1} \cdot l / 1.74\times10^{-6} cm^{-1}\ ohm^{-1}$$

$$= 4.5\times10^{4} mole/l \cdot \text{read out}$$

The conductivity of Λ_+ is assumed as 1/10 the Λ_-

$$\Lambda_+ = \left[4.5\times10^{4} mole/l \cdot \text{read out}\right] / 10 = 4.5\times10^{3} mole/l \cdot \text{read out}$$

The descending leg disappears at a molar ratio of 1:6 HTAB to cetyl alcohol. The initial conductance of 41.0 is a read value. Therefore the solute concentration can be calculated as

$$(41.0 \text{ read out}) / (45.0\times10^{3}+4.5\times10^{3})\ mole/l \cdot \text{read out}$$

$$= 8.28\times10^{-4}\ mole/l$$

The dissociation constant of the counter ion associated with the micelle is 0.0936 and is obtained from the calculations of the benzene titration into single surfactant HTAB system. Assuming the conductivity of the micelle aggregate is negligible, the conductivity of the counter ion bromide $\left[Br^-\right]$ associated with micelle is $(4.5\times10^{4}\ mole/l \cdot \text{read out}) \times 0.0936 = 4.212\times10^{3}\ mole/l \cdot \text{read out}$. Dividing the initial conductance difference of the curve that has a descending leg with the curve without descending

leg gives the micelle concentration. For example, the micelle concentration of HTAB to cetyl alcohol at molar ratio 1:3 is $(53.1-41.0)/4.212\times10^{3} = 2.87\times10^{-3}$ mole/l

Total concentration of HTAB in the system is

$0.15/364.46\times1000/25 = 1.65\times10^{-2}$ mole/l

The total concentration of HTAB is subtracted from the HTAB solute concentration and the micelle concentration. This value should be the concentration of ionic surfactant in the rod formation.

The distribution of ionic surfactant at various molar ratios of HTAB to cetyl alcohol are listed on Table 7-7.

Table 7-7 The Distribution of HTAB in the Mixed Emulsifier Systems

Molar ratio of HTAB to Cetyl alcohol	Solute Con. (M)	Micelle Con. (M)	Rod Formation Concentration (M)
1:6	8.28×10^{-4}	0	1.56×10^{-2}
1:3	8.28×10^{-4}	2.87×10^{-3}	1.28×10^{-2}
1:1	8.28×10^{-4}	9.97×10^{-3}	5.66×10^{-3}
1:0.5	8.28×10^{-4}	1.47×10^{-2}	9.35×10^{-4}
1:0.33	8.28×10^{-4}	1.65×10^{-2}	$-8.65\times10^{-4} \fallingdotseq 0$

The actual solute and micelle concentration should be lower than the calculated value, because the rod formation is assumed as non-conducting species, furthermore

the molar conductivity of the micelle should be the sum of counter ion and the micelle aggregates. Nevertheless the aggregate is assumed as non-conducting species. A negative value appears for the rod formation concentration at molar ratio 1:0.33 of HTAB to cetyl alcohol, and this value is quite close to zero. Figure 2-4 indicates the conductometric titration curve of titrating of benzene into the HTAB and cetyl alcohol mixed emulsifier system at molar ratio 1:0.33 is very close to the titrating benzene into HTAB single surfactant system.

7-3-3-2: The Formation of the mixed emulsifier system

The assumption is made that the optimum ratio of HTAB to cetyl alcohol in forming perfect crystals, will contribute the highest stability in the emulsion formation. According to the ultracentrifugation stability study, the molar ratio of HTAB to cetyl alcohol of 1:3 has the highest stability, therefore the complex formation should form the best crystals. The parameters of this system will be subscripted b. The ratio of $P(2)/P(2)_b$ is indicative of the degree of crystallinity of the complex formation while the micelles exist in the aqueous phase. The $P(2)/P(2)_b$ ratio, for the following molar ratios of HTAB to cetyl alcohol 1:1, 1:0.5 and 1:0.33,are 0.894, 0.419 and 0.189,respectively.

It is found that the slope of the descending leg (Figure 2-4) decreases and V1 increases (see Table 7-4) while the ratio between HTAB to cetyl alcohol decreases. V1 is related to the solubilization time, and therefore, it follows that V1 increases as the ratio between HTAB and cetyl alcohol decreases. In other words, V1 increases while there are free micelles available. Nevertheless, the range for the increase in V1 should be limited. Furthermore the slope of the descending leg should be constant.

The experimental data obtained with less alcohol in the mixed emulsifier system can be explained due to the loss of structure of the rod shaped crystals with excess HTAB. As the oil is added to the mixed emulsifier system, the rod formations will be destroyed while they diffuse to the oil droplets, meaning that small amounts of HTAB are being kicked out continuously.

Therefore the slope of the initial descending leg will change and V1 will increase. The degree of crystallinity can explain this phenomena quantitatively.

7-3-3-3: Check the suggested model

In order to check the suggested model, two sets of conductometric titration experiments were carried out:

I. Varying the amount of HTAB at the same molar ratio of HTAB and cetyl alcohol (Figures 7-8, 7-9)

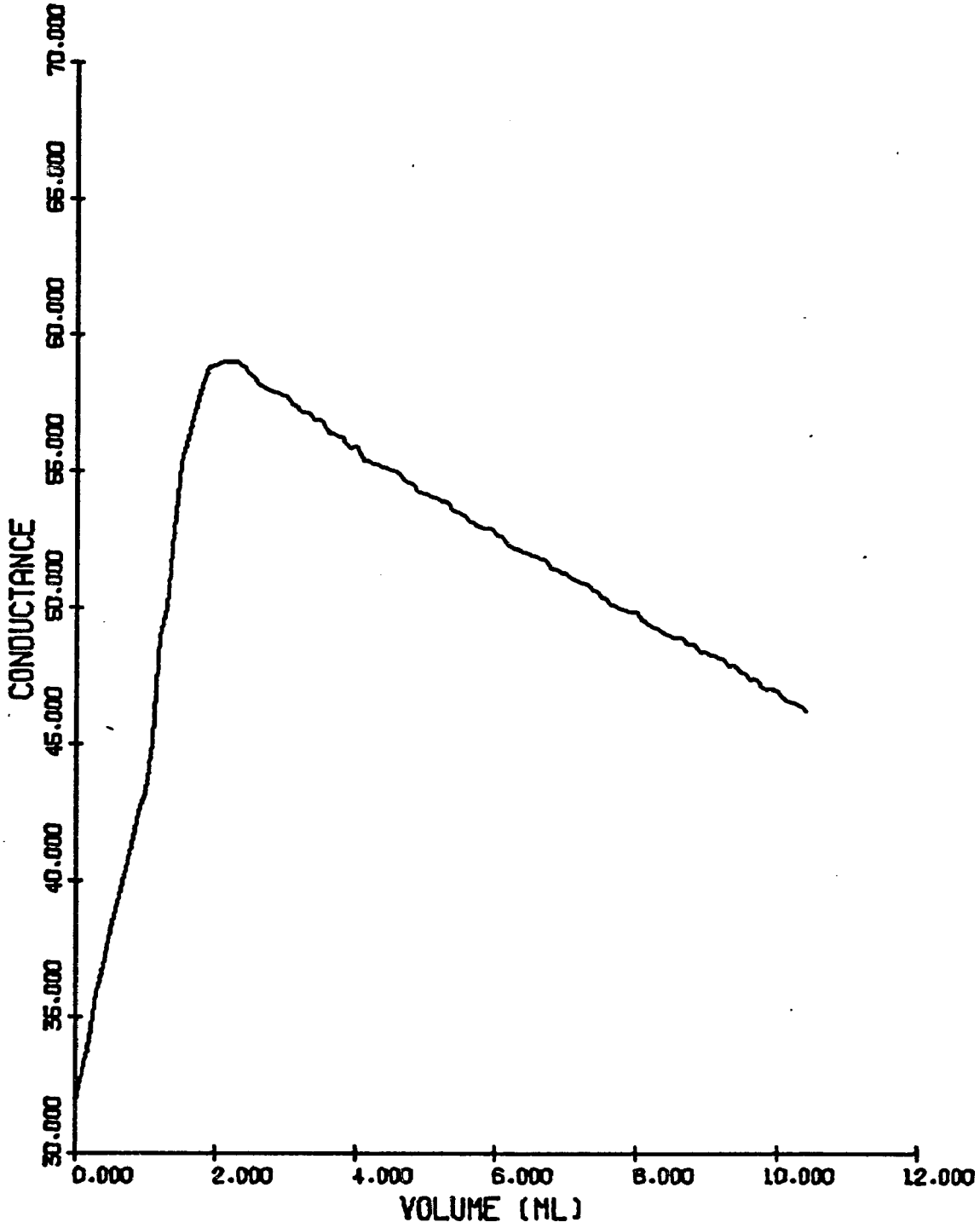

Figure 7-8 Conductometric titration curve for titrating benzene at constant rate of 1 c c /minute into 25 c c solution of 0.4% HTAB plus cetyl alcohol at a molar ratio 1:3.

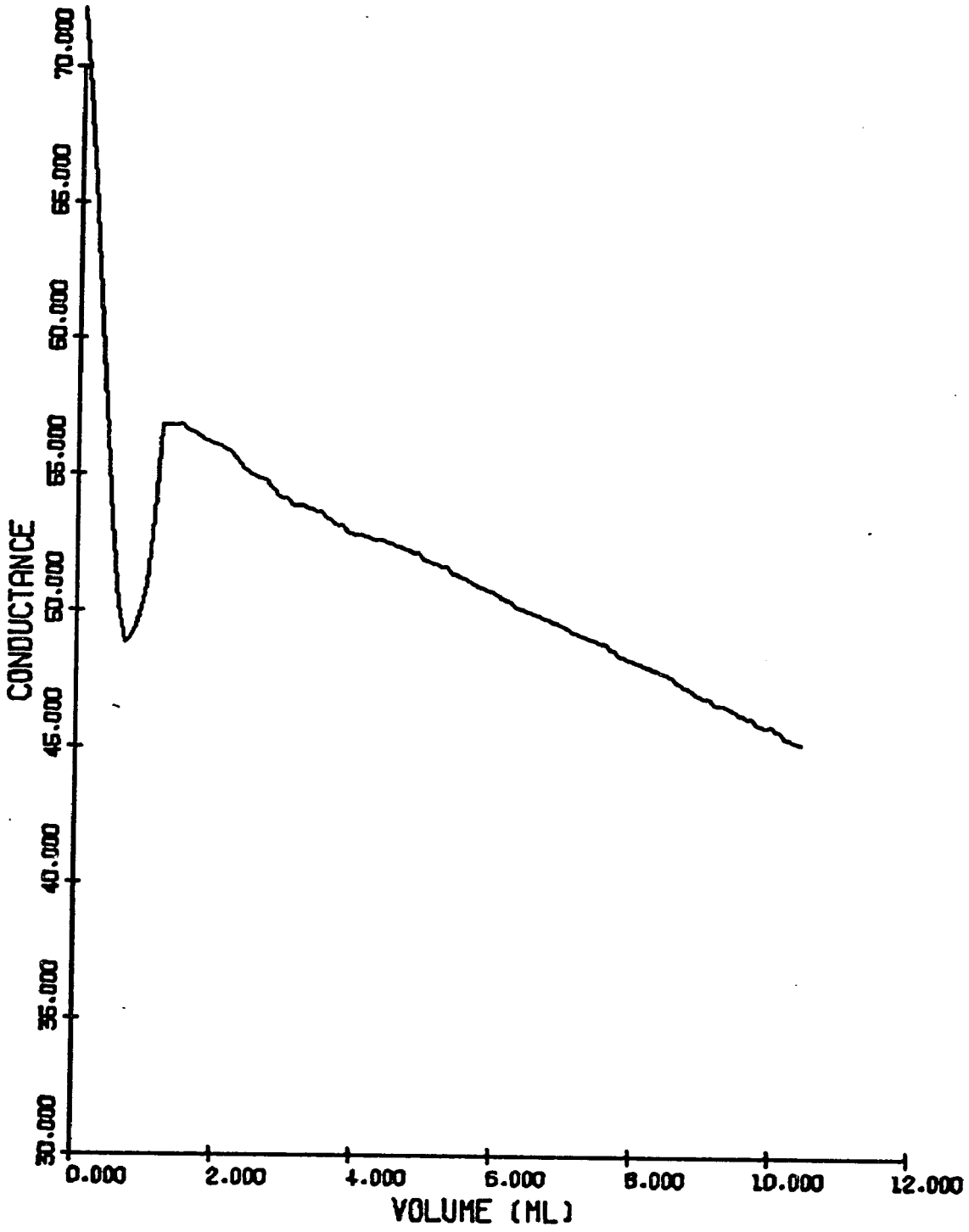

Figure 7-9 Conductometric titration curve for titrating benzene at constant rate of 1 c c /minute into 25 c c solution of 0.8% HTAB plus cetyl alcohol at a molar ratio 1:3.

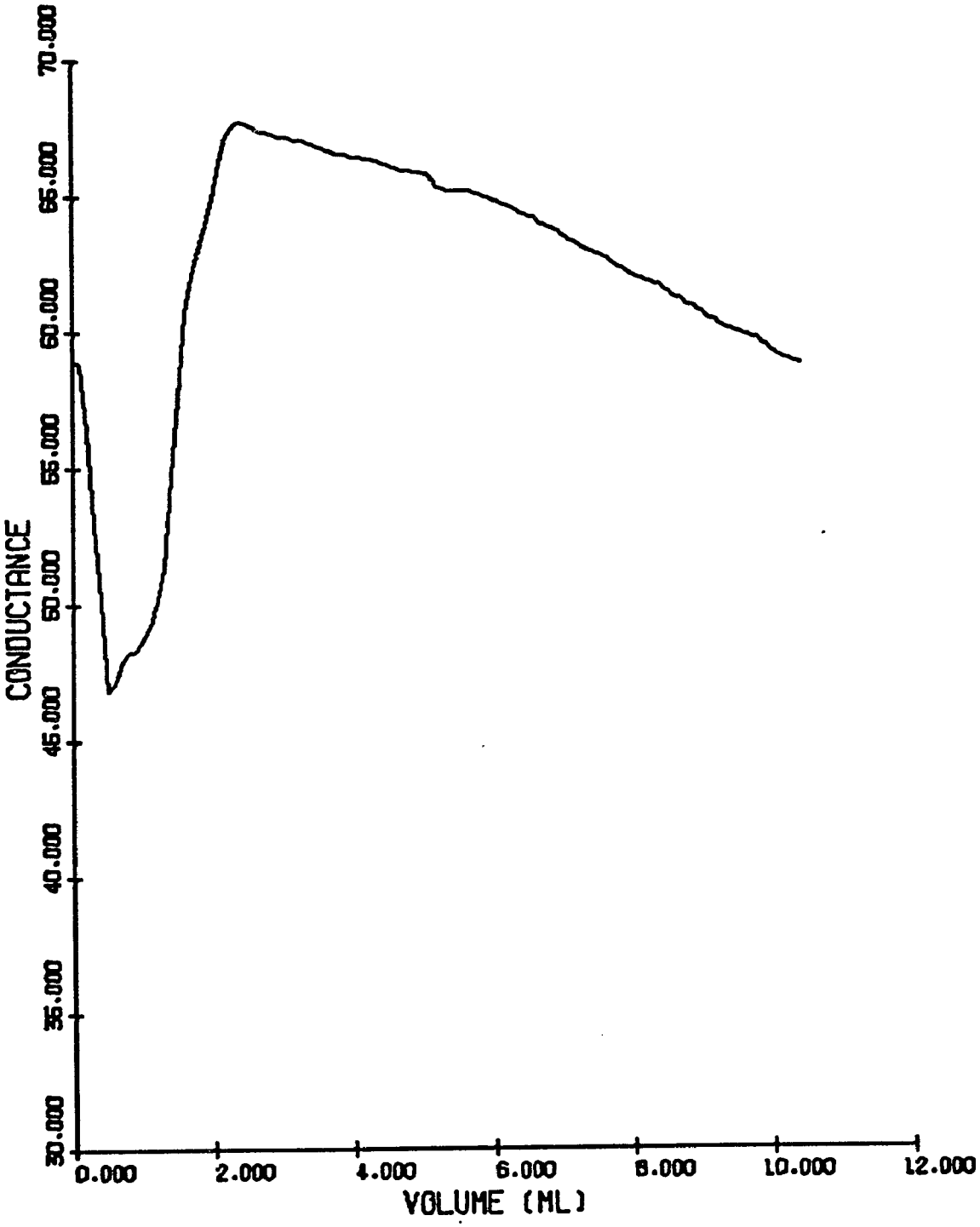

Figure 7-10 Conductometric titration curve for titrating benzene at constant rate of 1 c c /minute into 25 c c solution of 0.4% HTAB plus cetyl alcohol at a molar ratio 1:1.

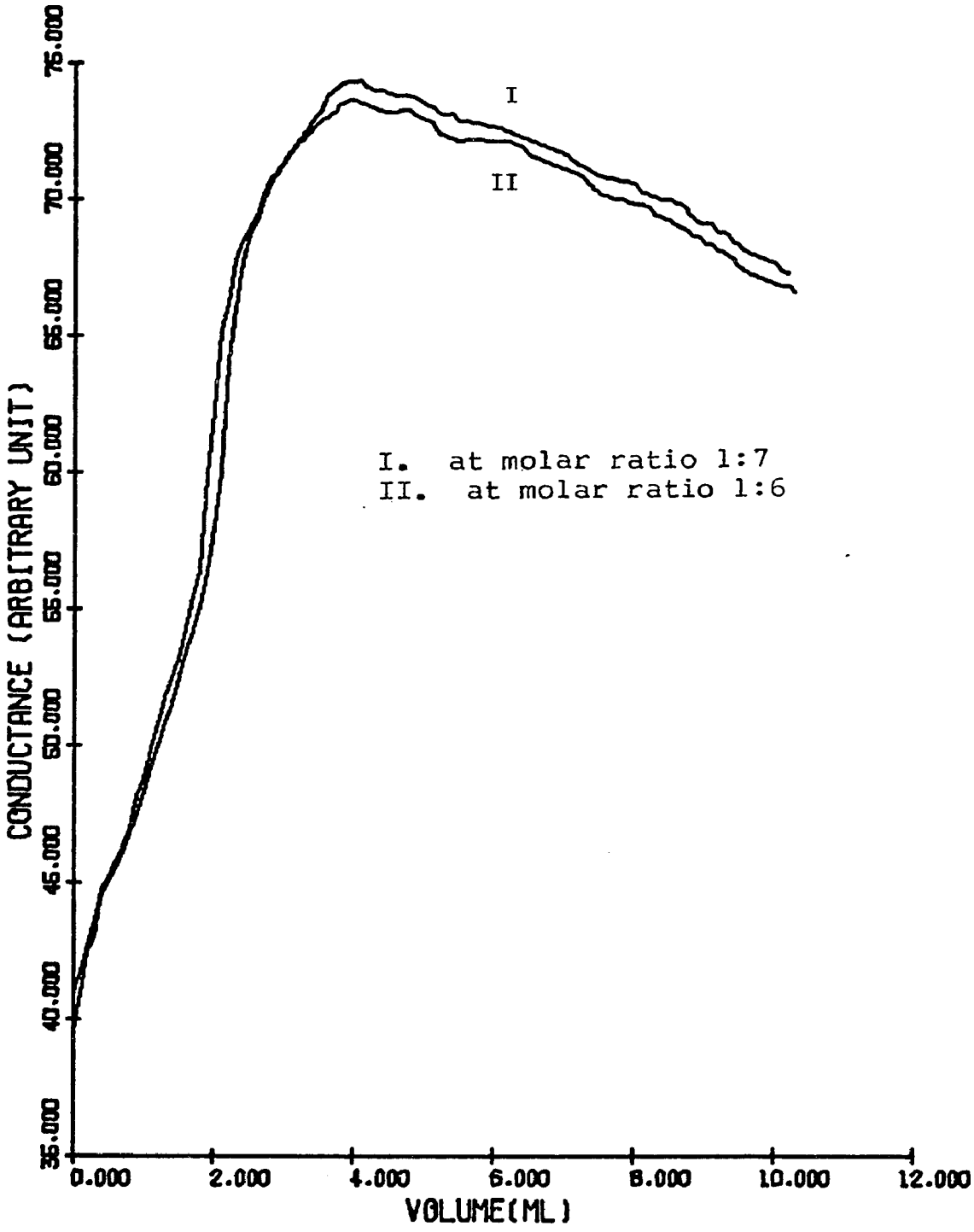

Figure 7-11 Conductometric titration curve for titrating benzene at constant rate of 1 c c /minute into 25 c c solution of 0.6% HTAB plus cetyl alcohol at molar ratios higher than 1:6.

II. Increasing the amount of cetyl alcohol at fixed amounts of 0.6% HTAB plus cetyl alcohol system, makes the ratio of HTAB:cetyl alcohol more than 1:6 (Figure 7-11).

Case I shows that at the same molar ratio but different amounts of ionic surfactant HTAB, the conductometric titration curves are completely different. For the titration curve in which benzene is titrated into 0.1 gm HTAB and 0.2 gm cetyl alcohol at a molar ratio of 1:3 in 25 cc. deionized water, no initial descending leg was found (Figure 7-8). This suggests that no micelles exist, while 0.1 gm of HTAB exists in 25 cc. deionized water (0.4%). As shown in Figure 7-6, a small initial descending leg was found while titrating benzene into 0.6% HTAB plus cetyl alcohol at a molar ratio of 1:3. That implies that few micelles exist in this system. Furthermore, increasing the amount of HTAB to 0.8% plus cetyl alcohol at a molar ratio of 1:3, while titrating benzene into this mixed emulsifier system, increases the portion of the initial descending leg (Figure 7-9). This suggests there are more micelles than 0.6% HTAB plus cetyl alcohol at a molar ratio of 1:3.

In order to further test this model, when titrating benzene into 0.4% HTAB plus cetyl alcohol at a molar ratio of 1:1, a significant initial descending leg was found (Figure 7-10). That means there are more micelles

in this system. Comparing Figure 7-8 and Figure 7-9 we can observe easily the number of micelles existing in aqueous solutions as a function of the amount of HTAB at a fixed molar ratio of HTAB to cetyl alcohol. Figure 7-3 & 7-7 tells us, for a fixed amount of HTAB, the number of micelles existing in aqueous solutions is a function of the amount of cetyl alcohol.

Case II shows there is no significant difference in the conductometric titration curve with a molar ratio of HTAB to cetyl alcohol beyond 1:6 (Figure 7-11). This can be explained as excess cetyl alcohol existing in the mixed emusifier system. There are no micelles available, therefore, while further increases are made in the amount of cetyl alcohol, the only location for it to go is into rod formation. The crystallinity will be destroyed but no significant change can be observed in the conductometric titration curve.

7-4 References

1. M.E.L. McBain, W.B. Dye and S.A. Johnston, J. Amer. Chem. Soc., 61, 549 (1939).

2. P. Mukerjee and K.J. Mysels, Critical Micelle Concentrations of Aqueous Surfactant Systems, NSRDS-NBS-36, 107 (1971).

3. W.J. Moore, Physical Chemistry, 4th ed., Prentice-Hall, 435 (1972).

4. W.C. Wu, Ph.D. Dissertation, Lehigh University, 23 (1977).

CHAPTER 8 CONCLUSIONS AND RECOMMENDATIONS

8-1 Conclusions

Conclusions can be drawn concerning the role of the mixed emulsifier system in the preparation of emulsions and latexes based on various indirect approaches, i.e. conductometric titration, adsorption isotherm, electron microscopy, ultraviolet absorption, ultracentrifugation and mathematical modeling.

The conductometric titration information indicated two completely different titration curves (Figure 2-3); the first resulting from the titration of benzene into the aqueous single surfactant system and the other from the titration of benzene into a aqueous mixed emulsifier system. The information suggests two completely different emulsification processes are involved. From the titration of benzene into varying molar ratios of the HTAB and cetyl alcohol mixed emulsifier system at a fixed concentration of ionic surfactant (Figure 2-4) shows that the amount of cetyl alcohol in the mixed emulsifier system plays a very important role in controlling the emulsification mechanism. From the titration of benzene into the mixed emulsifier systems containing various chain lengths of fatty alcohol mixed with HTAB at a fixed molar ratio (Figure 2-5), reveals that the emulsification mechanism of the mixed emulsifier system is a function of the chain

length of the fatty alcohol.

All of the above information implies that a complex formation in the mixed emulsifier system is formed during the emulsification process. Furthermore, Figure 2-6 shows that the conductometric titration curve is time-dependent. This suggests that the efficiency of emulsification process is a function of the pre-emulsification time.

Figure 2-7 shows that the mixed emulsifier system needs a certain stirring 1.5 hours to reach equilibrium. If the pre-emulsification time is less than 1.5 hours, the conductometric titration produces a higher initial conductance and a relatively small ΔH between two critical points. This information indicates that there must be a complex formation existing in the mixed emulsifier system which is related to conductance, and is a function of time. Nevertheless, the conductometric titration data can not give conclusive results.

The adsorption isotherms show that the surface coverages of sodium dodecyl sulfate on the cleaned monodisperse polystyrene latex with and without the addition of cetyl alcohol are quite different. The surface area covered by the sodium dodecyl sulfate molecule on the cleaned monodisperse latex with cetyl alcohol is much larger than without cetyl alcohol on the surface. This implies that, concerning surface area covered by cetyl alcohol can be

substituted for sodium dodecyl sulfate. In other words, while cetyl alcohol is adsorbed on the latex surface, less ionic surfactant is required to cover the particle surface in contributing to good stability. Therefore, if the same amount of ionic surfactant is applied to the monodisperse latex with and without cetyl alcohol on the particle surface, the system with cetyl alcohol on the latex surface needs less ionic surfactant to cover the particle surface. The excess ionic surfactant will be desorbed into the water phase in the form of micelles. This fact can be explained by the ascending leg of the conductometric titration curve for the titration of oil into the mixed emulsifier system.

Electron microscopy provided more information in understanding the details of the mixed emulsifier system. Rod formation of the mixed emulsifier system was observed (Figure 4-5 and Figure 4-8).

The particle size distribution of the stained styrene monomer emulsions along with the conductometric titration curve tells us the relationship of the volume of styrene monomer in the system to the number of particles and to the particle surface area. This information provides a very important breakthrough in explaining the conductometric titration curve. The initial descending leg is correlated to the solubilization process, because no

particles were observed in that region. The big particles were found at the end of the descending leg. This implies the end of the solubilization process and another process is replacing it. A sharp decrease in particle size distribution along the ascending leg of the conductometric titration curve suggests there is a break-down process occurring. The equilibrium part of the conductometric titration curve shows a decreasing number of particles as well as an increasing particle size. This is an indication of a particle growth stage.

Electron diffraction patterns of the rod complex formation (Figure 4-7) demonstrate the crystallinity of the rod complexes. This indicates HTAB and cetyl alcohol are alternately and regularly arranged in the crystalline rods. The crystalline rod formation can explain the particle size break-down along the ascending leg, and the large particle size at the end of the initial descending leg of the conductometric titration curve. While the droplet is being formed in the mixed emulsifier system, the rod formation will approach the hydropholic phase (oil phase). The rod formation will be destroyed by the oil, and the oil droplet surface will be covered by the well-arranged cetyl alcohol and HTAB. The excess HTAB obtained from rod crystal will be desorbed into the aqueous phase, and the conductance will begin to increase.

A different ultraviolet spectrum of the serum (water phase) of the ultracentrifuged benzene in water emulsion against mixed emulsifier system was observed (Figure 5-16) while the mixed emulsifier system was used as reference. This suggests the mixed emulsifier system must have a complex formation formed that is interfering with the benzene ultraviolet absorbance. The ultraviolet study of the concentration of benzene in the ultracentrifuged serum and the solubilized benzene in the deionized water show the benzene concentrations of both systems are similar (0.01M), which is the solubility of benzene in water. This indicates all the micelles will be pushed out of the water phase if enough ultracentrifugal force is applied.

The ultracentrifugation data verified that the stability of the emulsion prepared by using a mixed emulsifier system is a function of the fatty alcohol chain length and the molar ratio of HTAB to cetyl alcohol. Also, the ultracentrifugationdata verifies that ΔH on the conductometric titration curve is related to stability of the emulsion. The mathematical model summarizes the above information and gives a quantitative value in demonstrating the distribution of a single surfactant in the solute form and micelle form for titrating the oil in the single surfactant system. The model can also express quantitatively the distribution of ionic surfactant in the solute

form, micelle form and rod complex formation of the mixed emulsifier system at various molar ratios before titration.

The crystallinity of the mixed emulsifier system can be expressed numerically by the mathematical model.

Furthermore, a set of advanced interpretation of ultraviolet spectra in terms of relative peak heights has been proposed. The advantage of these interpretations are independent of the base line shift. The relative ratio at certain wavelengths can be obtained immediately. The absolute concentration can be obtained as long as the standard concentration spectrum is available.

The instability mechanism has been proposed based on the ultracentrifugation data. For a stable emulsion the oil droplet tries to keep its individuality in the cream phase until the oil phase separatation occurs. But, for an unstable emulsion the oil droplet begins to coalesce and no longer has a tendency to keep its individualty in the cream phase.

8-2 Recommendations for Future Research

For mixed emulsifier systems, rod shaped crystals play an important role in the preparation of emulsions and latexes. It is assumed that the crystallinity is dependent on the ratio of HTAB to cetyl alcohol. It would

be of great interest to study the crystallinity and the structure of these rods by using a diffraction pattern method at various ratios of HTAB to cetyl alcohol as well as different combinations of ionic surfactants and fatty alcohols.

Since the formation of a crystalline rod plays such an important role in the mixed emulsifier system during the emulsification process, it would be worthwhile to characterize the rod formation by studying the salt effect at various concentrations, the stability changes, as well as the change in crystallinity.

Appendix 1 Purification of the Styrene Monomer

A. Wash to remove inhibitor: The inhibitor, such as hydroquinone or t-butylpyrocatechol, is removed by washing the monomer with 10% aqueous NaOH. Roughly equal parts of the basic solution and the monomer are placed in a separatory funnel and mixed by shaking vigorously for 15 minutes. The heavier aqueous phase is drained off. The procedure is repeated twice until the liquids remain clear. The monomer is then washed with distilled water until litmus paper shows that all the base has been removed.

B. Dry: A drying agent such as anhydrous Na_2SO_4 is added to the monomer (100 g/l). With occasional tumbling, drying is complete in about 1/2 hr.

C. Distill: Add about 1 g/l CuCl stabilizer to the monomer and distill under dry N_2 at 20 torr and 40-43^{o}C.

Note: flush the distillation setup with N_2 for while before raising the temperature for distillation, in order to get rid of all the O_2 and then close the N_2 valve, let the vacuum pull some out and keep the distillation system free from O_2.

Appendix 2 The computer program for plotting conductance against added volume of surfactant solution and the concentration of surfactant in the aqueous phase

```
      PROGRAM CONDUCT(INPUT,OUTPUT,PLOT,TAPE99=PLOT)
      DIMENSION V(100),CONDUCT(100),XM(100)
      PRINT 199
  199 FORMAT (5X,*SAMPLE NO E*,/)
      PRINT 3
    3 FORMAT(//,10X,*CONDUCTANCE*,10X,*V*,10X,*M*,//)
      READ 1,N
    1 FORMAT(5I3)
      READ 2,(V(J),CONDUCT(J),J=1,N)
    2 FORMAT(12E10.0)
      DO 5 J=1,N
      VV=V(J)
      XM(J)=1000.*VV/(288.39*(25.0+VV))*0.04694
      PRINT 4,CONDUCT(J),V(J),XM(J)
    4 FORMAT(1X,F8.4,9X,F8.4,2X,F8.6,/)
    5 CONTINUE
      CALL NANPLT
      CALL FACTOR(0.7)
      CALL PLOT(0.0,-0.5,-3)
      V(N+1)=0.0
      V(N+2)=2.0
      CONDUCT(N+1)=0.0
      CONDUCT(N+2)=35.0
      CALL AXIS1(1.5,1.5,11HVOLUME (ML),-11,6.0,0.0,V(N+1),V(N+2),10.0)
     +CALL AXIS1(1.5,1.5,11HCONDUCTANCE,11,8.0,90.0,CONDUCT(N+1),
     +CALL SYMBOL(2.0,0.5,0.25,16HCONDUCTANCE PLOT,0.0,16)
      CALL LINE(V,CONDUCT,N,1,-1,11)
      CALL PLOT(0.0,0.0,3)
      XM(N+1)=0.0
      XM(N+2)=0.0088
      CALL AXIS1(0.0,8.0,8HMOLARITY,8,6.0,0.0,0.0,XM(N+2),10.0)
      CALL PLOT(0.0,0.0,3)
      CALL LINE(XM,CONDUCT,N,1,-1,47)
      CALL PLOT(10.0,-1.5,-3)
      CALL ENDPLT
      CALL EXIT
      END
```

Appendix 3 The computer program for plotting conductance/M against $\sqrt{M}$ as well as conductance against added volume of surfactant solution

```
      PROGRAM CONDUCT(INPUT,OUTPUT,PLOT,TAPE99=PLOT)
      DIMENSION V(100),CONDUCT(100),XM(100),MCON(100),SRM(100)
      REAL MCON
      PRINT 199
  199 FORMAT (5X,*SAMPLE NO A*,/)
      PRINT 3
    3 FORMAT(//,10X,*CONDUCTANCE*,12X,*V*,10X,*M*,8X,*MCON*,8X,*SRM*,//)
      READ 1,N
    1 FORMAT(5I3)
      READ 2,(V(J),CONDUCT(J),J=1,N)
    2 FORMAT(2E10.0)
      DO 5 J=1,N
      VV=V(J)
      XM(J)=1000.*VV/(288.39*(25.0+VV))*0.01
      SRM(J)=SQRT(XM(J))
      MCON(J)=CONDUCT(J)/XM(J)
      PRINT 4,CONDUCT(J),V(J),XM(J),MCON(J),SRM(J)
    4 FORMAT(12X,F8.4,9X,F8.4,2X,F8.6,5X,F8.2,2X,F8.6,/)
    5 CONTINUE
      CALL NAMPLF
      CALL FACTOR(0.7)
      CALL PLOT(0.0,-0.5,-3)
      V(N+1)=0.0
      V(N+2)=9.0
      CONDUCT(N+1)=0.0
      CONDUCT(N+2)=35.0
      CALL AXIS1(1.5,1.5,11HVOLUME (ML),-11,6.0,0.0,V(N+1),V(N+2),10.0)
     +,CONDUCT(N+2),10.0)
      CALL AXIS1(1.5,1.5,11HCONDUCTANCE,11,3.0,90.0,CONDUCT(N+1),
      CALL PLOT(6.0,0.0,3)
      CALL SYMBOL(2.0,0.5,0.25,16HCONDUCTANCE PLOT,0.0,16)
      CALL PLOT(1.5,1.5,-3)
      CALL LINE(V,CONDUCT,N,1,-1,11)
      CALL PLOT(6.0,0.0,3)
      SRM(N+1)=0.03
      SRM(N+2)=0.0
      MCON(N+1)=10000.0
      MCON(N+2)=4750.0
      CALL AXIS1(0.0,8.0,14HSQ RT MOLARITY,14,6.0,0.0,SRM(N+1),SRM(N+2)
     +,10.0)
      CALL AXIS1(16.0,0.0,13HCONDUCTANCE/M,-13,8.0,90.0,MCON(N+1),
     +,MCON(N+2),10.0)
      CALL PLOT(16.0,0.0,3)
      CALL LINE(SRM,MCON,N,1,-1,14)
      CALL PLOT(10.0,-1.5,-3)
      CALL EXIT
      END
```

Appendix 4 Calculation of the added volume of surfactant solution from known concentration of surfactant solution

$$C_M = \frac{Vxc}{M} \times \frac{1000}{25+V}$$

where C_M = the titrated surfactant concentration in molarity

V = the added volume

c = the concentration of surfactant solution

M = the molecular weight of surfactant

Example:

If $C_M = 8.54x10^{-3}M$

M = 288.38 for SDS

c = 1%

Then $8.54x10^{-3} = \frac{0.01V}{288.38} \times \frac{1000}{25+V}$

$$8.54x10^{-3} = \frac{10\ V}{7209.5+288.38V}$$

$$61.585+2.47V = 10V$$

$$7.53V = 61.585$$

$$V = 8.2 \text{ (c.c.)}$$

Appendix 5 Calculation of the surface coverage of each surfactant molecule on the monodisperse latex surface

$$A = \frac{3(Vo)(a)(de)(M)}{(V-Vi)(C)(No)(r)(d)}$$ (see equation 3-1)

For the system of this study

a = 11.97%, de = 1 gm/cm^3, M = 288.38 No = 6.023×10^{23},

r = $(0.45 \times 10^{-4})/2$ cm, d = 1.05 gm/cm^3

Example:

Sample B c = 1%, V = 8.948 cc, Vi = 8.2 cc

$$A = \frac{3 \times 5 \times 11.97\% \times 1 \times 288.38}{(8.948-8.2) \times 0.01 \times 6.023 \times 10^{23} \times (\frac{0.045 \times 10^{-4}}{2}) \times 1.05}$$

$$= 48.65 \times 10^{-16} \text{ cm}^2 = 48.865 \text{ A}^2$$

Appendix 6 The computer program for plotting the ultraviolet spectra from one set of data

```
      PROGRAM INK (INPUT,OUTPUT,PLOT,TAPE99=PLOT)
      DIMENSION X(200),Y(200),Z(200)
      READ 1,N
    1 FORMAT(5I3)
      DO 9 I=1,N
      READ 2, Z(I),Y(I)
    2 FORMAT(2F10.0)
    9 CONTINUE
      PRINT 199
  199 FORMAT (5X,*SAMPLE NO.0*)
      PRINT 4
    4 FORMAT(10X,*COND.*,2X,*VOL.*)
      PRINT 8 , ( I, Z(I),Y(I), I=1,N)
    8 FORMAT (5X,I3,5X,2F10.2)
      CALL NAMPLT
      CALL FACTOR(0.8)
      CALL PLOT(0.0,-0.5,-3)
      Z(N+1)=150.0
      Z(N+2)=30.0
      Y(N+1)=0.0
      Y(N+2)=0.125
      CALL AXIS1(1.5,1.5,15HWAVELENGTH (NM),-15
     +,6.0,0.0,Z(N+1),Z(N+2),10.0)
      CALL AXIS1(1.5,1.5,10HABSORBANCE,10
     +,8.0,90.0,Y(N+1),Y(N+2),10.0)
      CALL PLOT (1.5,1.5,-3)
      CALL LINE (Z,Y,N,1,0,0)
      CALL PLOT (10.0,-1.5,-3)
      CALL ENDPLT
      CALL EXIT
      END
```

Appendix 7 The computer program for plotting more than one set of data on the same plot

```
      PROGRAM CONDUC(INPUT,CUTPUT,PLOT,TAPE99=PLOT)
      DIMENSION X(1000),Y(1000)
      READ 1,M
      CALL NAMPLT
      CALL FACTOR(0.8)
      CALL PLOT(0.0,-0.5,-3)
      CALL SYMBOL(0.5,0.5,0.25,24HULTRAVIOLET ABSORBANCE CURVE,0.0,28)
      DO 5 L=1,M
      READ 1,N
    1 FORMAT(15I3)
      READ 2,(X(I),Y(I),I=1,N)
    2 FORMAT(2E10.0)
      PRINT 199
  199 FORMAT (5X,*SAMPLE NO.5-8*)
      PRINT 8,(X(I),Y(I),I=1,N)
    8 FORMAT(5OX,2F20.3)
      X(N+1)=1.8E+2
      X(N+2)=30.0
      Y(N+1)=0.125
      Y(N+2)=0.125
      IF( L .NE. 1 ) GO TO 20
      CALL AXIS1(1.5,1.5,15HWAVELENGTH (NM),-15
     +,6.0,0.0,X(N+1),X(N+2),10.0)
      CALL AXIS1(1.5,1.5,10HABSORBANCE,10
     +,8.0,90.0,Y(N+1),Y(N+2),10.0)
      CALL PLOT(1.5,1.5,-3)
   20 CALL LINE(X,Y,N,1,0,0)
      CALL PLOT(0.0,0.0,-3)
    5 CONTINUE
      CALL PLOT(10.0,-1.5,-3)
      CALL ENDPLT
      CALL EXIT
      END
```

Appendix 8 The computer program for plotting the comparison curves of experimental data and the theoretical model

```
      PROGRAM VOLUME (INPUT,OUTPUT,PLOT,TAPE 99=PLOT)
      DIMENSION V(100),T(100),P(20),F(100)
      DATA P(1)/11.85/,P(2)/0.07022/,P(3)/76.709/,P(4)/0.012361/,
     +P(5)/78.742/,P(6)/0.5172787/,V1/6.30/,V2/7.77/
      READ 1,N
    1 FORMAT(5I3)
      READ 2,(V(I),T(I),I=1,N)
    2 FORMAT(2F10.8)
      DO 4 I=1,N
      VV=V(I)
      A=0.0
      B=0.0
      C=0.0
      IF(VV.LE.V1) A=1.0
      IF(VV.LE.V1) B=0.0
      IF(VV.LE.V1) C=0.0
      IF(VV.GE.V2) A=0.0
      IF(VV.GE.V2) B=0.0
      F(I)=A*P(1)*EXP(P(2)*(VV-V1))+C*(P(5)*EXP(P(6)*(VV-V2)))
     +B*P(3)*EXP(P(4)*(VV-V1))+C*(P(5)*EXP(P(6)*(VV-V2)))
      PRINT 100,T(I),V(I),F(I),I
  100 FORMAT(5X,F8.2,3X,F8.2,5X,F10.2,3X,I3)
    4 CONTINUE
      CALL NAMPLT
      CALL FACTOR (0.8)
      CALL PLOT(0.3,-0.5,-3)
      T(N+2)=15.0
      V(N+1)=0.0
      V(N+2)=1.5
      CALL AXIS1(1.5,1.5,11HVOLUME (ML),-11,6.0,0.0,V(N+1),V(N+2),10.0)
      CALL AXIS1(1.5,1.5,11HCONDUCTANCE,11,6.0,90.0,T(N+1),T(N+2),10.0)
      CALL SYMBOL(0.5,0.25,
     +14HCOMPARISION OF MODEL TO EXPERIMENTAL DATA,0.0,41)
      CALL PLOT(1.5,1.5,-3)
      CALL LINE(V,T,N,1,0,0)
      CALL PLOT(0.0,0.0,3)
      F(N+1)=0.0
      F(N+2)=15.0
      CALL LINE(V,F,N,1,-1,11)
      CALL PLOT(10.0,-1.5,-3)
      CALL ENDPLT
      CALL EXIT
      END
```

Appendix 9 A photograph of the layer location in ultracentrifugal cell of SPINCO-E and the corresponding analysis

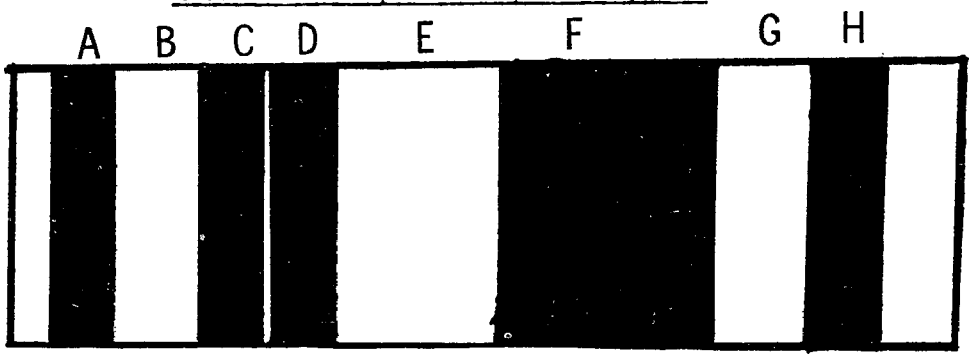

The regions A and H indicate the reference lines, the regions B and G are blocked by the cell. Region C is caused by an air bubble in the cell. Regions D, E, F represent the oil, cream and water phases respectively. The thickness of regions B to G can be measured individually by a travelling micrometer. The average value for each region is obtained by taking six measurements along the two edges of each region. The corresponding volume can be calculated by

$$V=4/360\times\pi\times h\left[(Ra+X)^2-Ra^2\right]=h/90\times\pi\times(2\times Ra+X^2)$$

where Ra is the distance from the center of the ultracentrifuge rotor to the oil/air interface. The radius of the rotor is 5.7 cm, therefore Ra = 5.7 + B + C; h is the thickness of the cell, which is 12 mm for these experiments, X is the distance from the oil layer to an interface. The distance between the two reference lines is 1.6 cm, the magnification of the plate has been calibrated to be 2.154, therefore the value of x in cm is divided by 2.154 before substitution into the volume equation.

VITA

Mr. Yungnien John Chou was born at Li-Yang, Kiang-Su, China on July 18, 1947. He moved to Taiwan with his parents in 1949. He is the only son of Mr. and Mrs. Chao Chan Chou. He graduated from Hsin Chu Boys' High School in 1966. He received the bachelor of Science degree in Chemistry from Cheng-Kung University, Tainan, Taiwan in June, 1970. He then served as second lieutenant in the Chinese Army in the capacity of platoon leader for one year, after which he taught chemistry at Hsin-Hui Agriculture and Technology Vocational High School for one year. In June 1972 he entered the graduate school of applied chemistry, College of Chinese Culture, Taipei, Taiwan during which time he was employed by Cheng-Fong Chemical Company, Taipei, Taiwan. He received his Masters in Applied Chemistry in June 1974.

He came to Lehigh University, Bethlehem, Pennsylvania for graduate study in August, 1974 and received a Master degree in Chemistry in October, 1976. While at Lehigh University, he was sponsored by a University Scholarship and the Emulsion Polymers Institute.

Mr. Chou is married to the former Chaochin Chien and is the father of three children Leslie, Johnny and Luann.